

Aus dem Institut für Schlaganfall- und Demenzforschung ISD

Klinik der Universität München

Direktor: Prof. Dr. Martin Dichgans

Contribution of the K63-deubiquitinase Cylindromatosis (CYLD) to neuronal cell death after focal cerebral ischemia

Dissertation

zum Erwerb des Doktorgrades der Medizin

an der Medizinischen Fakultät der

Ludwig-Maximilians-Universität zu München

vorgelegt von

Pierre Scheffler

aus Luxemburg

2023

Mit Genehmigung der Medizinischen Fakultät
der Universität München

Berichterstatter: Prof. Dr. Nikolaus Plesnila

Mitberichterstatter: PD Dr. Nicole Angela Terpolilli
Prof. Dr. Thomas Liebig

Dekan: Prof. Dr. med. Thomas Gudermann

Tag der mündlichen Prüfung: 16.02.2023

Meinen Eltern

TABLE OF CONTENTS

1	Introduction.....	1
1.1	Stroke	1
1.1.1	Definition	1
1.1.2	Epidemiology	2
1.1.3	Current treatments	3
1.1.4	Pathophysiology.....	4
1.2	CYLD and its implication in cell death	8
1.2.1	The CYLD protein	8
1.2.2	CYLD and ubiquitination	8
1.2.3	CYLD, programmed cell death and the NF- κ B pathway	9
1.2.4	CYLD, glutathione peroxidase 4 (GPX4) and ferroptosis.....	10
1.3	Aim of the study.....	11
2	Materials and Methods	13
2.1	Animals.....	13
2.1.1	CYLD knockout	13
2.1.2	Generation of inducible neuronal GPX4 and CYLD double knockout ...	13
2.2	Experimental design	15
2.3	Induction of focal cerebral ischemia	16
2.3.1	Anesthesia	16
2.3.2	Monitoring and maintenance of body temperature.....	16
2.3.3	Attachment of laser Doppler probe	16
2.3.4	Transient middle cerebral artery occlusion.....	17
2.4	Evaluation of neurological deficits	18
2.5	Quantification of infarct volume	21
2.6	Cerebral vasculature analysis	22
2.7	Gravimetric assessment of brain edema	24

2.8	Western blot analysis	24
2.9	Immunofluorescence	26
2.10	Statistical analysis	27
3	Results	28
3.1	CYLD deletion in the brain.....	28
3.2	Pattern of expression of CYLD in the brain	28
3.3	Expression of CYLD after cerebral ischemia	30
3.4	MCAo standardization	31
3.5	Cerebral vasculature analysis	32
3.6	Infarct volume and brain edema after focal cerebral ischemia in CYLD -/-..	33
3.7	Functional outcome after focal cerebral ischemia in CYLD -/-	35
3.8	Neuronal cell death after focal cerebral ischemia in CYLD -/-	35
3.9	Survival after conditional GPX4 knockout in CYLD -/-	37
3.10	Functional outcome after conditional GPX4 knockout in CYLD-/-	38
4	Discussion	39
4.1	Discussion of the methods	39
4.1.1	Animal models in stroke research.....	39
4.1.2	The use of filament MCA occlusion in mice as a stroke model	41
4.1.3	Measurement of cortical blood flow.....	44
4.1.4	Survey of neurological status.....	44
4.1.5	The role of anesthesia in experimental stroke models	45
4.1.6	Hypothermia in experimental stroke models	46
4.1.7	Determination of hemispheric swelling and edema	47
4.1.8	Cerebral vasculature analysis	47
4.1.9	The TUNEL assay.....	48
4.2	Discussion of the results.....	48
4.2.1	CYLD is expressed in neurons in the mouse brain	48
4.2.2	Cerebral ischemia decreases CYLD expression in the brain	49

4.2.3	CYLD deletion is neuroprotective after cerebral ischemia	50
4.2.4	CYLD deletion does not influence edema formation after cerebral ischemia	51
4.2.5	Neuroprotective effect of CYLD deletion does not result from vascular collateralization.....	52
4.2.6	Neuroprotective effect of CYLD deletion through decrease in necroptosis but not lipid peroxidation.....	52
4.3	Clinical relevance of the findings	54
5	Summary	55
5.1	English.....	55
5.2	Deutsch	57
6	Abbreviations.....	59
7	Acknowledgements	62
8	Curriculum Vitae.....	63
9	Presentations and publications.....	65
10	Citations.....	66

1 INTRODUCTION

1.1 STROKE

1.1.1 Definition

The American Stroke Association defines stroke as a neurological deficit attributed to an acute focal injury of the central nervous system by a vascular cause³. Depending on the affected area of the brain, patients may suffer from transient or permanent partial loss of voluntary movement, sensation, vision, or speech; severe strokes can result in a minimally conscious state or death.

In general, two main types of stroke can be distinguished: ischemic and hemorrhagic stroke. Hemorrhagic strokes are due to bleeding in the brain parenchyma or in the subarachnoid space. Intracerebral hemorrhage is frequently caused by hypertensive small vessel disease, which leads to the formation of small lipohyalinotic aneurysms, but can also be caused by intracranial vascular malformations, cerebral amyloid angiopathy or secondary hemorrhage after an ischemic stroke⁴. Subarachnoid hemorrhage is mainly caused by traumatic brain injury or rupture of aneurysms within the subarachnoid space⁵.

Ischemic strokes, on the other hand, are due to decreased cerebral blood supply caused by vessel occlusion through atherosclerosis or embolic events. The subsequent lack of oxygen supply leads to the degradation of the affected tissue. Ischemic strokes are more common than hemorrhagic ones, accounting for about 80% of all strokes^{6,7}. The focus of the study presented here lies on ischemic stroke.

1.1.2 Epidemiology

Stroke is responsible for 9% of all deaths globally⁸, and it is the sixth most common cause of disability-adjusted loss of life years⁸. In 2010, approximately 15 million people suffered a stroke, and there were 33 million stroke survivors, many of whom are struggling with permanent disabilities. Worldwide stroke incidence, prevalence and mortality have been continuously rising over the past decades. As a result, stroke prevalence is predicted to rise to 70 million by 2030 (Fig. 1)¹.

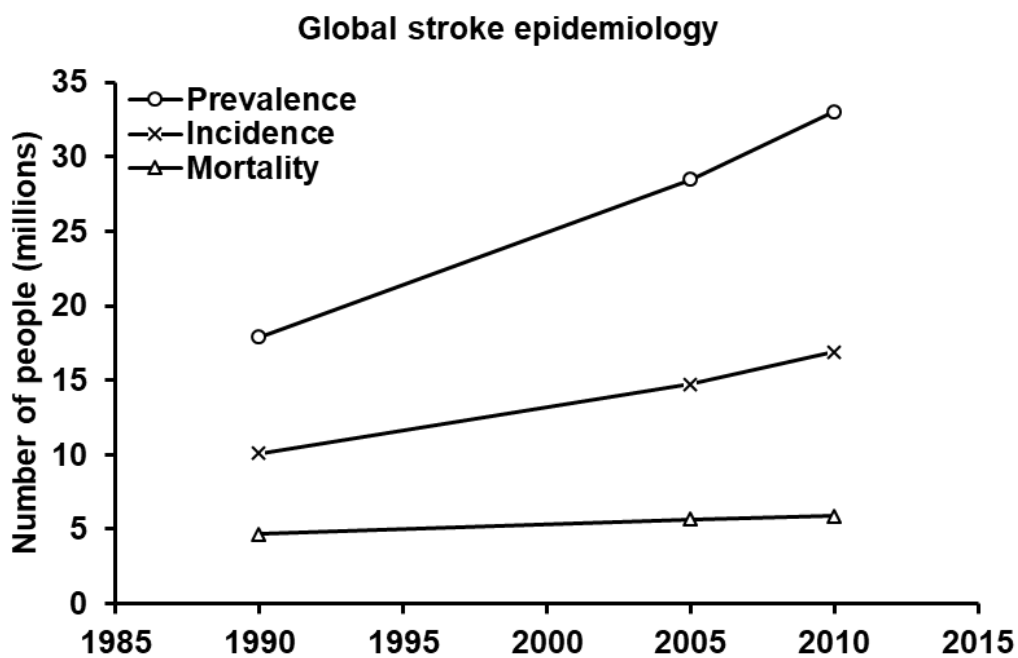


Figure 1: Rise of stroke prevalence, incidence and mortality over time. Data source: Feigin et al., *The Lancet*, 2014¹.

Beyond the health burden, stroke also has a considerable economic impact. In Europe, the total cost of stroke was approximately €60 billion in 2017, amounting to 0.4% of total gross domestic product. In Germany, stroke is related to 2.6% of total health care expenditures⁹.

These statistics illustrate that stroke has already become a significant public health problem that will continue to grow in the next decades. They also highlight the importance of further research into new stroke treatments that could potentially reduce the social and individual burden of the disease.

1.1.3 Current treatments

Despite the significant impact of stroke on public health, therapeutic options are still limited. Guidelines for an evidence-based approach to the treatment of stroke are regularly published by the American Stroke Association¹⁰.

1.1.3.1 Thrombolysis

During the first hours of an ischemic stroke, the goal is to minimize brain injury through rapid restoration of blood flow to the ischemic area. This can be achieved with intravenous (IV) thrombolysis. Alteplase, a recombinant tissue-type plasminogen activator (rt-PA), has been shown to improve functional outcome if administered up to 4.5 hours after the initial onset of symptoms, with earlier treatment leading to better outcomes¹¹. However, there are numerous contraindications to rt-PA use¹². For instance, IV thrombolysis cannot be used in patients with intracranial hemorrhage or therapeutic anticoagulation. As a result, only 6% to 8% of all ischemic stroke patients are eligible for rt-PA therapy^{13,14}.

1.1.3.2 Mechanical thrombectomy

In some patients with large artery occlusion, mechanical thrombectomy can be used either in addition or as an alternative to IV thrombolysis to achieve reperfusion. In this case, the thrombus is physically removed with an intraarterial stent retriever device. Mechanical thrombectomy has been shown to significantly improve functional outcome in several different trials¹⁵⁻²⁰.

1.1.3.3 Stroke units

After blood flow restoration or if the patient was not eligible for both thrombolysis and thrombectomy, patients are ideally admitted to a specialized stroke unit during the subacute phase of the stroke, usually with ECG and blood pressure monitoring, frequent laboratory studies including electrolytes, glucose and markers of inflammation, and early rehabilitation. Management of patients on a stroke unit alone reduces mortality by 28% and leads to improvements in functional outcome²¹. The aspects responsible for this effect remain unclear, although some researchers suggest that the treatment of acute complications like pneumonia, pulmonary embolism and recurrent stroke as well as early rehabilitation and psychological factors may contribute to it²².

1.1.3.4 Neurosurgical interventions

Some patients with large supratentorial strokes or infratentorial strokes may also need early neurosurgical intervention due to rising intracranial pressure. In young patients with malignant middle cerebral artery (MCA) infarction and brain edema, studies have shown that decompressive surgery within 48 hours of stroke onset reduces mortality and improves outcome²³. Patients with neurological deterioration after cerebellar infarction often undergo decompressive suboccipital craniectomy to reduce brainstem compression²⁴.

1.1.3.5 Secondary prevention

After the subacute phase, stroke treatment is currently limited to rehabilitation and secondary prevention. Secondary prevention includes lifelong antiplatelet treatment, usually with acetylsalicylic acid, which has been shown to reduce mortality and morbidity in stroke patients^{25,26}. Stroke patients also benefit from lifelong statin therapy²⁷.

To date, most guidelines for the treatment of stroke do not feature any neuroprotective agents. The only currently available acute stroke treatment possibly interfering with neuronal cell death is the administration of selective serotonin reuptake inhibitors (SSRIs). There is limited data suggesting that SSRIs, a class of drugs that are frequently prescribed for the treatment of depression, improve recovery after ischemic stroke independently of its effect on poststroke depression^{28,29}. The mechanism behind this effect is currently unclear; possible mechanisms include an increase in neurogenesis³⁰, neuroprotection through anti-inflammatory properties³¹, improved cerebral blood flow³² and modulation of the adrenergic neurohumoral system³³. However, the available data is still considered insufficient to justify the use of SSRIs outside of clinical trials²⁸.

1.1.4 Pathophysiology

In order to develop new therapeutic options for stroke, it is essential to understand the underlying pathomechanisms.

1.1.4.1 Excitotoxicity and mitochondria dysfunction

Compared to other organs, the brain tolerates only short periods of ischemia. This is partly due to its very high energy demand: The brain consumes 20% of blood oxygen despite accounting for only 2% of a human's total body weight³⁴. The brain's low

ischemic tolerance is further aggravated by its almost complete lack of energy storage options, thereby making the proper function of brain tissue highly dependent on a continuous supply of both oxygen and glucose.

A critical decrease of cerebral perfusion and oxygenation results in ischemic infarction with a central core undergoing rapid neuronal cell death and tissue necrosis. The core is surrounded by a larger area of the brain able to receive reduced blood supply through collaterals: the penumbra (Fig. 2). While tissue within the penumbra will still degrade eventually, cell death is delayed compared to the ischemic core due to the residual collateral perfusion.

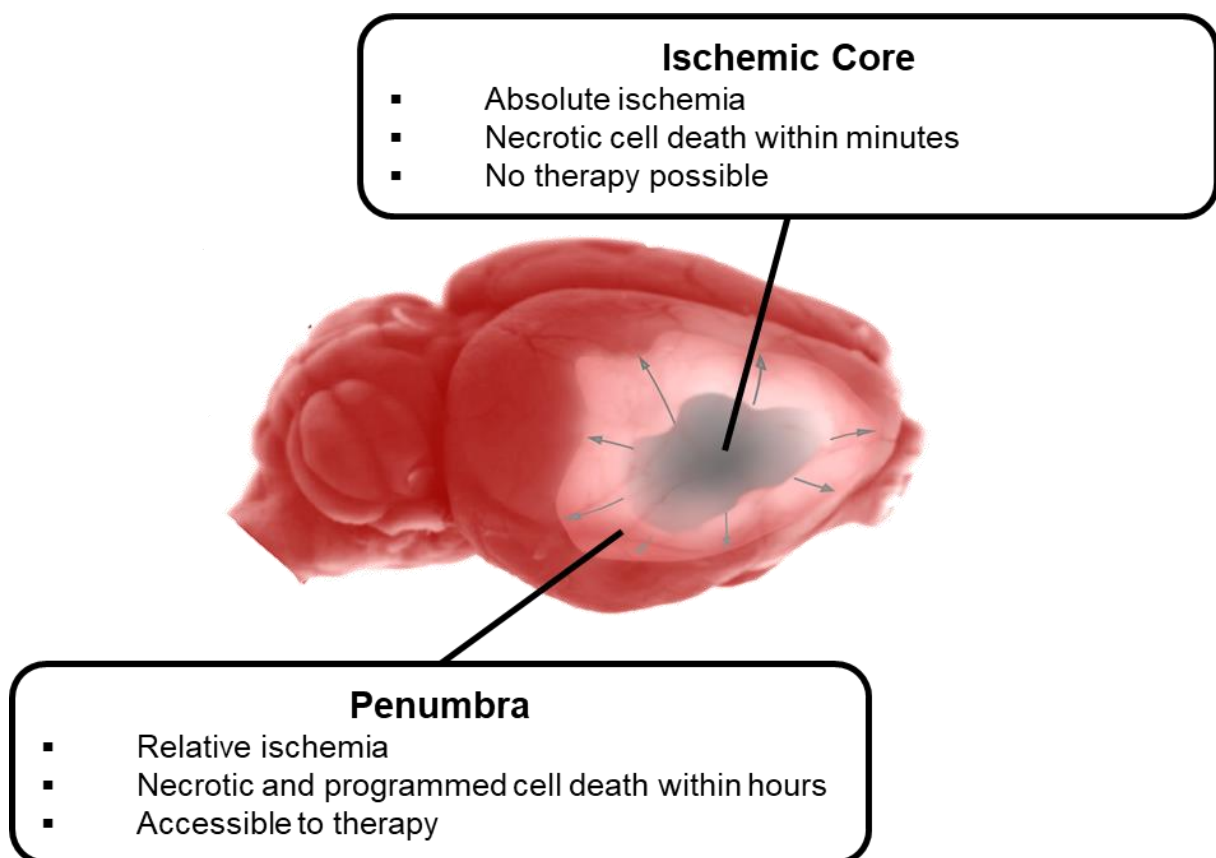


Figure 2: Different ischemic areas of a mouse brain after MCA occlusion. The ischemic core is depicted in grey, the penumbra in pale red, the healthy brain in deep red.

The brain mostly uses adenosine triphosphate (ATP) derived from oxidative phosphorylation of glucose supplied by the arterial circulation as source of metabolic energy to maintain transmembrane ion gradients in neurons. The sudden loss of energy in the event of an ischemic stroke leads to a rapid depletion of ATP reserves and subsequently to a loss of membrane ion pump function in neurons³⁵ (Fig. 3). This leads to the depolarization of neurons and the release of glutamate by excitatory

neurons. Glutamate in return activates α -amino-3-hydroxy-5-methyl-4-isoxazolepropionic acid (AMPA), N-methyl-D-aspartate (NMDA) and metabotropic glutamate receptors and thus triggers Na^+ , Cl^- and Ca^{2+} influx as well as K^+ efflux and further depolarization of neurons, leading to a vicious circle known as excitotoxicity³⁶.

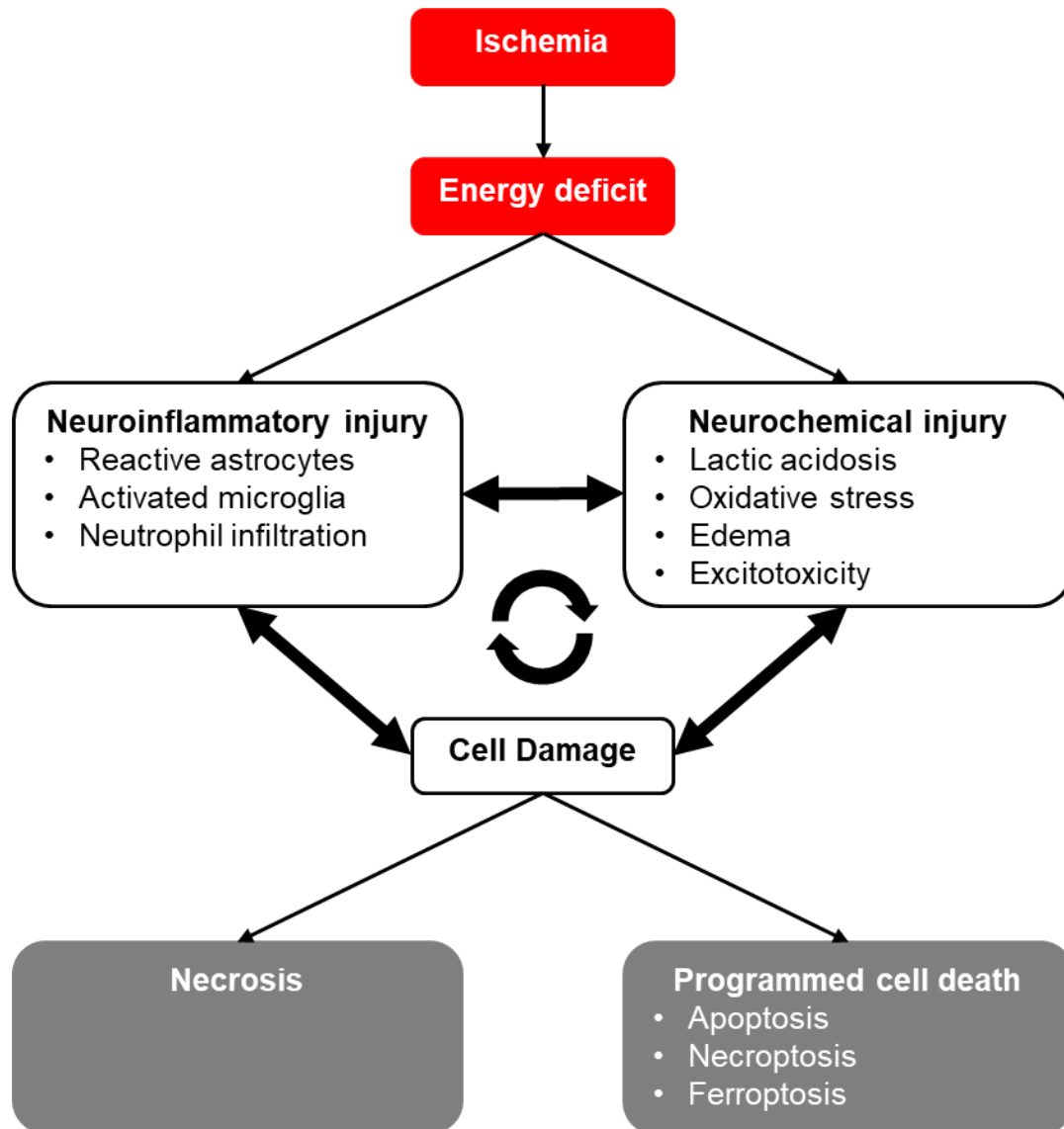


Figure 3: Ischemic cascade leading to brain damage and cell death.

In the ischemic core, perfusion is so low that the excitotoxicity-induced Ca^{2+} influx triggers lipolysis, proteolysis and deoxyribonucleic acid (DNA) fragmentation, which ultimately leads to necrotic cell death within minutes^{36,37}. Within the surrounding penumbra, blood flow is too low to maintain the physiological activity of brain cells, but still sufficient to partially preserve energy metabolism and prevent membrane failure^{38,39}. However, eventually, peri-infarct depolarizations within the penumbra will increase energy metabolism, thereby causing energy depletion and cell death^{40,41}. Excitotoxicity, hypoxia and the accumulation of free radicals will also trigger an

inflammatory reaction shown to lead to further necrosis⁴². In addition, the Ca²⁺ overload, oxygen radicals, inflammation, mitochondrial and DNA damage will all contribute to programmed cell death within the penumbra³⁶. As a result, the area of irreversibly damaged tissue will continuously increase until up to 48 hours after the onset of ischemia⁶.

Due to its rapid and irreversible degradation, the ischemic core cannot be realistically targeted by any form of acute therapeutic intervention. The slowly degrading penumbra, however, can potentially be saved; this makes the biochemical processes that lead to the degradation of the penumbra an attractive target for therapy.

1.1.4.2 Reperfusion injury and inflammation

Although reperfusion is in most cases beneficial, some aspects of it can lead to further damage, which is known as reperfusion injury⁴³. Reperfusion results in additional oxidative stress, which is mainly caused by mitochondria due to posttranslational modification of oxidative phosphorylation proteins⁴⁴, and by nicotinamide adenine dinucleotide phosphate (NADPH) oxidase through electron transfer to molecular oxygen⁴⁵. Reperfusion also facilitates leukocyte infiltration of the damaged tissue and thus increases inflammation⁴⁶. Inflammation and oxidative stress both contribute to blood-brain-barrier disruption, which leads to vasogenic edema and facilitates hemorrhagic transformation of the stroke⁴⁷.

1.1.4.3 Different forms of neuronal cell death

Although necrotic and apoptotic features are often prevalent in neuropathological conditions, there is now increasing evidence that cell death mechanisms are more diverse. Until recently, the delayed cell death mechanisms in the penumbra were associated with apoptosis, a regulated cell death mechanism^{48,49}. However, ischemic cerebral tissue presents cells with morphological cell death features shared between apoptosis and necrosis^{50,51}, suggesting various forms of controlled cell death.

The intracellular formation of reactive oxygen species (ROS) as well as the apoptotic/necroptotic signalling pathways have been identified as contributing processes⁵². Cyldromatosis (CYLD) and the antioxidant glutathione peroxidase 4 (GPX4) have emerged as key players in the signaling for necroptosis and ROS-mediated ferroptosis respectively.

1.2 CYLD AND ITS IMPLICATION IN CELL DEATH

1.2.1 The CYLD protein

The CYLD protein in human is encoded by a gene located on the long arm of chromosome 16 and on chromosome 8 in rodents⁵³. Its name is a reference to specific mutations in the CYLD gene associated with several autosomal dominant hereditary skin diseases including familial cylindromatosis and Brooke-Spiegler syndrome. These lead to the formation of tumors originating from skin appendages, such as spiradenomata, trichoepitheliomata and the eponymous cylindromata⁵⁴.

1.2.2 CYLD and ubiquitination

The CYLD protein possesses 3 cytoskeletal-associated protein glycine-rich (CAP-Gly) domains, which are usually found in proteins regulating the attachment to microtubules⁵⁵ (Fig. 4). It also has a catalytic domain similar to ubiquitin carboxy-terminal hydrolases (UCH) allowing it to serve as a deubiquitinating enzyme⁵⁶, and a TNF receptor-associated factor 2 (TRAF2) binding motif⁵⁷, a protein involved in programmed cell death as explained in detail below.



Figure 4: Overview of CYLD structure. CYLD features 3 CAP-Gly domains, a TRAF2-binding motif (TBM) and a ubiquitin-specific protease (USP) domain. Figure adapted from Harhaj and Dixit⁵⁷

Ubiquitin is an 8.5 kDa regulatory protein first isolated in 1975 and occurring ubiquitously in eukaryotic cells, hence its name⁵⁸. Ubiquitin is usually attached post-translationally with its C-terminal glycine to other proteins in a process called ubiquitination. This can modify the protein's function and turnover in different ways, depending on the type of ubiquitination⁵⁹. Ubiquitin can either be attached to a structurally different protein or to another ubiquitin molecule. Ubiquitin is thus able to create polyubiquitin chains. Depending on whether a single ubiquitin molecule or a whole polyubiquitin chain is attached to a protein, the process is called mono- or polyubiquitination. Polyubiquitination can then be further differentiated depending on the type of link between the ubiquitin molecules⁶⁰. Links between ubiquitin molecules are established between the to-be-added ubiquitin molecule's C-terminal glycine and either the already attached ubiquitin molecule's N-terminus or one of several lysines within the ubiquitin's polypeptide chain. The lysines within the ubiquitin molecule

which can be linked are K6, K11, K27, K29, K33, K48 and K63⁶¹. The function of most forms of ubiquitination is poorly understood. Monoubiquitination is usually associated with membrane trafficking and endocytosis^{62,63}, while exclusively K48-linked polyubiquitination targets proteins for proteasomal degradation⁶⁴.

CYLD is a K63-deubiquitinating enzyme. K63-ubiquitination is involved in various processes as diverse as endocytic trafficking, inflammation, translation, and DNA repair⁵⁹.

1.2.3 CYLD, programmed cell death and the NF- κ B pathway

One of the target proteins of CYLD is the receptor-interacting protein 1 (RIP1), which is involved in a caspase-independent programmed cell death pathway called necroptosis. Necroptosis morphologically resembles necrotic cell death but is activated through cell signaling pathways in the absence of intracellular apoptotic signaling. Necroptosis is thought to contribute to cell death in the penumbra during stroke, and an inhibitor of necroptosis, Necrostatin-1, reduced the infarct volume in mice after MCA occlusion⁶⁵.

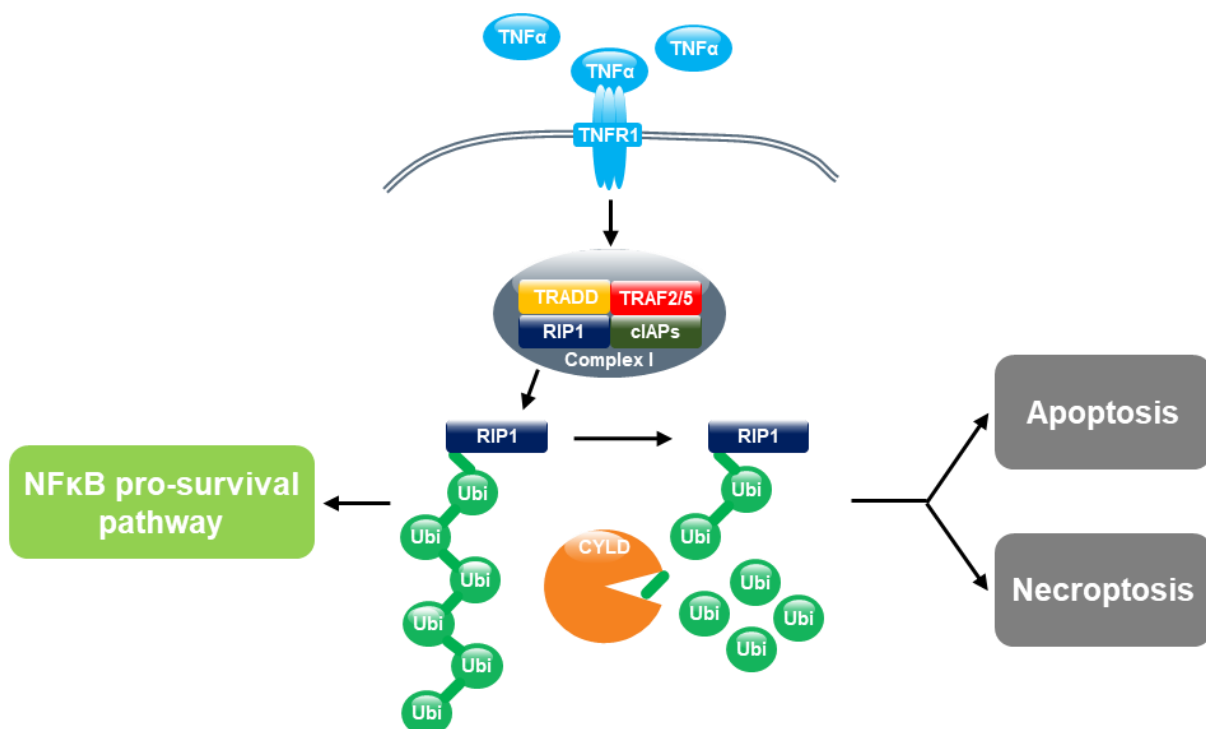


Figure 5: CYLD implication in the TNFR1 biochemical pathway. CYLD is a Lysin 63-Deubiquitinase targeting RIP1 and thus pushing the balance towards programmed cell death.

Necroptosis is initiated by the binding of tumor necrosis factor alpha (TNF α) to the TNF receptor 1 (TNFR1); this leads to the intracellular assembly of the so-called TNFR

complex 1 (Fig. 5). TNFR complex 1 consists of the TNF receptor-associated death domain (TRADD), the TNF receptor-associated factors 2 and 5 (TRAF2/TRAF5), the cellular inhibitor of apoptosis proteins (cIAPs) and RIP1⁶⁶.

The function of TNFR complex 1 depends on the ubiquitination of RIP1⁶⁷. RIP1 can be K63-ubiquitinated by the cIAPs⁶⁸. In this case, RIP1 can recruit the transforming growth factor beta activated kinase 1 (TAK1), and TAK1-binding proteins 2 and 3 (TAB2/TAB3), which leads to the formation of a protein complex called nuclear factor kappa-light-chain-enhancer of activated B cells (NF- κ B)⁶⁹. NF- κ B acts as a cell survival signal and inhibits programmed cell death⁷⁰. If RIP1 is deubiquitinated by CYLD, however, it leads to the formation of complex 2, which consists of RIP1, RIP3, TRADD, the FAS-associated protein with a death domain (FADD) and Caspase 8. Caspase 8 then triggers apoptosis⁷¹. If Caspase 8 is inhibited, phosphorylation of RIP1 and RIP3 through an unknown mechanism leads to necroptosis⁷².

1.2.4 CYLD, glutathione peroxidase 4 (GPX4) and ferroptosis

Release of reactive oxygen species is known to trigger ferroptosis, an iron-dependent form of programmed cell death that has first been described in 2012⁷³ (Fig. 6). It is triggered by inhibition of the cystine/glutamate antiporter System X_c⁻, for example through high extracellular glutamate concentrations. This leads to a lack of intracellular cystine and subsequently cysteine, which is needed for the regeneration of glutathione. Glutathione acts as an antioxidant within the cell; its absence – even under physiological conditions – leads to the accumulation of reactive oxygen species, which ultimately lead to the destruction of the cell.

Glutathione peroxidases are enzymes catalyzing the reduction of peroxides by glutathione. Among these, glutathione peroxidase 4 (GPX4) seems to play a key role, as its deletion leads to intrauterine death⁷⁴. Its main function seems to be the reduction of phospholipid hydroperoxides, which is why it is also called phospholipid hydroperoxide glutathione peroxidase (PHPGPX)⁷⁵. It was recently found that GPX4 is crucial for inhibition of ferroptosis: Its overexpression and knockdown modulated the lethality of ferroptosis inducers, and depletion of glutathione causes its inactivation⁷⁶. GPX4 has also been shown to be located in neurons⁷⁷. A neuron-specific conditional knockout seems to lead to rapid neurodegeneration⁷⁸ or death. Previous work showed that neuronal cell death in these animals occurs by increasing lipid oxidation⁷⁹.

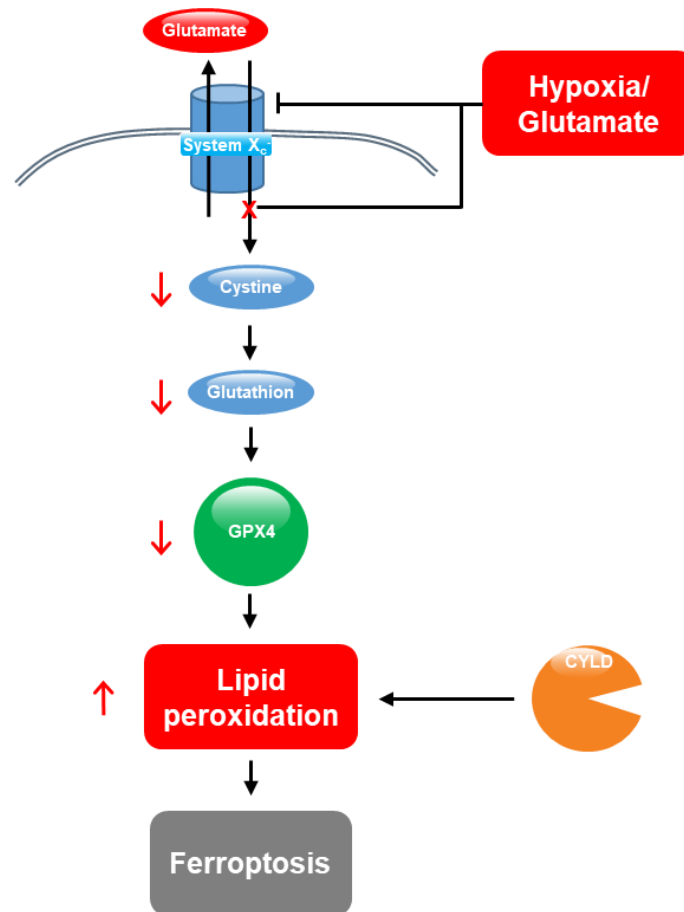


Figure 6: Contribution of CYLD in GPX4 induced-ferroptosis. Previous results have shown lower lipid peroxidation upon reduction of CYLD mRNA, suggesting a link between CYLD and lipid peroxidation.

Interestingly, it was recently shown that a siRNA-mediated knockdown of CYLD leads to a reduction of lipid peroxidation. Therefore, CYLD may also be involved in ferroptosis, suggesting a crosstalk between these two cell death mechanisms prevailing in stroke pathology⁸⁰. However, the interactions between these processes are not well understood.

1.3 AIM OF THE STUDY

Programmed cell death mechanisms like necroptosis and ferroptosis are involved in the degradation of the penumbra during stroke. CYLD is thought to play an important role in necroptosis and may also be involved in ferroptosis. Therefore, the aim of this study was to

(1) Investigate the role of CYLD in ischemic stroke, its mechanism of action and its impact on lesion size, edema formation and neurological outcome to see whether CYLD qualifies as a target molecule for future stroke therapy.

(2) Analyze whether CYLD is significantly involved in the induction of lipid oxidation during neuronal cell death using double-knockout mice with a regular CYLD and an inducible, potentially lethal GPX4 knockout. We evaluated whether a deletion of CYLD has a positive effect on the survival of these animals.

2 MATERIALS AND METHODS

2.1 ANIMALS

All animal procedures were approved by the Animal Care Committee of the Government of Upper Bavaria (Protocol Number 55.2-1-54-2532-7-14). Animals were kept under controlled temperature and humidity conditions with standardized light and dark cycles and free access to food pellets and tap water. C57BL/6 mice were obtained from Charles River (Erkrath, Germany). CYLD knockout and CYLD and tamoxifen-inducible GPX4 double-knockout mice were used in this study.

2.1.1 CYLD knockout

CYLD knockout mice (CYLD^{-/-}) bred for at least 5 generations on a C57BL/6N background were kindly provided by Prof. Dr. Reinhard Fässler (Max Planck Institute of Biochemistry, Munich). The CYLD^{-/-} mice were generated with a targeting construct in which the ATG-containing exon 4 of the CYLD gene was disrupted by insertion of a cassette containing a lacZ reporter and a neomycin gene⁸¹. Before and after each experiment, the knockout mice were genotyped to verify the lack of the CYLD gene and the presence of the lacZ reporter gene. Besides increased susceptibility to develop skin tumors while aging, the CYLD^{-/-} mice are fertile, normal in size and do not display any obvious physical or behavioral abnormalities. We used CYLD wildtype (WT) littermates as controls.

2.1.2 Generation of inducible neuronal GPX4 and CYLD double knockout

In order to investigate the relationship between CYLD and neuronal ferroptosis, we created a double knockout mouse model with both a permanent CYLD knockout and a tamoxifen-inducible GPX4 knockout in cells expressing the Ca²⁺/calmodulin-dependent protein kinase II α (CamKII α).

Our inducible GPX4 knockout uses Cre-Lox recombination. The Cre recombinase is an enzyme that catalyzes the recombination between short DNA sequences called LoxP (locus of x-over P1), which results in the deletion of the DNA segment between two sites⁸². Our model uses an inducible Cre recombinase that has been fused to a modified ligand binding domain recognizing tamoxifen, so that nuclear translocation and thus recombination only occurs after administration of tamoxifen⁸³; this allows us to investigate the impact of gene deletions that would otherwise lead to intra-uterine

death. In addition, the inducible Cre recombinase was put under the control of the CamKII α promoter. CamKII α is a brain-specific enzyme⁸⁴ that is found in glutamatergic, but not in GABAergic pre- and postsynaptic densities in the cortex, thalamus and hippocampus^{85,86}. CamKII α -controlled Cre expression thus allows for gene inactivation restricted to excitatory neurons in the brain. In summary, the CamKII α Cre/loxP-flanked GPX4 mice show a completely unremarkable phenotype unless exposed to tamoxifen, which leads to the brain-specific deletion of GPX4.

CamKII α Cre/loxP-flanked GPX4 mice with C57BL/6 background were kindly provided by Marcus Conrad (Institute of Clinical Molecular Biology and Tumor Genetics, Helmholtz-Zentrum Munich). The exact method used to generate these mice is described by Seiler et al.⁸⁷. The double knockout model was created by breeding CYLD^{-/-} and mice with floxed GPX4 and CamKII α -controlled, tamoxifen-inducible Cre recombinase according to the breeding scheme illustrated below (Fig. 7).

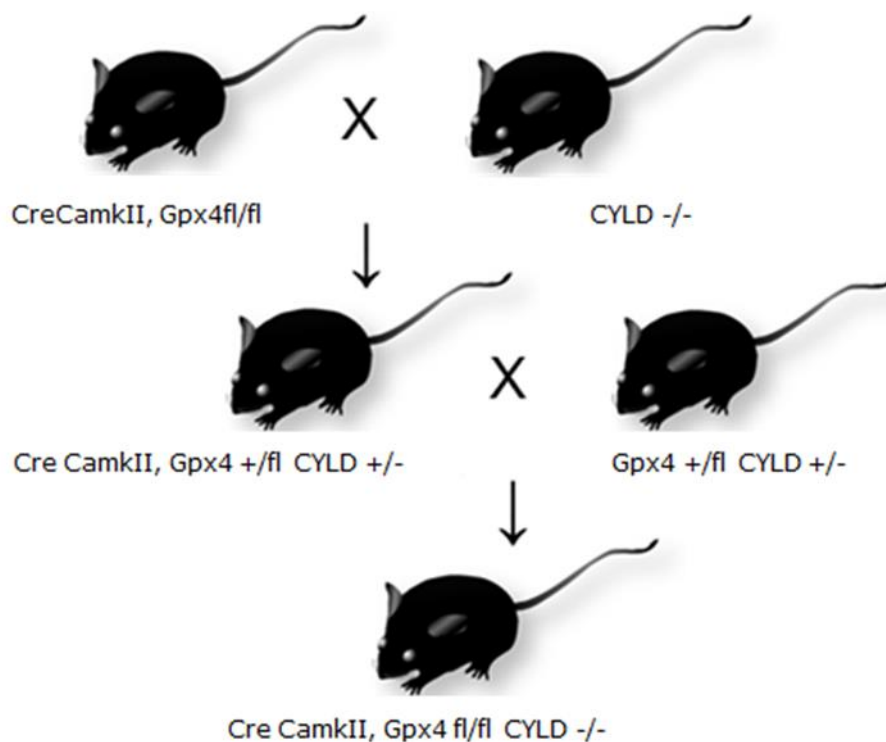


Figure 7: Breeding scheme used to generate the double transgenic mouse line.

2.2 EXPERIMENTAL DESIGN

At the time of experimentation, mice were approximately 8 weeks old. Animals of both sexes were used in the experiments. Most experiments involved filament middle cerebral artery occlusion (MCAo) as described below. We performed behavioral testing 1 hour and at 24 hours after focal cerebral ischemia (Fig. 8). 24 hours after ischemia, the brain was removed as described below. Depending on the experiment, the brain was either frozen with dry ice, a part of the penumbra was collected for western blot analysis, or the hemispheres were separated and collected for edema measurement.

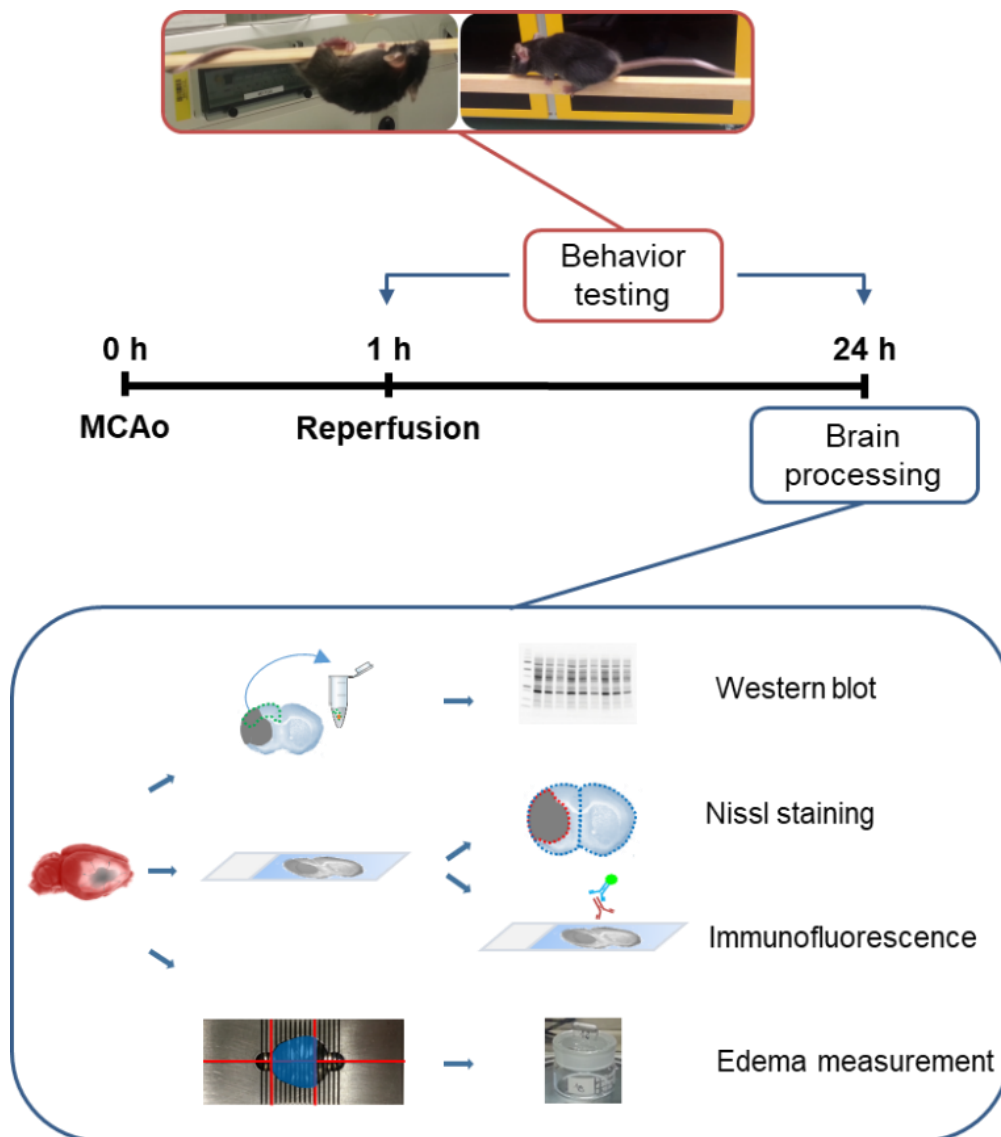


Figure 8: Timeline for filament middle cerebral artery occlusion in mice. 60 minutes after the initial drop in laser Doppler measurement over the MCA territory, the modified Bederson score is evaluated and the filament is surgically removed. 23 hours later, the animal is sacrificed and the brain removed, frozen using dry ice and stored at -80 degrees Celsius until further processing.

All experiments were performed by an investigator blinded to the genotype of the animals and in a randomized manner. For comparison of stroke size, edema measurement, neurological outcome and survival, a group sizes of 10 animals per group was calculated; for histological examination, western blotting and cerebral vasculature analysis, 5 animals per group were used.

2.3 INDUCTION OF FOCAL CEREBRAL ISCHEMIA

In order to induce focal cerebral ischemia in our mice, we used transient filament middle cerebral artery occlusion. This method had already been established in our laboratory and was performed as already described in prior publications^{88,89}.

2.3.1 Anesthesia

Introduction of anesthesia was performed in a separate box with 5% Isoflurane, 65% N₂O and 30% O₂ for 1 minute. During the attachment of the laser Doppler probe, anesthesia was maintained with 3% Isoflurane, 67% N₂O and 30% O₂ administered via a face mask; during the transient middle cerebral artery occlusion, anesthesia was maintained with 2% Isoflurane, 68% N₂O and 30% O₂. Duration of anesthesia was between 20 and 30 minutes. To prevent the animal's eyes from drying out, eye ointment (Bepanthen Augensalbe, Roche, Germany) was applied before starting the surgery.

2.3.2 Monitoring and maintenance of body temperature

To prevent hypothermia under general anaesthesia, core body temperature was measured intraoperatively with a rectal probe and maintained at 37 °C using a feedback-controlled heating pad (FHC, Bowdoinham, USA). Following anesthesia, animals were allowed to recover in an incubator at 32 °C (Drägerwerk AG, Lübeck).

2.3.3 Attachment of laser Doppler probe

All surgery was performed under a surgical microscope (M80, Leica Biosystems, Wetzlar, Germany). Changes in regional cerebral blood flow (CBF) during MCA occlusion were measured with a laser Doppler flowmetry unit (Periflux System 5000 LD, Perimed, Stockholm, Sweden). The laser doppler probe was attached at the beginning of the surgical intervention. The animals were first placed in a prone position. An incision was made above the left temporal muscle, between the left eye and ear. Then the left temporal muscle was separated from the skull until the middle cerebral artery became visible through the skull. Thereafter the laser Doppler probe was placed

on the skull above the middle cerebral artery. Once a decent laser Doppler signal over 150 LD units was found, the probe tip was attached to the skull with acrylic glue (INSTA-CURE Glue, Plastruct, City of Industry, CA, USA) and a respective accelerator (INSTA-SET Accelerator, Plastruct, City of Industry, CA, USA).

2.3.4 Transient middle cerebral artery occlusion

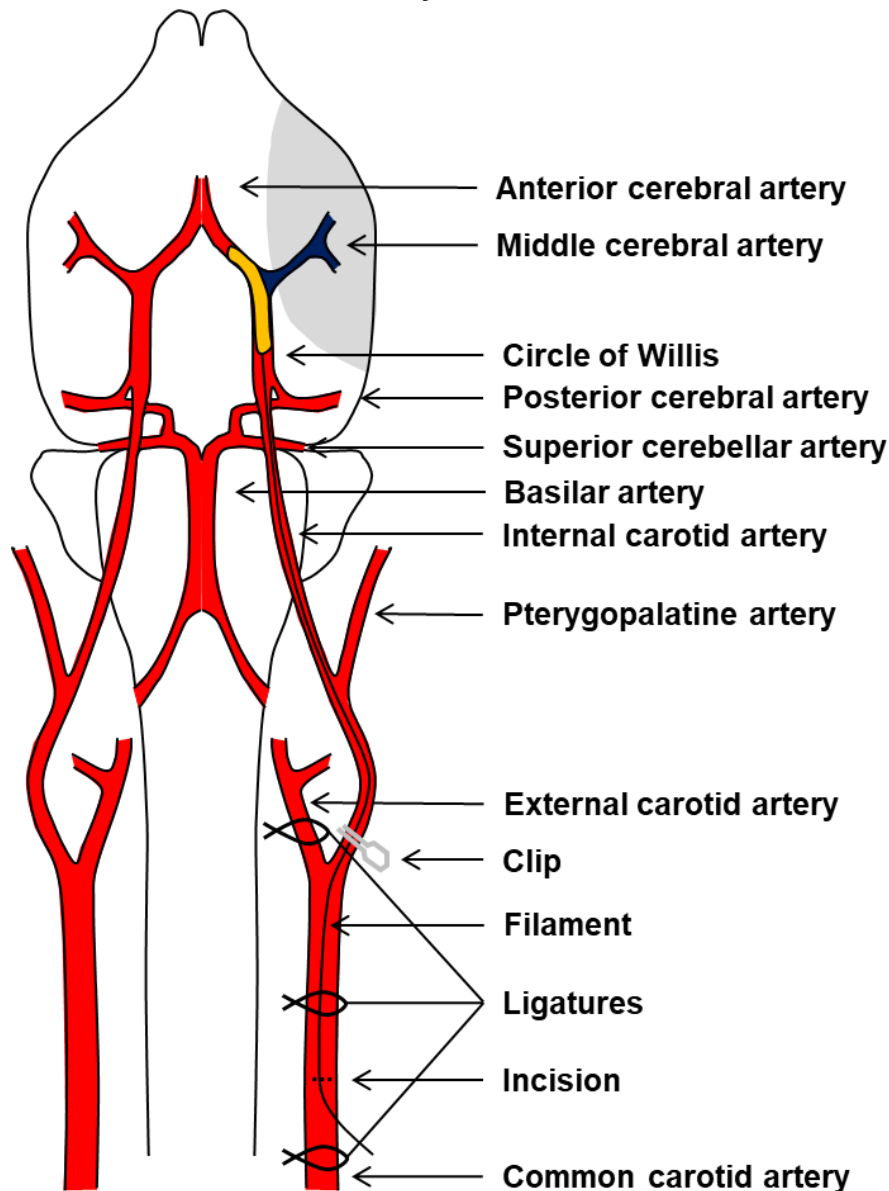


Figure 9: The intraluminal filament model of middle cerebral artery occlusion in mice.

The mice were then placed in a supine position. A cervical midline incision through skin and subcutaneous tissue was made. The submandibular glands were separated in the middle. A retractor was used to lateralize the opening and the ipsilateral salivary gland in order to provide access to the left lateral cervical region. The omohyoid muscle was dissected and the underlying connective tissue was separated atraumatically until the left carotid sheath became visible (Fig. 9). The carotid sheath was then opened up

to the carotid bifurcation. Then the left common carotid artery was ligated at its proximal end. Afterwards, the external carotid artery was also ligated right after the carotid bifurcation. After both the proximal common carotid artery and the external carotid artery were ligated, a surgical clip was temporarily placed on the internal carotid artery in order to prevent back flow. Using micro-scissors, a small opening was cut into the common carotid artery and a thread with a silicon-coated tip was introduced. The thread was pushed forward until it sat right behind the surgical clip. A loose knot was then placed just above the opening in order to prevent bleeding and to hold the filament in place. After removing the surgical clip, the thread was advanced until it occluded the origin of the ipsilateral middle cerebral artery in the circle of Willis. At this point, a significant drop of the laser Doppler signal indicated successful occlusion of the middle cerebral artery.

Once the MCA had been occluded, the loose knot distal to the opening in the common carotid artery was closed tightly in order to prevent any kind of filament displacement. The retractor was removed and the skin wound above the surgical site was closed with two sutures. Afterwards, anesthesia was discontinued and mice were placed in a heated chamber for recovery.

60 minutes after the occlusion, mice were re-anesthetized and reperfusion was initiated by removing the filament from the common carotid artery. The common carotid artery was ligated and the skin wound was closed with two sutures. Anesthesia was discontinued and mice were handled as described above. Mice were returned to their original cage and placed in a warming cabinet heated to 35 °C overnight.

24 hours after ischemia, animals were sacrificed by cervical dislocation. The brain was removed from the skull. The olfactory bulbs were removed and the brain was rapidly frozen using dry ice. It was stored at -80 °C until further processing.

2.4 EVALUATION OF NEUROLOGICAL DEFICITS

We evaluated neurological deficits after MCA occlusion with a modified version of the neurological grading system established by Bederson et al.⁹⁰.

Our score ranges from 0 to 4 and is evaluated according to the criteria in the table below.

Modified Bederson Score	Description
0	The mouse shows no deficits
1	The mouse shows contralateral whisker hyposensitivity or an asymmetric righting reflex, but no circling
2	The mouse circles to either side while having normal posture at rest
3	The mouse leans to the contralateral side at rest
4	The mouse does not move at all

The evaluation takes 30 seconds per mouse and was performed 60 minutes after MCA occlusion (before thread removal) as well as 24 hours after MCA occlusion.

To evaluate the neurological outcome after GPX4 knockout, we used a more complex neurological scoring system based on the neurological severity score developed by Shapira et al.⁹¹ (Fig. 10). In addition to motor function, this score also evaluates other neurological aspects such as arousal, exploration and coordination.

Score	Description
General condition	
0	Smooth fur, clean body openings, clear eyes
1	Minor fur defects
2	Major fur defects, dirty body openings, increased muscle tonus
3	Cloudy eyes, cramps, paralysis
Ability to leave a 1m diameter circle	
0	Less than 2 minutes
0,5	Stops on the boundary
1	Stays within the boundary
3	Does not move
Reaction upon acoustic stimulus	
0	Yes
1	No
Exploration	
0	Normal
1	Awake, but passive
2	Comatose/ no spontaneous movement
Rearing	
0	Yes
1	No
Tail suspension	
0	Hindlimbs straight
1	Hindlimbs crossed over
Clinging to rough surface	
0	Yes
1	No
Holding on to square rod (edge length 7 mm)	
0	With 4 limbs
0,5	With 3 limbs
1	Falls down after rotating rod
2	Falls down immediately
Holding on to round rod	
0	With 4 limbs
0,5	With 3 limbs
1	Falls down after rotating rod
2	Falls down immediately
Crossing a beam with 3 cm width	
0	Normal
1	Unstable/ Missteps
2	Refuses to move
3	Drops down after a few steps
4	Drops down immediately
Crossing a beam with 2 cm width (scoring identical to 3 cm beam)	
Crossing a beam with 1 cm width (scoring identical to 3 cm beam)	

Figure 10: Overview of the extended neuroscore scoring sheet used in our experiments for rating neurological outcome. The mice are assessed and receive a score in every single category. The final score represents the sum of all individual scores.

2.5 QUANTIFICATION OF INFARCT VOLUME

To quantify the infarct volume, we used fresh frozen sections that were prepared and analyzed according to the following protocol.

The frozen brain was placed on a tissue holder with the olfactory bulbs facing up, covered with embedding medium (Tissue-Tek®, Sakura Finetek Germany GmbH, Staufen im Breisgau) and cut using a cryostat (Leica Biosystems, Wetzlar, Germany). We collected 12 coronal sections of 10 µm thickness at a distance of 750 µm from each other, starting at the end of the olfactory bulbs. The sections were then mounted onto slides, stained using a cresyl violet solution (Nissl-staining), covered with a coverslip and digitized using a microscope equipped with an image sensor (Axio Imager, Zeiss, Oberkochen, Germany) (Fig. 11).

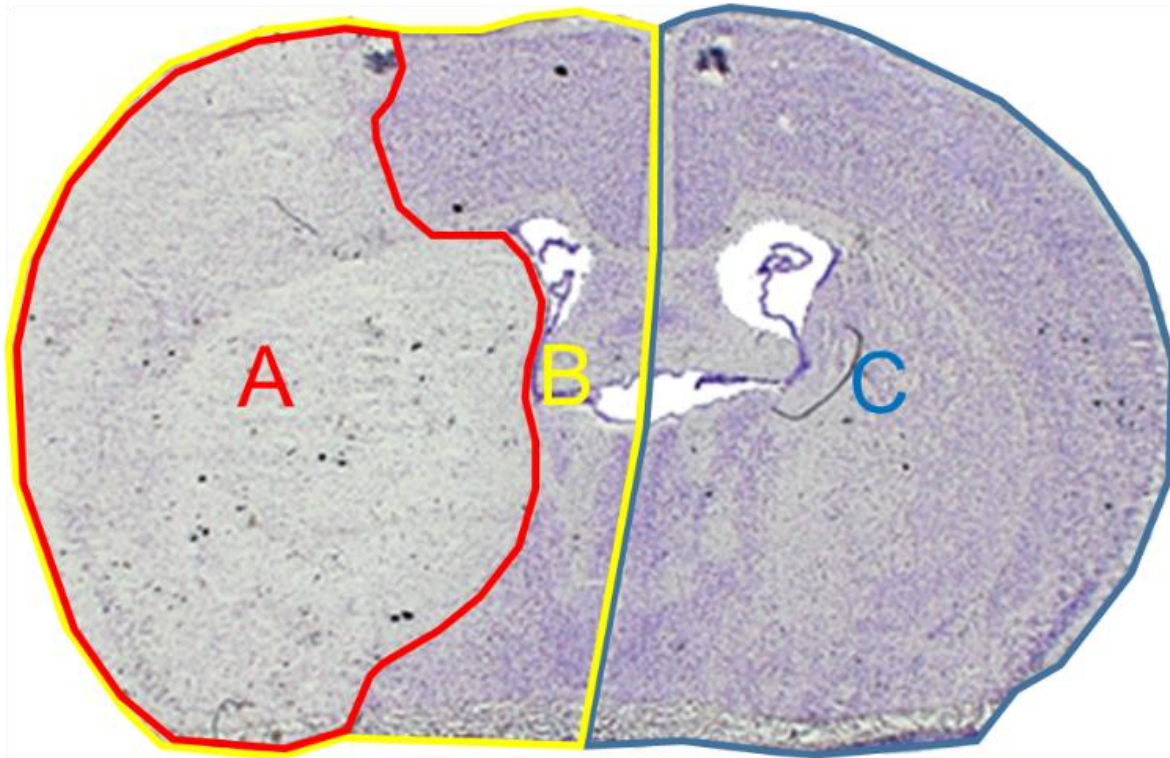


Figure 11: Illustration of the stroke size measurement process using Nissl-stained sections. Area A represents the lesion, area B corresponds to the ipsilateral hemisphere, area C corresponds to the contralateral hemisphere

We measured the surface area on each section for the lesion (A) and for the ipsilateral (B) and the contralateral hemisphere (C) using image analysis software (Axiovision, Zeiss). We correct for an increase in stroke size due to hemispheric swelling by using the following formula, assuming that both hemispheres should have an equal area:

$$\text{Corrected lesion area} = C - (B - A)$$

The corrected total infarct volume was determined based on the corrected lesion area (D) and the distance between sections (0,75 mm) as follows:

$$\text{Corrected lesion volume} = 0,75 \text{ mm} * (D_1 + D_2 + \dots + D_{12})$$

2.6 CEREBRAL VASCULATURE ANALYSIS

Collaterals may influence the size of an infarct following MCA occlusion. To determine whether control and CYLD knockout mice had the same degree of collateralization between the basilar and the middle cerebral artery territory, we evaluated the size of the posterior communicating artery using ink perfusion as established by Murakami et al.².

Mice received analgesia and anesthesia with midazolam, medetomidine and fentanyl. We then performed a thoracotomy, punctured the left ventricle with a butterfly, cut open the right atrium and transcardially perfused mice with saline followed by 4% paraformaldehyde (PFA). After having evacuated all the blood through the right atrium, we injected 200 μ l of ink into the ventricle to visualize cerebral vasculature. We removed the brain as previously described and kept it in 4% PFA for 24h. The brains were briefly rinsed in PBS and then imaged with a CCD camera. The morphology of the posterior communicating artery (PCOM) was graded from 0 (no PCOM) to 3 (fully developed PCOM; Fig. 12).

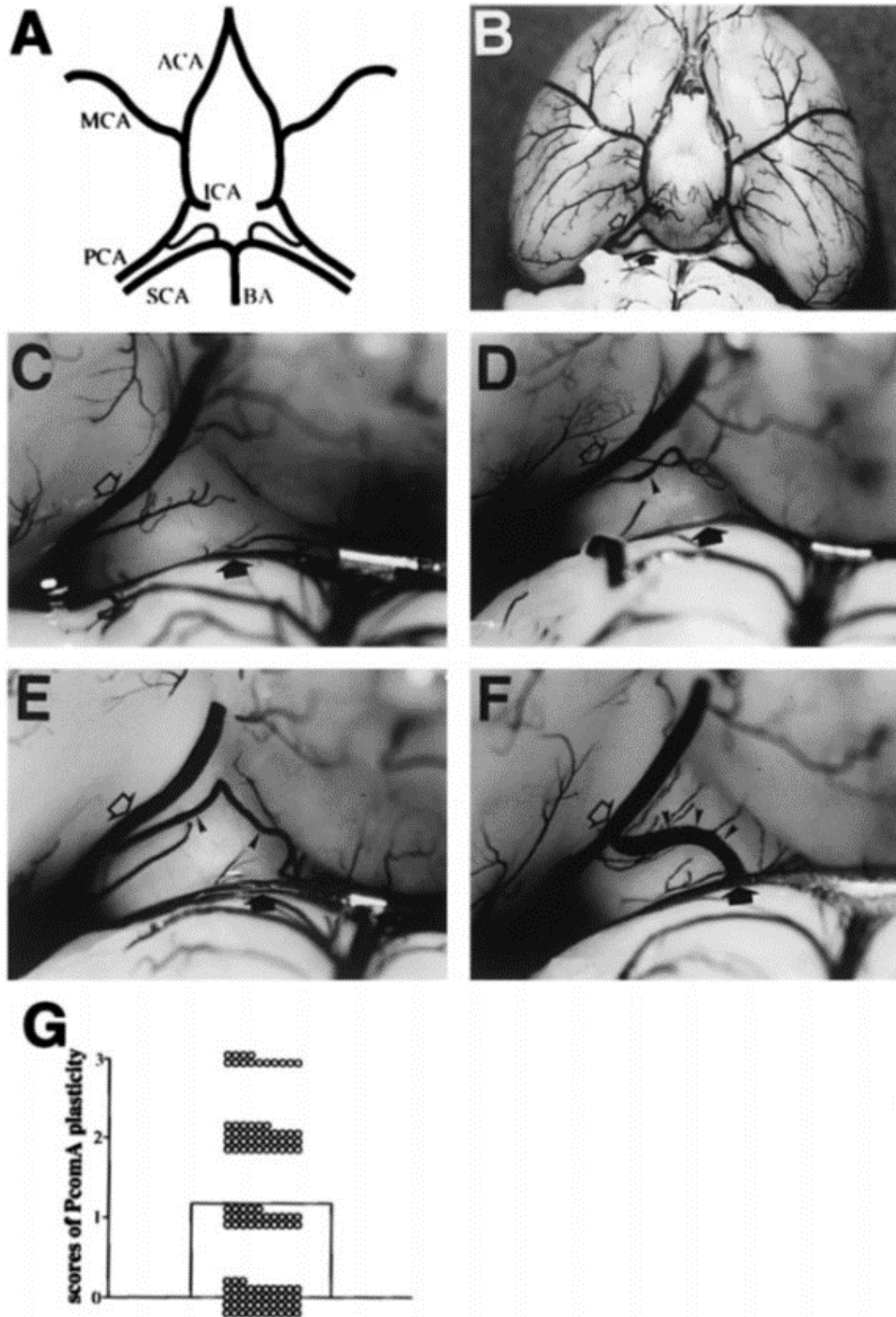


Figure 12: Illustration of the PCOM scoring system after ink perfusion from Murakami et al. ² Image A and B show the circle of Willis in mice both schematically (A) and imaged with a dissection microscope after ink perfusion (B). The morphology of the posterior communicating arteries was graded 0 (depicted in image C), 1 (D), 2 (E) or 3 (F); Image G shows the distribution of PCOM scores in CD-1 mice.

2.7 GRAVIMETRIC ASSESSMENT OF BRAIN EDEMA

To determine the extent of edema in CYLD WT and CYLD ^{-/-}, we performed a separate series of MCA occlusion, with brain removal occurring again after 24 hours.

The assessment of hemispheric swelling was performed as described in our previous publications⁹². Immediately after brain removal, the olfactory bulbs and the cerebellum were separated from the cortex using a mouse brain slicer matrix (Zivic Instruments, Pittsburgh, USA), and both hemispheres were split. We placed the hemispheres into separate, airtight glass vials, which we weighed beforehand using a high precision scale. The glass vials were then weighed again; we calculated the wet weight of a hemisphere by subtracting the glass vial's empty weight. The glass vials were manipulated exclusively with cotton gloves to avoid measurement errors due to fingerprints on the glass.

Afterwards, we opened the glass vials and placed them in a heating chamber; we dried the hemispheres at 110 °C for 24 hours. We determined the hemispheres' dry weight by measuring the glass vials' weight again and subtracting the corresponding empty weight. We obtain the percentage hemispheric water content using the following formula:

$$\text{Hemispheric water content (\%)} = \left(\frac{\text{wet weight} - \text{dry weight}}{\text{wet weight}} \right) * 100\%$$

2.8 WESTERN BLOT ANALYSIS

Brains were removed 24 hours after MCA occlusion. We removed the brain as previously described and, using a brain matrix, retrieved a 2 mm thick coronal section, starting at a distance of 2 mm from the end of the olfactory bulbs. The section was then cut horizontally in half using a razor blade; the lower half was discarded. The cortex was separated from the corpus callosum and the striatum. Then, the cortex from the ipsilateral and the contralateral side were collected in two separate Eppendorf tubes, which were weighed beforehand. We weighed the tubes again, subtracted the empty weight to determine total tissue weight, and added ten times the tissue weight in RIPA buffer (radioimmunoprecipitation buffer: 150 mmol/l NaCl; 50 mM Tris; 1% Triton X-100; 0,5% sodium deoxycholate; 0.1% sodium dodecyl sulfate) in order to achieve equal protein concentration in all tubes.

We performed tissue homogenization by adding metal beads to the tubes and putting them in a shaker. Afterwards, we removed the beads and centrifuged the tubes. We transferred the supernatant into new Eppendorf tubes and stored it at -80 °C.

We determined the protein concentrations of our samples according to Bradford using a bicinchoninic acid (BCA) protein assay kit (Thermo Fisher Scientific, Waltham, Massachusetts, USA). We added 2 µl of each sample to 150 µl of RIPA buffer and 150 µl of BCA reagent mix, and measured the samples' light absorption at 560 nm. We calculated protein concentrations by comparing the light absorption of our samples to a standard curve established with wells containing known concentrations of bovine serum albumin (BSA). Then, we added additional RIPA buffer to each sample until we reached a protein concentration of 1.75 mg/ml.

For protein denaturation, we mixed 15 µl of our samples with 5 µl of 4x-Laemmli-buffer (200 mmol/l Tris, 8% sodium dodecyl sulfate, 0.4% bromophenol blue, 40% glycerol), heated them at 95 °C for 5 minutes and centrifuged them at 16000 g for 10 minutes at 4 °C.

For the gel electrophoresis, we used precast gels (BioRad Laboratories, Hercules, California, USA). We filled the sample pockets with 20 µl of each sample solution and western blot protein ladder to a single pocket. Electrophoresis was performed at 80V for 10 minutes, then at 150V for 30 minutes.

Protein was transferred from the gel on a PVDF membrane using wet transfer by applying an electric potential of 100V for 1h. The presence of protein on the membrane was subsequently verified using Ponceau S staining. The membranes were stored in tris-buffered saline (TBS).

The membranes were subsequently blocked with 5% milk powder in TBS-Tween 20 (TBS-T) for 30 minutes. For detection of CYLD, we incubated the membrane with a goat anti-CYLD antibody (LS/B4323, LSBio, Seattle, WA, USA) in blocking solution overnight at 4 °C. To account for differences in protein concentration, we also incubated the membrane with a β-actin antibody (1:1000) (Sigma-Aldrich, St. Louis, MO, USA). After washing, the membrane subsequently incubated with an anti-goat horseradish peroxidase (HRP) secondary antibody (1:10 000) (Agilent Technologies, Santa Clara, CA, USA). For imaging, we added ECL western blotting substrate (Thermo Fisher Scientific, Waltham, Massachusetts, USA); the final image was taken under UV light.

We calculated the western blot band intensity using using ImageJ⁹³. We adjusted the band intensity for total sample protein concentration by expressing band intensity as a fraction of β -actin band intensity.

2.9 IMMUNOFLUORESCENCE

For immunofluorescence on vibratome sections, Mice were transcardially perfused with saline followed by 4% PFA. Brains were extracted as described above and kept for 24h in the same fixative. The brains were briefly rinsed in PBS and embedded in 4% low melting temperature agarose. Serial sections (50 μ m) were cut with the vibratome and collected with a brush in 12 well plate containing PBS. The free-floating sections were kept at 4°C until further processing. The immunostaining was performed by incubating the sections in blocking solution (10% goat serum in tris buffer saline (TBS) containing 0.3% triton x100) for 3 hours. This step blocks unspecific binding and improves tissue permeabilization with the presence of triton in the buffer. The sections were then incubated overnight at 4°C in primary rabbit anti-CYLD (1:100) (ab137524, Abcam, Cambridge, MA, USA) and mouse anti-Tuj-1 (1:500) (A488-435L, BioLegend, San Diego, CA, USA). After washing (3 times 15 min in TBS-Triton 0.03%), the sections were incubated for 3 hours in secondary, fluorescent Alexa Fluor 555 anti-mouse and Alexa Fluor 488 anti-rabbit antibodies (1:500) (Jackson ImmunoResearch, West Grove, PA, USA) and DAPI (1:20000) (Invitrogen, Waltham, MA, USA). After washing, the sections were mounted on glass slides, coverslipped with an aqueous mounting medium (FluoroMount, Thermo Fisher Scientific) and sealed with nail polish.

For immunofluorescence with fresh frozen sections, cryosections from the infarct volume measurement groups were used. The sections were dried at room temperature for 30 minutes, fixed in 4% PFA for 10 min and permeabilized in a mix of 67% ethanol and 33% acetic acid for 5 minutes. After washing, the sections were blocked for 30 min with 5% BSA, incubated for 2 h in a primary Mouse Anti-NeuN-Antibody (1:500) and for 1 h in a secondary, fluorescent Alexa 555 Anti-Mouse antibody (1:500). For the terminal deoxynucleotidyl transferase dUTP nick end labeling (TUNEL) sections, staining was performed with a detection kit (ApopTag, Merck Millipore, Burlington, MA, USA) according to the manufacturer's instructions. The sections were then incubated with DAPI (1:10000) for 5 min, mounted with an aqueous mounting medium (FluoroMount) and sealed with nail polish.

Imaging was done at 20x magnification with a Leica confocal microscope (SP5), choosing the most lateral part of the cortex as the region of interest. For the TUNEL stainings, 3 sections per mouse were imaged, located at a distance of 3, 4.5 and 6 mm from the olfactory bulb. Cell counting was done manually with ImageJ and its Cell Counter plugin. Cells were divided into 2 categories, depending on whether they were predominantly NeuN- or TUNEL-positive. For each image, the total number of surviving neurons was then divided by the total number of counted cells. For each mouse, the average ratio of all 3 sections was calculated, and the ratios for CYLD^{-/-} and CYLD WT animals were compared.

2.10 STATISTICAL ANALYSIS

Statistical analysis was performed using a statistical software package (SigmaPlot 13, Systat Software GmbH, Erkrath, Germany). Quantitative data was expressed as mean \pm standard deviation. Differences between two groups were tested using the Mann-Whitney U test. Differences between survival distributions were tested using the log-rank test. P values below 0.05 were considered significant.

3 RESULTS

3.1 CYLD DELETION IN THE BRAIN

In order to address the role of CYLD in the brain, we first wanted to verify the knockout of our CYLD^{-/-} mice. We confirmed the CYLD deletion in the brain by polymerase chain reaction (PCR) and by western blotting (Fig. 13).

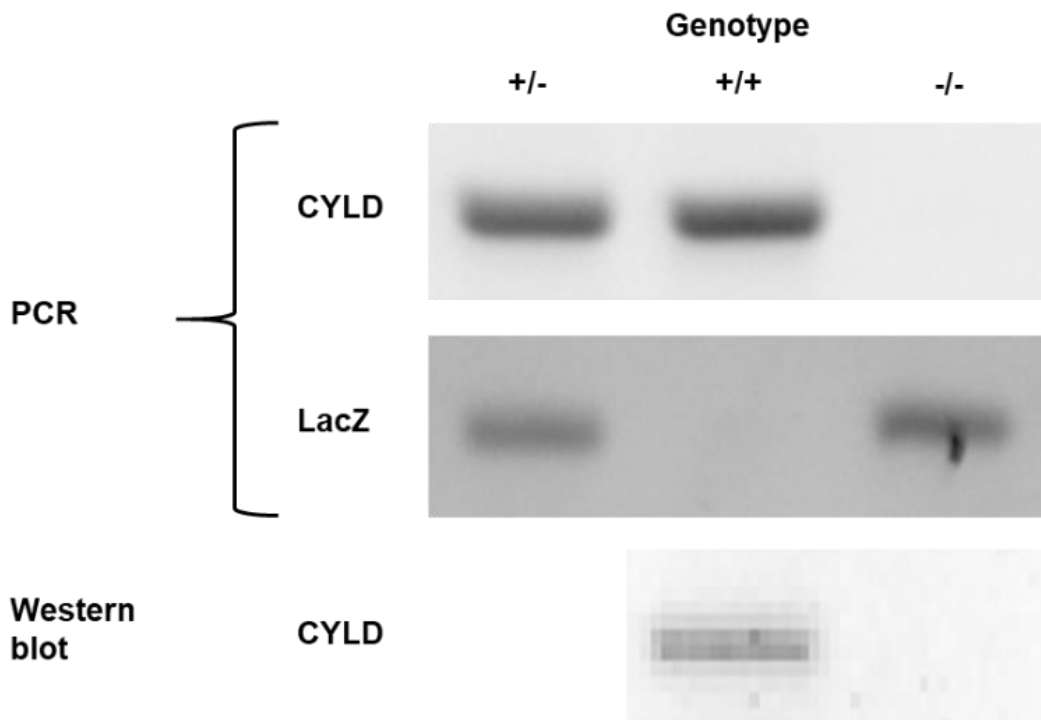


Figure 13: CYLD knockout validation by PCR and western blotting.

In the PCR, amplification of the CYLD gene yielded no band for the CYLD^{-/-} animals, but resulted in a band for the C57BL/6 animals. At the same time, amplification of the LacZ reporter gene confirmed the knockout by showing a band for the CYLD^{-/-} animals but none for the C57BL/6 mice.

3.2 PATTERN OF EXPRESSION OF CYLD IN THE BRAIN

As the CYLD^{-/-} mice possess a LacZ reporter gene instead of CYLD, we used the LacZ expression to determine the cellular expression of CYLD in the brain of CYLD^{-/-} mice. We performed immunohistochemistry for the LacZ reporter with a β -Galactosidase staining and combined it with a DAPI and a NeuN staining in brain sections of CYLD^{-/-} animals. We also performed CYLD stainings in brain sections of C57BL/6 animals (Fig. 14).

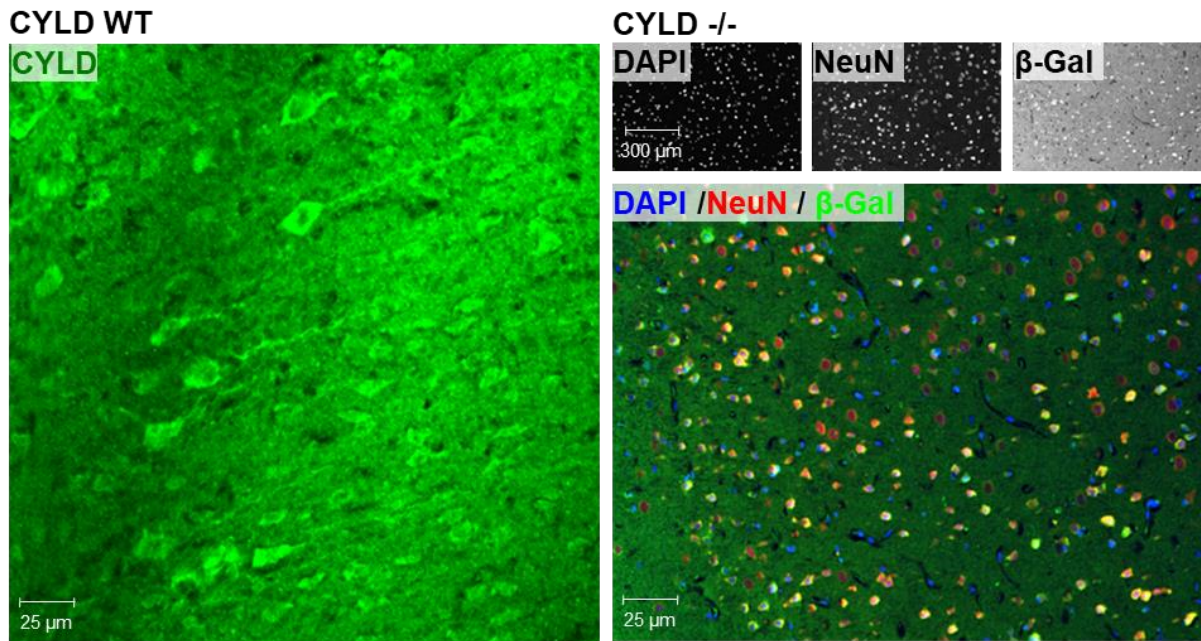


Figure 14: CYLD is deleted in neurons in CYLD knockout mice. Patterns of CYLD expression in 10 μ m fresh frozen mouse brain sections. The left side shows a high magnification CYLD immunofluorescence staining in green in a C57Bl6 mouse. The right side shows the staining of a CYLD $-/-$ mouse cortex section with DAPI (blue), NeuN (red) and β -Galactosidase (green) as well as the individual stainings of the same section in black and white.

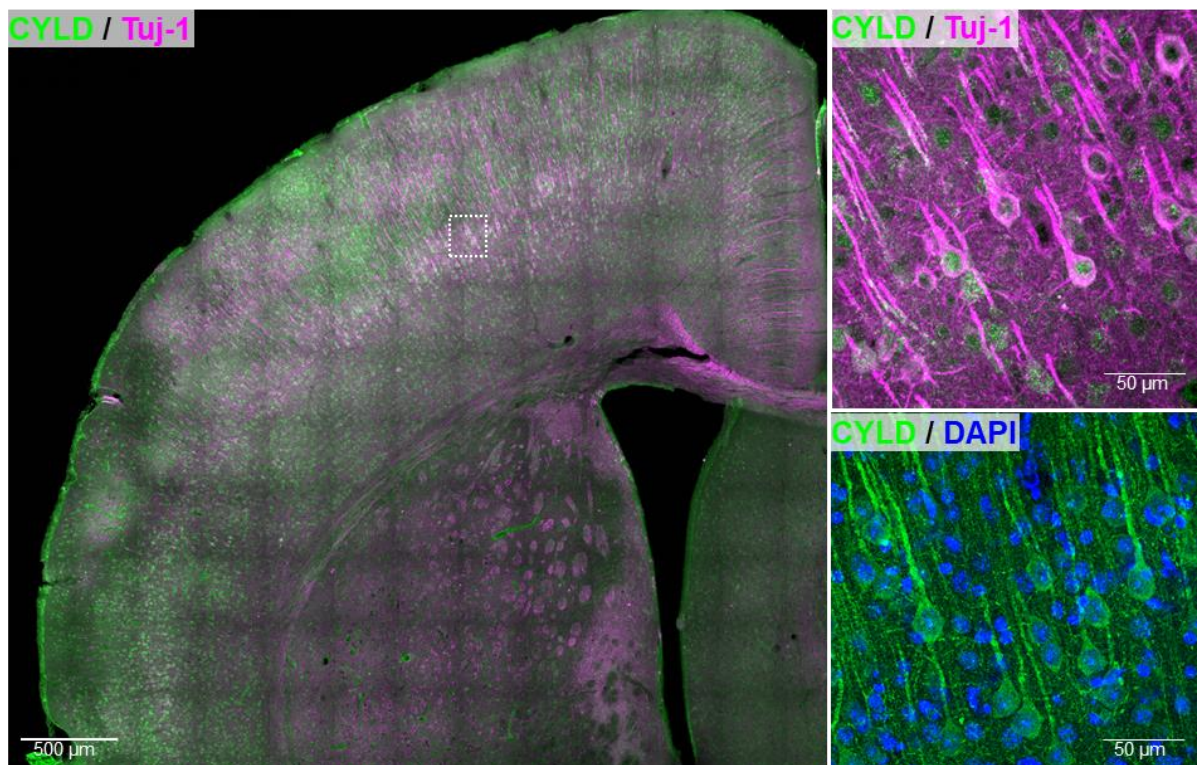


Figure 15: CYLD expression in the brain. CYLD protein in naïve mouse brain is expressed in majority in neurons as depicted by the double staining CYLD and the neuronal marker *tuj-1* (labels cell body, dendrites and axons). At subcellular level CYLD is present in the cell bodies as well as in the apical dendrites. However the level in the dendrites seems to be variable from neuron to neuron.

We found that the LacZ reporter is expressed in various regions of the brain spanning from the olfactory bulbs to the cerebellum. It was mostly expressed in many, but not all NeuN-positive neurons. CYLD was mainly identified in neurons. In terms of distribution, the staining was most intense in the perinuclear cell body, but in some neurons, we also found intense dendritical staining. As a result, we performed immunofluorescence stainings with CYLD, DAPI and the Neuron-specific class III beta-tubulin Tuj 1, which labels neuronal cell bodies, dendrites and axons (Fig. 15).

This staining confirmed CYLD's colocalization with Tuj-1 and thus presence in neuronal cell bodies and dendrites, but also revealed a faint colocalization with nuclear DAPI.

3.3 EXPRESSION OF CYLD AFTER CEREBRAL ISCHEMIA

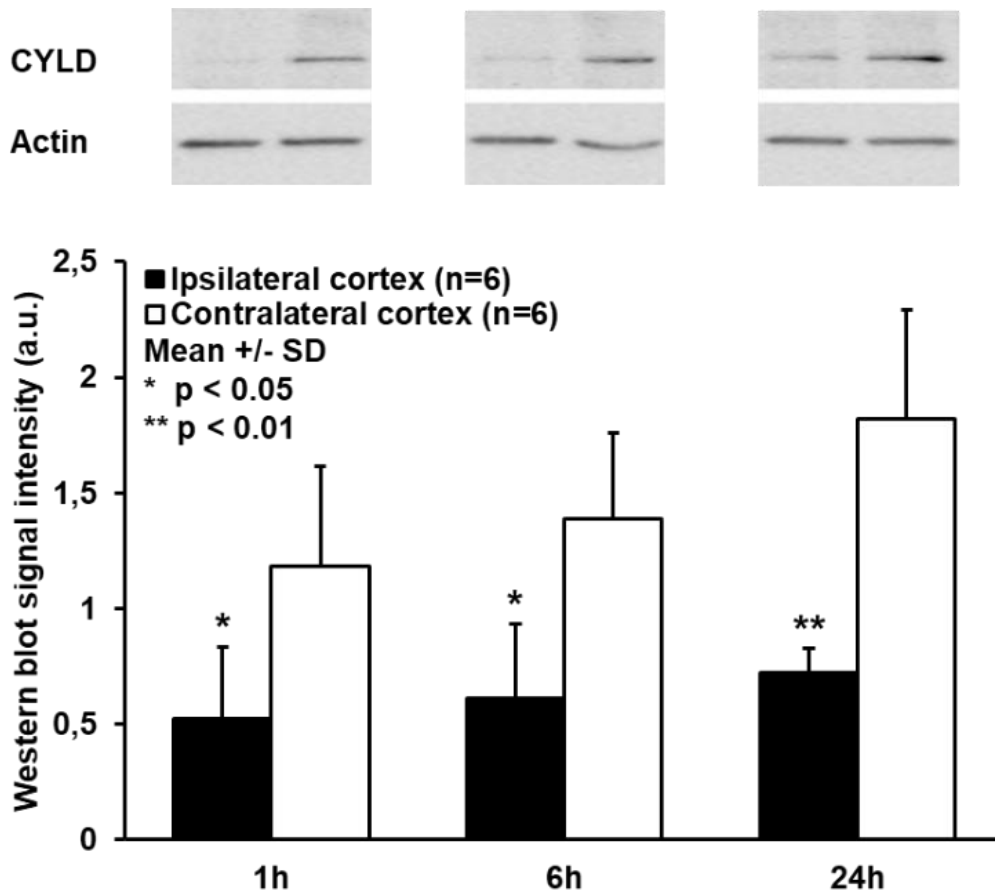


Figure 16: Effect of cerebral ischemia on CYLD protein expression in the brain. Comparison of CYLD expression after MCA occlusion in the ipsi- and contralateral hemispheres of C57Bl6 mice.

To evaluate the changes of CYLD expression upon cerebral ischemia, we induced cerebral ischemia in C57BL/6 male mice using the transient filament middle cerebral occlusion model. We determined the levels of CYLD protein in cortical extracts from the peri-infarct region by western blot at 1h, 6h and 24 h after reperfusion (Fig. 16).

Our western blot analysis showed a significant decrease of CYLD-expression in the penumbra on the ipsilateral side in comparison to matching region in the contralateral side at the three studied times after reperfusion (0.5 ± 0.3 , 1.2 ± 0.4 in penumbra vs contralateral, $P=0.026$ after 1h; 0.6 ± 0.3 , 1.4 ± 0.4 in penumbra vs contralateral, $P=0.015$ after 6h; 0.7 ± 0.1 , 1.8 ± 0.5 in penumbra vs contralateral, $P=0.002$ after 24h).

3.4 MCAO STANDARDIZATION

In order to assess the reproducibility of our MCA occlusion model, we performed a preliminary series with C57BL/6 animals (Fig. 17).

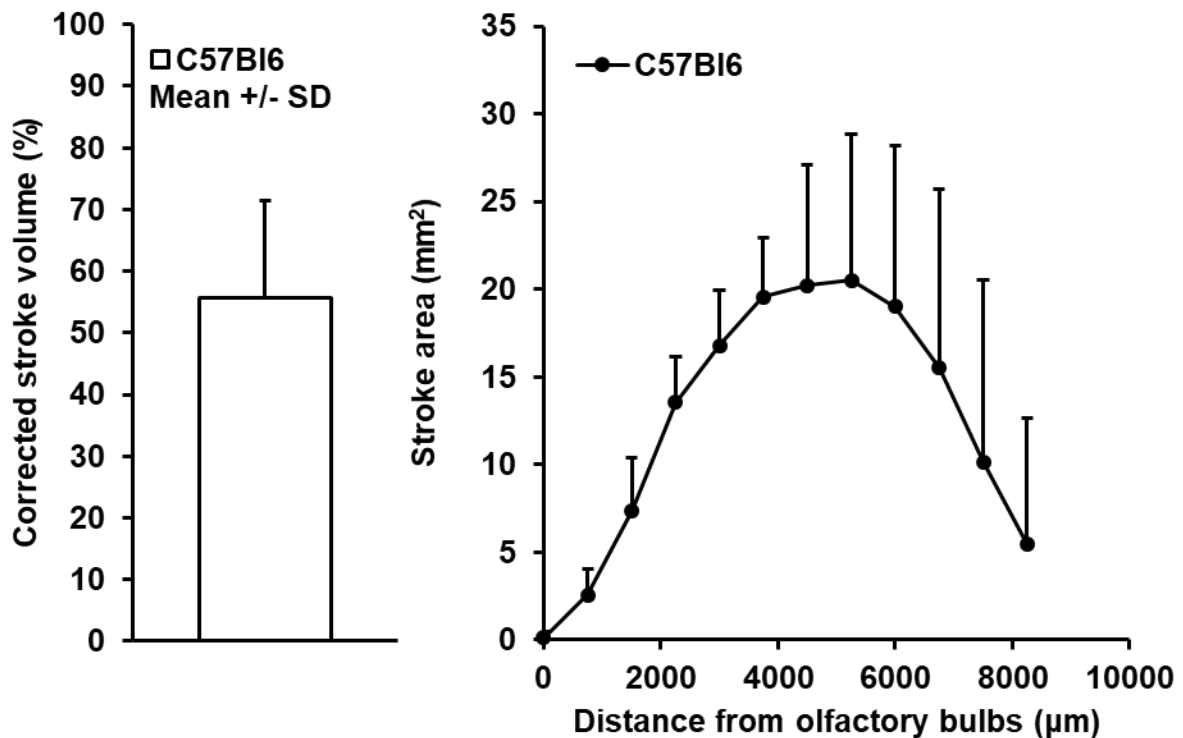


Figure 17: Corrected stroke volume and stroke area by depth for C57BL/6 mice. Due to partial reduction of posterior cerebral artery perfusion during MCA occlusion, a large variation in stroke area is found in the posterior parts of the brain.

We found that C57BL/6 animals had an average corrected stroke volume of 43% with a standard deviation of 16%. In terms of distribution, we have found that the stroke is largest in the central part of the brain, which is considered to be mostly MCA territory. We have found a larger standard deviation in the posterior parts of the brain, representing a larger variation in lesion size due to the variability of the vasculature feeding the PCA territory.

3.5 CEREBRAL VASCULATURE ANALYSIS

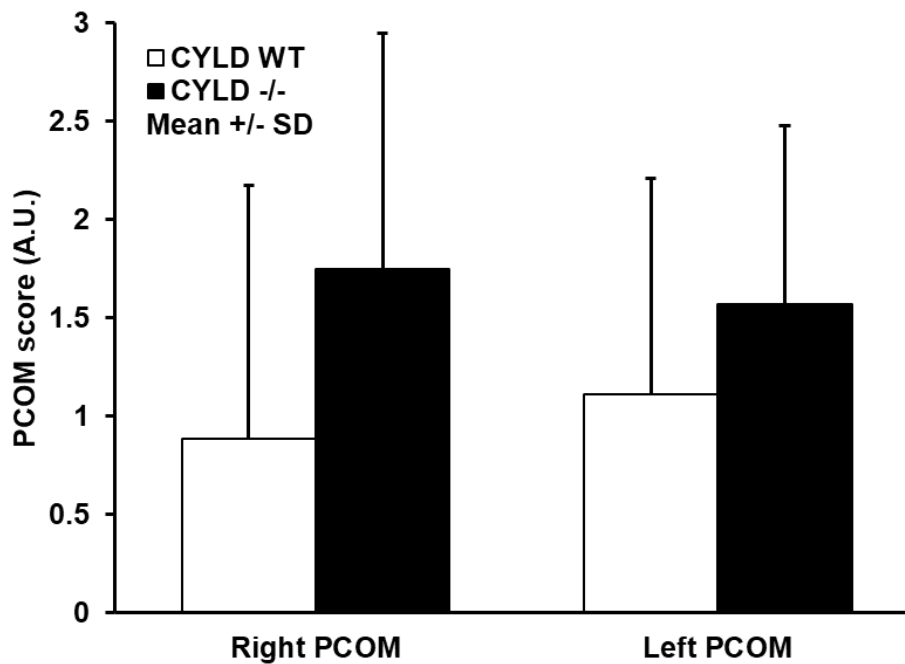


Figure 18: PCOM anatomical analysis in CYLD knockout mice. To exclude anatomic differences that could cause different susceptibility to middle cerebral artery occlusion in CYLD wild-type and knock-out mice, we analyzed the presence of collaterals in the PCOM using ink perfusion.

Cerebral vasculature analysis showed no difference in PCOM size on the left (1.6 ± 0.9 , 1.1 ± 1.1 in CYLD^{-/-} vs WT). However, there was a slight, non-significant trend in CYLD animals towards larger PCOM arteries on the right size (1.8 ± 1.2 , 0.9 ± 1.3 in CYLD^{-/-} vs WT, $P=0.18$) (Fig. 18).

3.6 INFARCT VOLUME AND BRAIN EDEMA AFTER FOCAL CEREBRAL ISCHEMIA IN CYLD ^{-/-}

To determine the contribution of CYLD to cerebral ischemia we evaluated the effect of CYLD deletion on the infarct volume and edema formation at 24 hours after MCAo (Fig. 19).

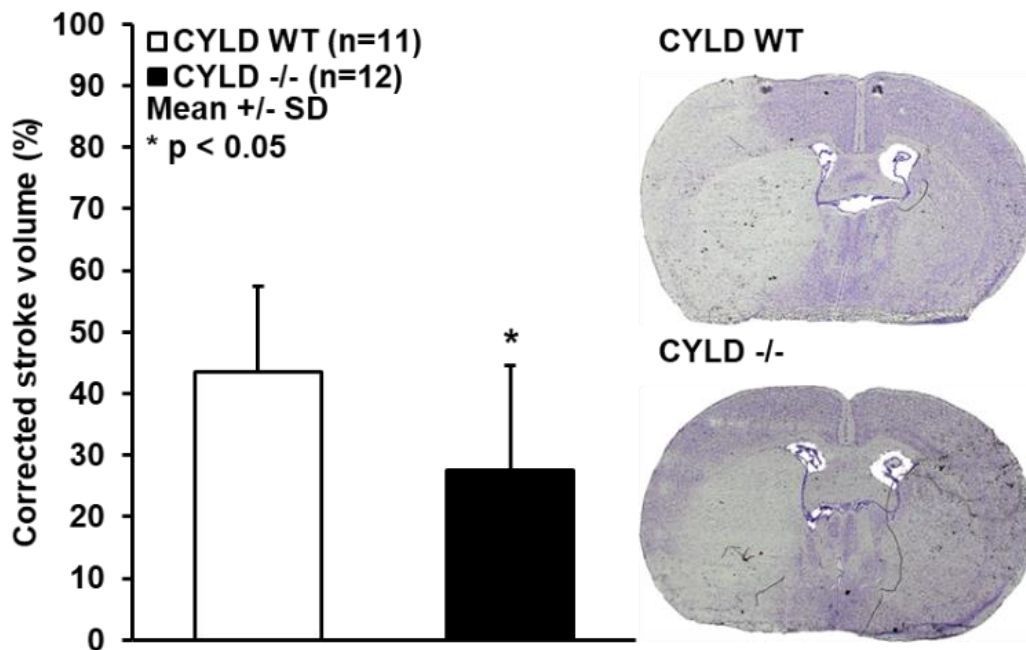


Figure 19: Effect of CYLD deletion on infarct volume at 24h after MCA occlusion. Stroke volume of CYLD WT and ^{-/-} mice after MCA occlusion. The stroke volume has been adjusted for brain size and hemispheric swelling.

We found a significant difference in lesion volume in CYLD ^{-/-} animals compared to their WT littermates. After accounting for hemispheric swelling, lesion volumes of CYLD ^{-/-} were on average 37% smaller than those in the control group (28 ± 17 %, 44 ± 14 % in CYLD ^{-/-} vs WT, P=0.021).

We could not find a significant difference in edema formation between the CYLD^{-/-} and CYLD WT groups, suggesting a neuroprotective mechanism in the reduction of infarct size (Fig. 20). Edema in CYLD^{-/-} was on average 4.2 % compared to the contralateral hemisphere versus 3.6% in WT animals (4.2 ± 0.8 %, 3.6 ± 1.2 % in CYLD^{-/-} vs WT).

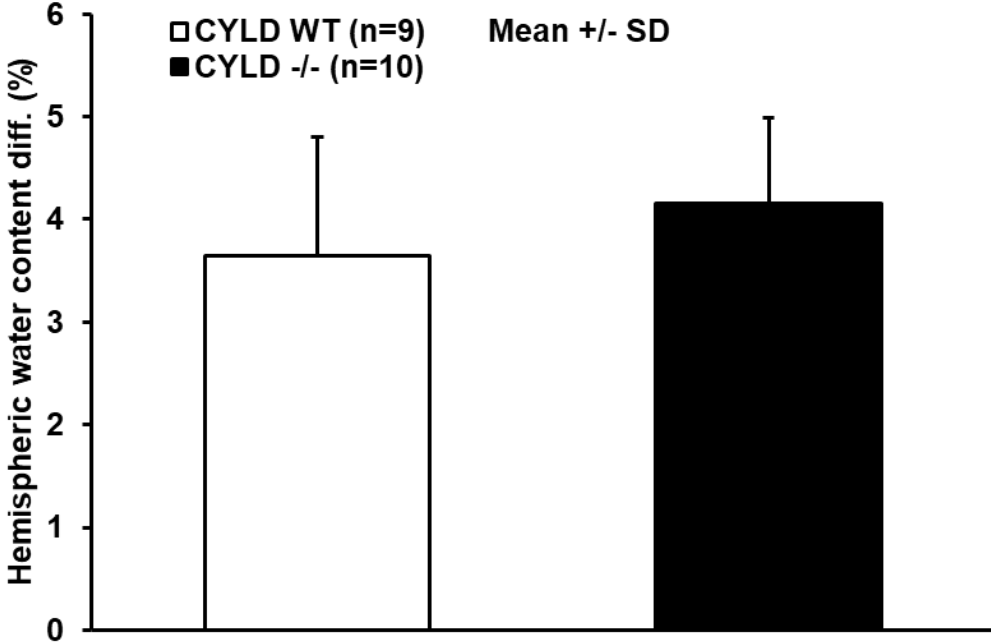


Figure 20: Effect of CYLD deletion on edema formation at 24h after MCA occlusion. Comparison of the difference in water content due to postischemic edema of both hemispheres after MCA occlusion in CYLD WT and -/- mice.

3.7 FUNCTIONAL OUTCOME AFTER FOCAL CEREBRAL ISCHEMIA IN CYLD ^{-/-}

To determine whether the neuroprotective effect of CYLD after MCAo is associated with functional improvement, we evaluated the behavior of the animals at 1h and 24h after reperfusion. The modified Bederson score was used to evaluate global neurological function (Fig. 21).

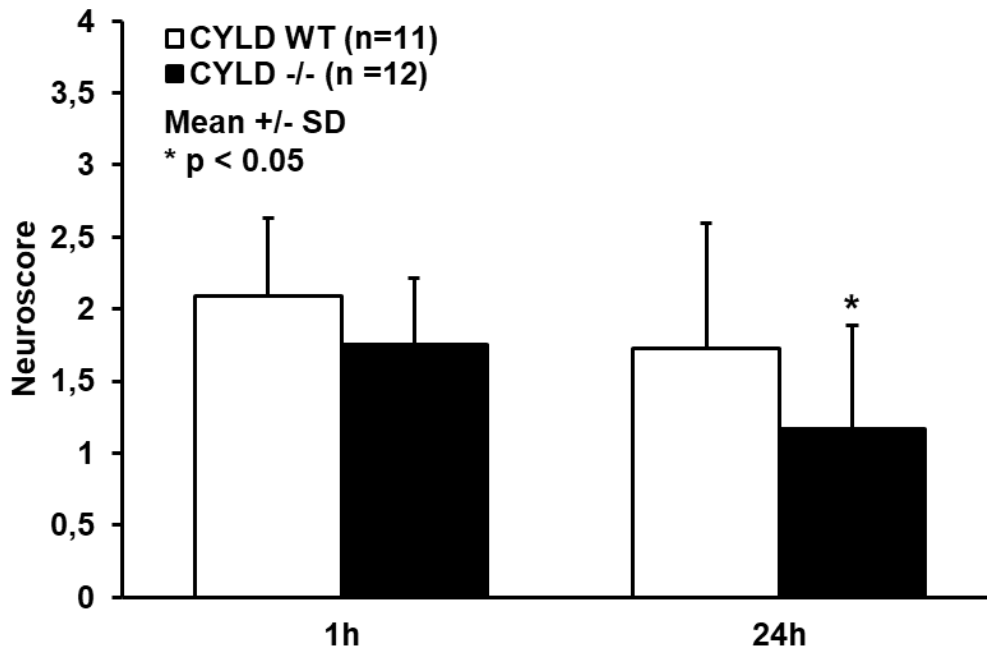


Figure 21: Effect of CYLD deletion on neuroscore. Modified Bederson score of CYLD WT and ^{-/-} mice before filament removal 1 hour after MCA occlusion and before sacrifice 24 hours after MCA occlusion.

There was no significant difference in functional outcome between the groups at 1h after ischemia. However, we observed a significant improvement in the neurological score at 24h after reperfusion in the CYLD ^{-/-} animals in comparison to their control littermates (1.2 ± 0.7, 1.7 ± 0.5 in CYLD ^{-/-} vs WT, P=0.05); indicating that CYLD deletion promoted functional recovery after cerebral ischemia.

3.8 NEURONAL CELL DEATH AFTER FOCAL CEREBRAL ISCHEMIA IN CYLD ^{-/-}

To understand whether the reduction of infarct volume is correlated to neuroprotection, we evaluated the neuronal cell death by co-staining with TUNEL to depict cells having undergone programmed cell death and the neuronal specific marker NeuN. We counted the number of TUNEL and NeuN positive cells in the cortical peri-infarct area at 24 hours after reperfusion (Fig. 22, Fig. 23).

We found a significant decrease in the ratio of TUNEL to NeuN and TUNEL positive cells in CYLD^{-/-} animals compared to the WT littermates, indicating that CYLD deletion promoted neuronal survival (74 ± 14 , 40 ± 13 in CYLD^{-/-} vs WT, $P=0.01$).

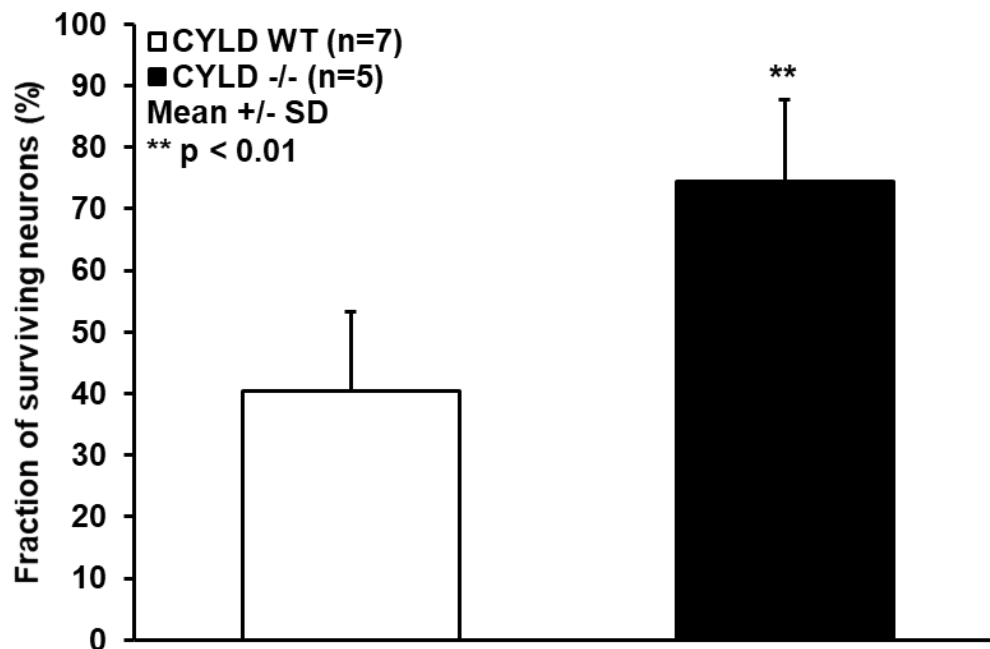


Figure 22: Effect of CYLD deletion on neuronal survival at 24h after MCA occlusion. Ratio of NeuN-positive to the sum of NeuN- and TUNEL-positive cells in 10 μ m fresh frozen cortical sections of CYLD WT and CYLD^{-/-} mice.

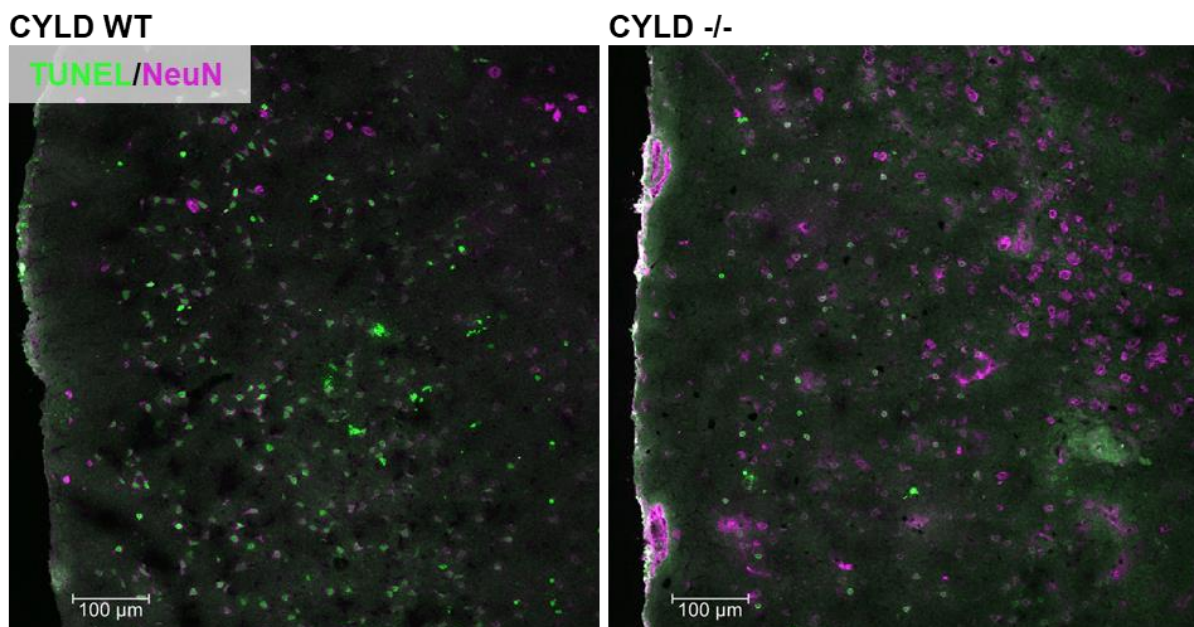


Figure 23: Cell death by TUNEL labeling in CYLD knockout mice 24 hours after MCA occlusion. Comparison of 10 μ m fresh frozen cortical sections of CYLD WT and CYLD^{-/-} mice. Green staining: Terminal deoxynucleotidyl transferase dUTP nick end labeling (TUNEL). Violet staining: NeuN. TUNEL detects the DNA fragmentation resulting from apoptotic programmed cell death, NeuN is used as a biomarker for living neurons.

3.9 SURVIVAL AFTER CONDITIONAL GPX4 KNOCKOUT IN CYLD ^{-/-}

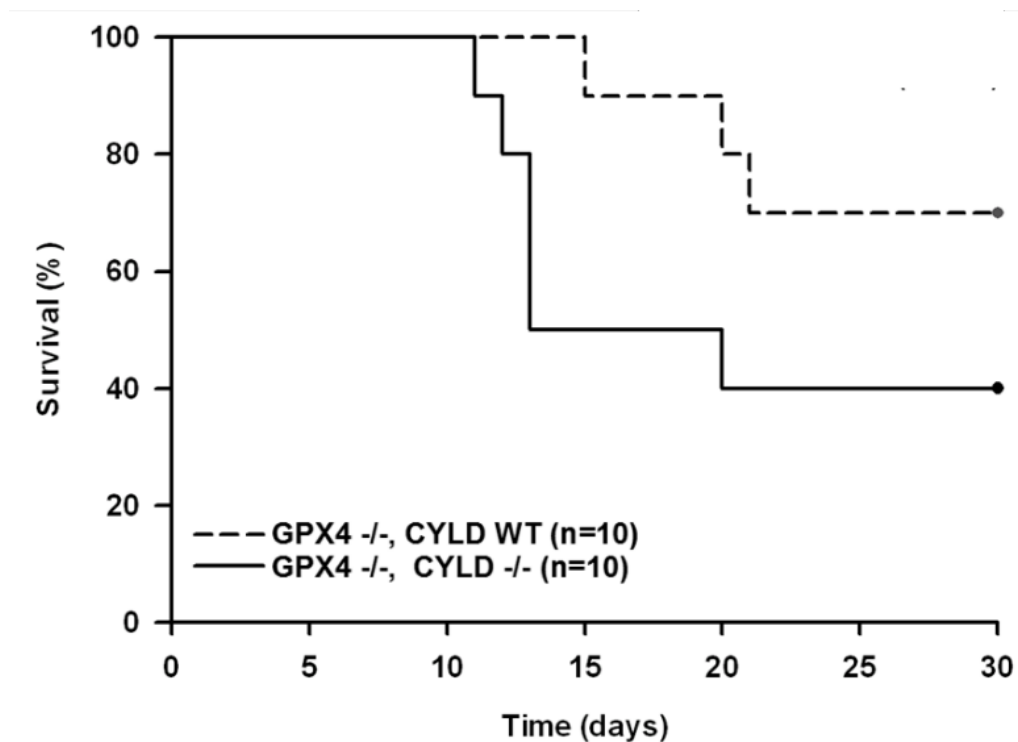


Figure 24: Effect of knocking out CYLD gene on survival of transgenic mice where GPX4 is specifically deleted in neurons at adult age.

In order to evaluate the relationship between CYLD and ferroptosis, we induced a neuronal GPX4 knockout in both CYLD ^{-/-} and WT mice and studied its effect on survival (Fig. 24). We could not find a significant difference in survival between both groups (27 ± 2 d, 20 ± 3 d in CYLD ^{-/-} vs WT).

3.10 FUNCTIONAL OUTCOME AFTER CONDITIONAL GPX4 KNOCKOUT IN CYLD^{-/-}

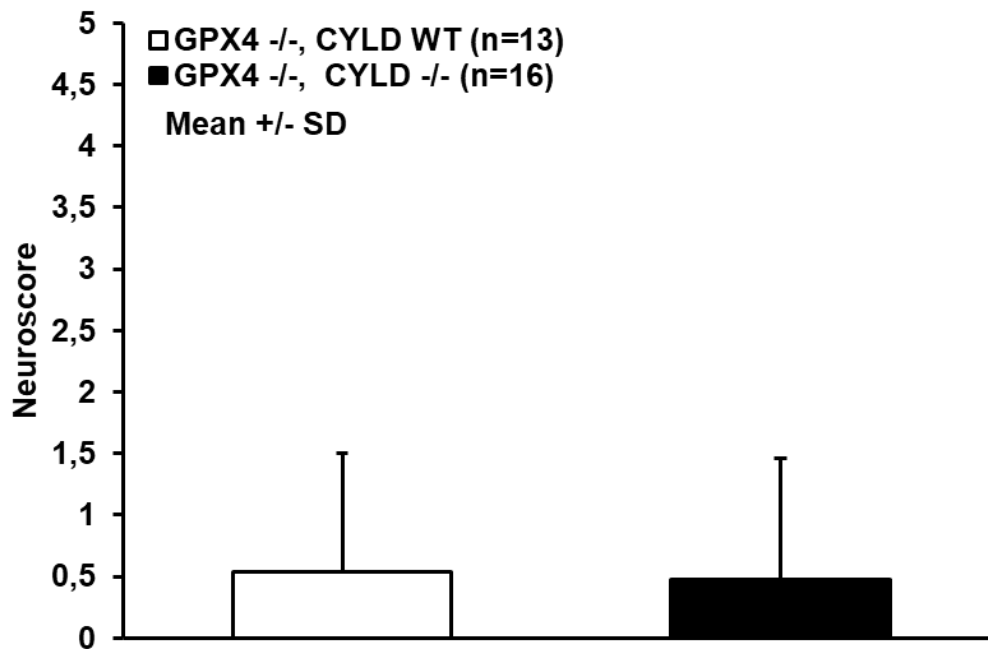


Figure 25: Effect of CYLD knockout on the extended neuroscore of GPX4 conditional knockout 7 days after the first tamoxifen injection causing the specific deletion of GPX4 in neurons.

In addition to survival, we also looked at functional outcome in CYLD^{-/-} and WT mice after induction of a neuronal GPX4 knockout (Fig. 25). All mice started out at a score of 0. At 1 week, we could not see a significant difference in functional outcome between both groups (0.47 ± 0.99 , 0.54 ± 0.97 in CYLD^{-/-} vs WT)

4 DISCUSSION

4.1 DISCUSSION OF THE METHODS

4.1.1 Animal models in stroke research

Animal studies are an indispensable tool for scientific studies. Unlike *in vitro* experiments, animal experiments allow manipulation and investigation of living, functional tissue. This is especially important in neuroscientific research, where not only single cell metabolism, but also cell structure and connections to other cells contribute to organ function. Compared to studies in humans, animal experiments can be performed with genetically almost identical individuals and few confounding factors such as preexisting medical conditions. Regarding stroke research, patients in clinical studies usually show large variations in size, localization and cause of stroke, whereas the controlled conditions of the experimental stroke models lead to comparable lesions, thus enhancing standardizability and reproducibility.

We have chosen to use mice for our current study. Mice are routinely used in various stroke models and have already been used as experimental animals in previous studies of our group⁹⁴⁻⁹⁶. Mice have multiple advantages over other animals. They can be bred quickly due to their short generation time of about 10 weeks. Due to their small body size, they also require very little space and food. Moreover, inbreeding has led to significant genetic homogeneity among mice of a certain strain. In addition, the ethical acceptance of the use of rodents in medical research compared to larger animals is significantly higher. Another important advantage of mice over other animals is their fully deciphered genome and the large number of available genetic modifications, including the CYLD and conditional GPX4 knockouts we used. In comparison, knockouts in rats have only been possible since 2003⁹⁷, and as a result, the number of available knockout models is much smaller. Compared to pharmacological inhibition, gene knockouts do not suffer from issues like partial agonism, differences in drug elimination or affinity to substances other than the target molecule, and are thus better suited to investigate the function of specific genes.

In our research, we exclusively used mice with a C57BL/6 background. We chose the C57BL/6 strain because it is one of the most widely used mouse strains in research⁹⁸. To minimize the possibility of differences in genetic background between knockout and

control animals, we exclusively used wildtype littermates in the control group. All animals used in our experiments were approximately 8 weeks old. At this age, animals are large enough to allow an intraluminal thread in the carotid artery to advance through the skull base and induce MCA occlusion, but too young for age-related diseases to significantly impact our results.

Even though mice have many important advantages in stroke research compared to other animals, they also have some disadvantages. Their small size for example complicates surgical procedures, although this problem can be partially mitigated through the use of microsurgical techniques and appropriately sized instruments⁹⁹. Another disadvantage is that mice do not possess a gyrencephalic brain, which reduces the transferability of some results to humans. While gene knockouts are an important research tool, they may not always have the desired effect on the phenotype. Knockouts can be compensated for through genetic redundancy (when a similar gene exists at a different location in the genome) or functional redundancy (other pathways compensate for the knockout).

Aside from the disadvantages that are inherent to mouse models, the results found in animal studies in general often cannot be reproduced in humans. Although there is an abundance of substances that have shown neuroprotection in animals, none of those who have made it to clinical trials have proven effective in humans^{100,101}. This translational gap is not exclusive to neuroprotection research; studies in cancer research have also shown that only a third of highly cited animal research is tested in humans, and out of these, only 8% succeed in phase I trials¹⁰².

There are several explanations for this translational gap. Much of it may be due to genetic differences. Although mice and other mammals share many similarities with humans, their physiology is distinct enough to show different outcomes given the same treatment. Some diseases such as cancer and Alzheimer's disease feature a complex underlying molecular pathogenesis that makes it difficult to adequately model these diseases in animals. However, this does not apply to ischemia, which by definition originates from restriction of blood supply, and can be modeled relatively easily. The existing models also show a high correlation in terms of clinical course and treatment effect when compared to the corresponding human diseases: For instance, studies investigating the effect of alteplase in the mouse thrombin injection stroke model have found that the animals show a similar therapeutic window to humans, and that alteplase

also shows a deleterious effect beyond the therapeutic window¹⁰³. Others have called into question the methodological quality of animal studies in neuroprotection research¹⁰⁴; this has led to the publication of the STAIR (Stroke Therapy Academic Industry Roundtable) recommendations in 1999 that intend to improve the quality of preclinical studies investigating acute stroke research¹⁰⁵.

In the end, while the potential shortcomings of animal studies need to be taken into consideration, there is no adequate substitute for animal models in stroke research, and we consider them to be crucial for our investigations.

4.1.2 The use of filament MCA occlusion in mice as a stroke model

Due to the large differences in individual location, size and symptoms, stroke is a highly variable condition. Research on stroke pathophysiology and possible therapies thus necessitated the development of stroke models in which most of these parameters were standardized.

In general, a distinction is made between global and focal ischemia models¹⁰⁶. Global ischemia models, like the two-vessel-¹⁰⁷, three-vessel-¹⁰⁸ and four-vessel-occlusion models¹⁰⁹, require occlusion of both carotid arteries and, depending on the model, also occlusion of either the basilar artery or both vertebral arteries. These models are usually used to simulate cardiac arrest; as a result, they are not relevant to our study and will not be described in detail. Focal ischemia models are more appropriate for the simulation of human strokes. Most focal ischemia models induce an ischemic lesion in the MCA territory, which is the region most frequently affected by ischemia in humans¹¹⁰⁻¹¹². The most common of these models are described below.

In the craniectomy model, the parotid gland, temporal muscle and skull overlying the MCA are surgically dissected or removed, the dura is opened and the MCA is subsequently either permanently occluded by electrocoagulation and transection¹¹³, or temporarily occluded with a surgical clip¹¹³ or a hook¹¹⁴. This model shows good reproducibility in stroke size and deficits; its main disadvantage is the opening of the neurocranium and dura mater, which requires certain surgical skills to perform, can lead to brain and vessel injury as well as inflammation, and affects intracranial pressure, cerebrospinal fluid (CSF) circulation and blood-brain barrier function.

The photothrombosis model relies on the injection of photoactive dyes like rose Bengal or erythrosin B and the subsequent irradiation of the intact skull^{115,116}. This leads to intravascular reactive oxygen species accumulation, focal endothelial damage, platelet aggregation and ultimately vessel occlusion within the irradiated area. The procedure is minimally invasive and the resulting lesion is highly reproducible; however, the resulting lesion is usually small and there is very little ischemic penumbra.

Focal ischemia can also be induced through application of the vasoconstrictive substance Endothelin-1 either directly onto the MCA, onto the cortical surface or through intracerebral injection. The resulting vasoconstriction leads to stroke. Unfortunately, Endothelin-1 also directly influences astrocytes and neurons, for example through facilitation of axonal sprouting, and can thus influence the results depending on the experiment¹¹⁷.

Embolitic strokes can be simulated through the intraarterial injection of either micro- or microspheres¹¹⁸ or thromboembolic clots¹¹⁹. Among these, the thromboembolic clot MCAo is particularly interesting, as it is the model that is pathophysiologically closest to embolic stroke and is thus ideally suited for thrombolysis research. However, due to differences in vessel occlusion and spontaneous lysis, this technique suffers from a large variability in stroke size and location, and thus low reproducibility¹²⁰.

Lastly, the most commonly used method to induce thromboembolic strokes is the filament MCA occlusion model¹²¹⁻¹²³, which we already described in detail in the methods section. To summarize the procedure, this model uses a specially prepared (in our case silicon-coated) thread that is advanced through the internal carotid artery into the circle of Willis until it occludes the ipsilateral middle cerebral artery. This method does not require craniectomy and thus avoids CSF leakage, blood-brain barrier disruption or direct damage to the brain. The resulting stroke size is reproducible and, as the thread can be removed at any time to cause reperfusion, can be influenced through duration of ischemia. Filament MCAo also has the advantage of modeling transient ischemia, as the MCA is usually only occluded for a limited amount of time until the filament is retracted again. Disadvantages of this model are possible vessel damage during filament insertion, such as endothelial damage in the internal carotid artery or intracranial perforation of the vessel wall and subsequent subarachnoid hemorrhage. The model also lacks a direct ischemia and reperfusion control; however, this can be compensated for through monitoring of the regional

cerebral blood flow. The lesion volume in filament MCAo is also relatively large compared to the average stroke in humans, which only affects about 4.5 to 14% of the hemisphere¹²¹, thereby reducing the transferability of results to humans.

Out of all these models, we chose the filament MCA occlusion model. We wanted an animal model with focal ischemia that leads to reproducible stroke volumes. We also preferred models with transient ischemia, as transient ischemia more accurately reflects the situation in human stroke: spontaneous recanalization occurs in the majority of ischemic stroke patients within 12 hours after onset of symptoms¹²⁴. Transient ischemia also usually leads to a larger penumbra due to the reperfusion of tissue at risk. Out of the listed models, only filament MCAo and certain variations of the craniectomy model fit these criteria. In our view, the benefits of ischemia without the possible complications of a craniectomy far outweigh the drawbacks of filament MCAo.

In the filament MCA occlusion model, duration of ischemia is an important factor, as it leads to large variations in infarct volume and neurological deficits¹²⁵. In rats, animals with 30 minutes of ischemia had mild motor deficits and recovered completely within one week. Animals with 60 minutes of ischemia initially had severe deficits and improved significantly, but no longer reached baseline levels. Animals with permanent ischemia showed the most severe failures and did not recover. The number of dead neurons doubled with prolongation of the ischemia time from 30 to 60 minutes and increased sixfold with permanent ischemia. A similar observation was made by Memezawa et al., who demonstrated a development of selective neuronal necrosis in the striatum at 15 minutes of ischemia, a complete necrosis in the striatum and selective neuronal necrosis in the neocortex after 30 minutes, and further cortical necrosis after 60 minutes¹²⁶. The cortical necrosis continued to increase with prolonged ischemia until it reached its maximum at 3 hours of ischemia.

As our aim was to investigate neuronal survival within the penumbra, we wanted the largest possible penumbra for our model. As a result, we chose an intermediate ischemic duration of 60 minutes, resulting in a moderately sized ischemic core with a large surrounding penumbra.

4.1.3 Measurement of cortical blood flow

One of the disadvantages of the filament MCA occlusion model is its lack of direct ischemia control. In order to verify cerebral ischemia, cerebral blood flow in the region of interest needs to be monitored.

One of the most accurate methods to determine CBF is by analyzing the distribution of previously injected, labeled substances, such as ^{14}C -iodoantipyrine^{127,128} or fluorescent microspheres¹²⁹. Unfortunately, these methods require the analysis of histological sections to determine blood flow, thus making them unsuitable for intraoperative CBF monitoring.

Non-invasive CBF measurement is feasible using modern imaging techniques such as nuclear magnetic resonance (MRI) imaging¹³⁰, computed tomography (CT)¹³¹ or positron emission tomography (PET)¹³². However, the required devices are very expensive and not widely available; in addition, these techniques only provide a snapshot of cerebral perfusion instead of a continuous measurement. In our case, it would also be technically difficult to perform imaging during surgery for perfusion control.

Laser Doppler Fluxmetry (LDF) is a non-invasive technique that allows that allows continuous measurement of microcirculatory blood flow¹³³. The calculation of flow velocity is based on the Doppler shift a beam of laser light undergoes when reflected by passing erythrocytes.

Overall, the LDF is appropriate for the study because it is non-invasive and allows for a simple and immediate evaluation of local perfusion to verify ischemia. Compared with autoradiography and labeled microspheres, LDF also shows a good correlation with actual blood flow^{134,135}. Disadvantages in CBF measurement with LDF compared other methods are its limited measurement depth of up to 400 μm ¹³⁶, allowing it to only measure CBF at the brain's surface, and the fact that LDF provides only relative, not absolute CBF values. However, for our purposes, penetration depth does not matter, and ischemia is determined through a large drop in CBF, so that absolute values are not needed.

4.1.4 Survey of neurological status

In many experimental stroke studies, stroke volume is the primary endpoint. However, from a clinical point of view, the functional outcome is the most relevant parameter.

Therefore, different scores have been designed to measure neurological outcome in animal stroke models.

We used a modified version of a score initially published by Bederson et al.⁹⁰. Some of the grading criteria were modified to allow for more reliable scoring, as we used different animals and a different stroke model than in the original study. We checked for discrete neurological deficits by testing whisker sensitivity and the mice's righting reflex. In addition, we extended the score to include "leaning to the contralateral side at rest" and "no spontaneous movement" to characterize severe neurological impairment.

The other neuroscore used in our study represents a modified version of a score developed by Katz et al.¹³⁷. This score was originally developed for the neurological evaluation of rats in global ischemia but is also used in subarachnoid hemorrhage models. It tests a selection of reliable criteria for the general neurological assessment of animals, including awareness, respiration, cranial nerve functions, motor functions, sensory functions and coordination. While we omitted some of the less reliable criteria of the original score, including olfactory and vision testing, we extended the scoring for motor, coordination and vestibular deficits by letting mice walk over beams of different widths and hold on to rods with different shapes, and we added scoring for the mouse's general condition.

4.1.5 The role of anesthesia in experimental stroke models

For surgical anesthesia, we had to choose between several different anesthetic agents and routes of administration. Anesthetics are usually administered either via injection or via inhalation. Frequently used injection narcotics in rodents are a combination of ketamine and xylazine, or midazolam, medetomidine and fentanyl (MMF)^{138,139}. In rats and mice, these are often administered via intraperitoneal injection; this means that the level of sedation cannot be easily modified intraoperatively, and that sedation will only slowly wear off after surgery unless reversal agents are used.

Compared to injection narcotics, inhalational anesthetics such as halothane or isoflurane can be controlled simply through an increase or reduction in inhalation concentration, and at the end of the procedure, stopping the anesthetic will lead to a rapid awakening of the animal. As a result, we chose inhalation sedation for our experiments. We opted for anesthesia with isoflurane because it is relatively

inexpensive and widely used in animal research, including experimental stroke research.

Unfortunately, many narcotics, including isoflurane, were found to have neuroprotective effects in various studies. Administration of Isoflurane led to reduced stroke sizes and improved functional outcome in rats in both MCA occlusion and global ischemia models. Several molecular mechanisms have been proposed to explain this effect, including a decrease of sympathetic activity¹⁴⁰, an increase in p38 mitogen-activated protein kinases¹⁴¹, inhibition of the mitochondrial permeability transition pore¹⁴², and inhibition of ubiquitin-conjugated protein aggregation¹⁴³. There is also some evidence that isoflurane counteracts the formation of free radicals and the accumulation of intracellular calcium¹⁴⁴. Isoflurane has also been shown to reduce neuronal apoptosis, brain edema¹⁴⁵ and blood-brain barrier disruption¹⁴⁶. Other volatile anesthetics, such as sevoflurane, desflurane, enflurane and halothane, have similar effects¹⁴⁷.

Usage of a neuroprotective anesthetic could also influence the results of our study. We have tried to minimize the effect of anesthesia on focal cerebral ischemia by keeping the duration of surgery below 30 minutes and by interrupting anesthesia during ischemia. Even if our results were influenced by the neuroprotective effects of anesthesia, both knockout and control animals have been exposed to the same anesthetic procedure, meaning that any difference in outcome should be independent of anesthesia.

4.1.6 Hypothermia in experimental stroke models

The neuroprotective effects of hypothermia are widely known and are for example used in heart surgery to minimize the brain damage during an artificially induced cardiac arrest. Various authors have shown that both intraoperative¹⁴⁸⁻¹⁵⁰ and postoperative¹⁵¹ hypothermia have a highly neuroprotective effect in cerebral ischemia models. In case of transient MCA occlusion, previous publications have shown an influence of body temperature on infarct volume in both rats¹⁵² and mice¹⁵³.

It is known that during and after anesthesia, mice exhibit a disturbed temperature autoregulation⁹⁹. Without temperature control, anesthetized mice show a reduction in body temperature by several degrees within minutes. It has also been shown that, in

the first few hours after focal cerebral ischemia, animals experience hypothermia due to hypothalamic damage, which, again, has an effect on outcome^{153,154}.

In order to minimize the effects of body temperature on stroke size, we kept the body temperature at a constant 37 °C during surgery with an auto-regulating heating pad controlled through a rectal temperature probe. After surgery, we kept the mice in an incubator at 32 °C.

4.1.7 Determination of hemispheric swelling and edema

Hemispheric swelling due to edema can increase the apparent volume of ischemic tissue, without necessarily being accompanied by an increase in cell death. Although stroke volume correction can account for hemispheric swelling, it is not a good proxy for edema formation in stroke. As we have shown in earlier work from our group, measurement of brain water content can give more reliable results¹⁵⁵.

The gravimetric assessment of brain water content is a well-established method to quantify cerebral edema. It has been used for edema measurement in ischemia at least since 1961¹⁵⁶; since then, it has been used in numerous publications by our group and others¹⁵⁷⁻¹⁵⁹. Based on the results of Slivka et al., we chose to measure brain water content at its peak 24 hours after cerebral ischemia in order to maximize any measurable differences in edema formation¹⁵⁸.

4.1.8 Cerebral vasculature analysis

MCA occlusion was found to be susceptible to variations in vasculature in previous studies. Barone et al. have compared MCA occlusion in different mouse strains and found that BABL/C mice show significantly larger stroke sizes than BDF mice after MCA occlusion. However, they also found that BABL/C mice lack a posterior communicating artery more frequently than BDF mice. They concluded that differences in sensitivity to cerebral ischemia may at least in part be related to PCOM anatomy¹⁶⁰.

To account for these variations, Murakami et al developed a scoring system for quantification of PCOM size after carbon black ink perfusion². The scoring system was originally developed for use in a global ischemia model, but given the importance of PCOM collateralization in MCA occlusion, its results are also relevant to the latter.

Although Baron et al. compared different mouse strains in their study, it is possible that similar variations in vasculature are caused by single gene knockouts such as the CYLD knockout. As we suspected CYLD to influence stroke volume mainly through its

involvement in programmed cell death, we had to exclude a vascular cause. Cerebral vasculature analysis through ink perfusion and PCOM scoring is well suited for this and was already used by our group for analysis in prior publications⁸⁹.

4.1.9 The TUNEL assay

TUNEL stands for terminal deoxynucleotidyl transferase dUTP nick end labeling. The method works by using the terminal deoxynucleotidyl transferase enzyme to add labeled (in our case fluorescent) deoxyuridine triphosphate (dUTP) molecules to the ends of DNA fragments. TUNEL is essentially a marker for DNA fragmentation, as more fragmented DNA will have a larger number of free DNA ends that will be labeled, which in return will increase signal intensity.

TUNEL was originally developed as a method for detection of apoptotic programmed cell death, based on previous in vitro studies which suggested that DNA fragmentation is characteristic for programmed cell death¹⁶¹. However, initial publications demonstrated that the method was unable to differentiate between programmed cell death and necrosis¹⁶². Subsequent changes in protocol have since led to an improvement of TUNEL specificity for apoptotic cells^{163,164}. As a result TUNEL can nowadays be considered a reliable tool for labeling of apoptotic cells.

Recent publications have revealed that TUNEL not only labels apoptotic cells, but also cells dying through the RIP3- (and subsequently CYLD-) mediated necroptotic pathway^{165,166}. We concluded that the TUNEL assay is an appropriate method for labeling CYLD-mediated cell death.

4.2 DISCUSSION OF THE RESULTS

4.2.1 CYLD is expressed in neurons in the mouse brain

Large, proteome-wide analyses have found that CYLD is expressed in most tissues across the human body to various degrees, with low tissue specificity¹⁶⁷. CYLD expression in the brain was verified in 2000 using RT-PCR⁵⁵ and in 2008 with western blotting¹⁶⁸. Feng et al. were the first to perform CYLD immunofluorescence staining and subsequent confocal microscopy on murine neuronal cell cultures¹⁶⁹. They found that in neurons, CYLD is mostly located within the nucleus; their stainings show only faint CYLD immunofluorescence in the cytoplasm.

To the best of our knowledge, we show for the first time the cellular and subcellular distribution of CYLD in actual brain tissue. Our immunofluorescence shows that CYLD is mainly found in neuronal cell bodies and dendrites, and to a lesser extent within the nucleus of these neurons. These results do not match the findings previously published by Feng et al. However, instead of cell cultures, we used fresh frozen and vibratome sections of mouse brains; it is possible that the discrepancy is due to differences in neuronal environment and function. This theory is partially supported by the findings of Dosemeci et al., who examined the presence of CYLD in postsynaptic densities using electron microscopy and western blotting¹⁷⁰. They showed that CYLD accumulates in the postsynaptic densities upon depolarization, suggesting that subcellular location of CYLD can change depending on neuronal activity.

The high expression of CYLD in neurons compared to other brain cells indicates that CYLD has an important role in neurons. In previous publications, CYLD has already been shown to be involved in necroptotic cell death of hippocampal neurons¹⁷¹. In addition, accumulation of CYLD in postsynaptic densities and its activity as a K63-deubiquitinating enzyme suggest a role in protein turnover¹⁷² and neuronal plasticity¹⁷³. Interestingly, we have found that not all NeuN-positive neurons show strong CYLD expression. As of now, we can only hypothesize why CYLD is not evenly expressed across neurons. Thein et al. show that CYLD frequently colocalizes with CaMKII under different conditions in the postsynaptic density and that CaMKII-mediated phosphorylation enhances CYLD's deubiquitinase activity, implying that CYLD's function within the postsynaptic density depends on CaMKII¹⁷². CaMKII itself shows a heterogeneous distribution across neurons⁸⁴, and it is possible that strong CYLD expression is linked to CaMKII expression.

4.2.2 Cerebral ischemia decreases CYLD expression in the brain

In our western blot analysis, we found a significant decrease of CYLD within the penumbra as soon as 1 hour after the onset of ischemia, which persists at least up to 24 hours. To our knowledge, such a decrease in CYLD expression within the brain after stroke has not been described before. This finding is unlikely to be related to general protein degradation in the necrotic tissue as actin levels remained stable in the penumbra samples in comparison to the contralateral side. The decrease in CYLD could be related to hypoxia within the penumbra: Previous studies found that CYLD mRNA transcription is inhibited by Snail¹⁷⁴ and Hes1¹⁷⁵, both of which are upregulated

by hypoxia^{176,177}. CYLD expression was also shown to be significantly reduced in hypoxic regions of human glioblastoma¹⁷⁸. A decrease in CYLD could be part of a neuronal survival mechanism: Under hypoxic stress, CYLD downregulation could reduce programmed cell death in order to minimize damage. However, not all publications are consistent with our findings. Feng et al. performed oxygen and glucose deprivation in neuronal cell cultures¹⁶⁹. They report that CYLD expression gradually increases within 8 hours after oxygen-glucose deprivation (OGD) and declines afterwards. Like the differences in subcellular CYLD expression we discussed earlier, these discrepancies could be due to differences between the in vitro OGD model and in vivo pathophysiology.

4.2.3 CYLD deletion is neuroprotective after cerebral ischemia

Our results show for the first time that CYLD^{-/-} mice who have had transient middle cerebral artery occlusion have significantly smaller infarcts than their CYLD WT littermates. So far, no prior publications have demonstrated protection against ischemia in CYLD-deficient brain tissue. Recently, Ganjam et al. showed that CYLD knockout mice develop smaller lesions after traumatic brain injury compared to their wildtype littermates¹⁷⁹. Although etiologies are very different, the pathophysiology of ischemic stroke and traumatic brain injury show certain similarities: they can lead to either programmed cell death or necrosis¹⁸⁰⁻¹⁸², and they are both associated with excitotoxicity, reduced cerebral blood flow and accumulation of reactive oxygen species^{182,183}. This means that CYLD could protect against traumatic brain injury and ischemic stroke through a shared mechanism. Other studies have also shown that blocking other enzymes in the necroptosis cascade leads to reduced stroke size in animals. The most prominent example is necrostatin 1, whose neuroprotective properties were described alongside the necroptotic cascade itself. Necrostatin 1 is thought to inhibit RIP1 and thus lead to a reduction of necroptotic cell death during stroke⁶⁵. It has subsequently also been found to be neuroprotective in traumatic brain injury¹⁸⁴. Moquin et al. show that CYLD directly deubiquitinates RIP1 and thus facilitates necroptosis¹⁸⁵. As CYLD and Necrostatin 1 share the same target, CYLD deficiency could cause neuroprotection through its interference with the necroptosis pathway. However, necrostatin 1 has also been described as an inhibitor of the indoleamine-2,3-dioxygenase IDO, which has been shown to have immunomodulatory properties¹⁸⁶. As inflammation is also involved in postischemic brain damage, the

neuroprotective effect of necrostatin 1 may also be mediated through immunosuppression.

Although the extent of ischemic lesions is strongly associated with functional outcome, separate measurements of neurological deficits are still relevant, as in a clinical setting, neurological outcome and not stroke size will ultimately determine the patient's quality of life.

The decrease in infarct size in CYLD knockout mice is accompanied by better recovery of function, although both groups show a slight improvement in the modified Bederson score from 1 hour to 24 hours after ischemia. This type of recovery is consistent with previous studies; Xianji et al. for example performed transient MCA occlusion in mice with neurological scoring at the same time points and found similar results¹⁸⁷. Early neurological improvement could be due to reperfusion and functional recovery of the penumbra. We did not find a significant difference 1 hour after onset of transient focal cerebral ischemia suggesting that both CYLD knockout and wildtype littermates were similarly impacted by the occlusion, However, CYLD knockout mice showed a significant functional improvement compared to their wildtype littermates after 24 hours. This result is in line with our expectations, as we assumed that a CYLD knockout would lead to better neuronal survival within the penumbra, which should result in faster functional recovery after reperfusion.

4.2.4 CYLD deletion does not influence edema formation after cerebral ischemia

In order to minimize the influence of cerebral edema on lesion volume, we corrected the stroke volume for any hemispheric swelling as described earlier. Our results suggest that the reduction of stroke size we saw is not due to cerebral edema. To confirm our findings, we decided to evaluate the effect of a CYLD knockout on edema formation in stroke separately using a more precise gravimetric measurement of the hemispheric water content after MCA occlusion.

We did not observe a significant difference in edema formation between CYLD^{-/-} and WT animals. Although this confirms that the reduced stroke size in CYLD^{-/-} must be due to reduced tissue infarction, this is a surprising result, as one would assume that any reduction of stroke size also leads to less edema formation through a reduction of cellular and blood-brain barrier injury. Our results are also not consistent with the

findings of Ganjam et al., who describe a significant reduction in edema formation after traumatic brain injury¹⁷⁹. Although traumatic brain injury and ischemic stroke are completely different pathologies, they both lead to hemispheric swelling through a combination of cytotoxic and vasogenic edema^{188,189}. Our result highlights the discrepancy in the mechanisms behind edema formation between both pathologies. We conclude that while CYLD deficiency reduced edema induced by traumatic brain injury, this deficiency has no influence on edema formation after stroke.

4.2.5 Neuroprotective effect of CYLD deletion does not result from vascular collateralization

Another possible influence on stroke size is the amount of vascular collateralization, which we investigated using ink perfusion. We found that CYLD knockout animals show no difference in PCOM size on the left side compared to wildtype animals, but we found a slight trend towards a larger PCOM on the right side in the knockout mice. CYLD may influence vasculature as it also plays a role in angiogenesis. It has been shown that CYLD inactivation in tumor cells enhances their angiogenic potential^{190,191}. Curiously, other publications have shown that CYLD mediates endothelial cell migration and that its knockdown thus impairs angiogenesis¹⁹².

Based on our results, collateralization should not have affected stroke size in our experiments, especially as MCA occlusion was always performed on the left side, where we clearly could not find any difference in vasculature between groups. Previous data also suggests that vascular collateralization is not related to the neuroprotective effect of a CYLD knockout, as it could not explain CYLD's neuroprotective effect in traumatic brain injury where collateralization is irrelevant⁸⁰. In addition, improved vascularization would not explain the functional improvement in CYLD knockout animals over time, as better collateralization should lead to significantly better motor function right after the onset of ischemia instead of a delayed effect after 24 hours.

4.2.6 Neuroprotective effect of CYLD deletion through decrease in necroptosis but not lipid peroxidation

Our further investigation using TUNEL and NeuN labeling revealed that a CYLD knockout increases the ratio of NeuN to TUNEL positive cells in periinfarct tissue after MCAo, suggesting a decrease in neuronal cell death in the penumbra. Although NeuN and TUNEL represent two different labeling techniques that are essentially independent, there was almost no overlap. NeuN seems to label only living neurons,

while TUNEL seems to be highly specific for cells undergoing programmed cell death. Our finding suggests that CYLD-deficient neurons may indeed be more resistant to ischemic stress, and that the higher neuronal survival may indeed be secondary to a reduction of programmed cell death, potentially necroptosis.

To understand whether CYLD signaling pathways would as well contribute to ferroptosis and lipid peroxidation we generated conditional neuronal GPX4 knockout in the CYLD knockout background and followed the neurological function and the survival rate. This investigation was initiated following preliminary *in vitro* study showing that knockdown of CYLD using siRNA leads to reduced lipid peroxidation in a glutamate-induced neuronal cell death model⁸⁰, suggesting a relationship between CYLD and lipid oxidation in neuronal cell death. Deletion of GPX4 is lethal and when induced in adult mice the deletion leads to massive neuronal loss through increased lipid peroxidation⁸⁷, which could potentially be prevented by CYLD deletion and thereby promote survival.

However, our double knockout model showed no significant differences in outcome between CYLD^{-/-} and CYLD WT mice after conditional neuronal GPX4 knockout. Both experienced a similar decline of neurological function and a similar survival. As a result, we think it is unlikely that CYLD plays a major role in the ferroptosis pathway. It is much more likely that CYLD's role in programmed cell death is indeed mediated mostly through the necroptosis pathway. However, one has to consider the limitations inherent to our chosen model. We have induced a GPX4 knockout exclusively in neurons expressing CaMKII and investigated if the presence of an additional CYLD knockout led to any changes in survival or neurological function. By doing this, we are already assuming that GPX4 plays a central role in ferroptosis – which, according to the literature, it does⁷⁶. In addition, we have no way to determine the role of CYLD in ferroptosis in cells other than CaMKII-positive neurons, as the Cre-recombinase was only expressed in these cells. And while we can say with a high level of confidence that CYLD does not play a central role in GPX4-mediated ferroptosis, we cannot exclude that CYLD is involved in ferroptosis, but its role is not crucial enough to stop neurodegeneration and death from a GPX4 knockout.

4.3 CLINICAL RELEVANCE OF THE FINDINGS

So far, we have presented evidence that deletion of CYLD reduces stroke size and improves functional outcome in mice, and that it leads to increased neuronal survival in the penumbra zone after stroke. We conclude that CYLD may be an appropriate target for neuroprotective therapy after stroke. However, the question remains how this knowledge can be applied in a clinical setting. In order to gather our data, we used a gene knockout, which at the moment is neither feasible nor desirable in humans. Thus we need to find another way to block CYLD after stroke. In order to make use of these findings, further research will be necessary in order to create a CYLD inhibitor. General deubiquitinase inhibitors like PR-619¹⁹³, cyclopentone prostaglandins¹⁹⁴ or chalcone compounds¹⁹⁵ may work in vitro, but their effect may be too unspecific and their side effects too severe to be clinically useful, especially as many of these substances are actually believed to trigger apoptosis and cell death through inhibition of deubiquitinases other than CYLD¹⁹⁶. As a result, any clinical application would probably require a CYLD-specific inhibitor. Such an inhibitor would also need to be able to penetrate the blood-brain-barrier in order to have any neuroprotective effect. One question our study could not answer is how immediate the neuroprotective effects of CYLD inhibition are. In our knockout model, CYLD deletion is permanent. In humans however, unless prophylaxis is an option, any CYLD inhibitor would have to be administered within a few hours in order to provide any clinically relevant neuroprotection.

In conclusion, while we believe that CYLD is a promising target for future stroke therapy, we also think that further research will be necessary in order to determine its clinical significance.

5 SUMMARY

5.1 ENGLISH

Stroke is responsible for 9% of deaths around the world and is the sixth most common cause of disability-adjusted life years lost. Despite its impact on society and on public health, currently available treatment options are limited. In order to develop new therapeutic strategies for stroke, it is important to understand its pathophysiology. Ischemic stroke is caused by occlusion of a cerebral blood vessel. In case of ischemic stroke, two zones can be differentiated: the ischemic core, in which perfusion is so low that cells die within minutes by necrosis, and the penumbra, an area with reduced perfusion where tissue function is impaired, but structure is still intact and where cells die within hours through necrosis and programmed cell death such as apoptosis, necroptosis and ferroptosis.

CYLD is a K63-deubiquitinase that has been shown to be part of the necroptosis cascade. It has also been shown to be related to lipid peroxidation, which is involved in GPX4-mediated ferroptotic cell death. As a result, we decided to investigate the role of CYLD in ischemic stroke to see whether it qualifies as a target for future stroke therapy. In our studies, we used CYLD knockout mice. We subjected these to filament middle cerebral artery occlusion, measured their stroke volume and functional outcome and compared them to their wildtype littermates. We also used Western blotting to look into the expression of CYLD after stroke in the penumbra region in C57BL/6 mice. In addition, we used immunofluorescence to localize CYLD in the brain. Finally, in order to investigate the link between CYLD and ferroptosis, we created a double knockout model with a permanent CYLD knockout and an inducible neuronal GPX4 knockout.

Our investigations revealed that CYLD is primarily located in neurons in the brain. It is found mostly in the perinuclear region within the cell body, but also to a varying degree within apical dendrites and to a lesser degree within the nucleus. We found that CYLD^{-/-} animals develop smaller strokes in the MCAo model than CYLD WT littermates. They also show better functional outcome 24 hours after MCA occlusion. However, we could not find any difference in edema formation between both groups. Upon stroke, CYLD expression within the penumbra also seems to significantly decrease. In our CYLD/GPX4 double knockout model, we could not find any difference in either survival or functional outcome between CYLD^{-/-} and WT mice.

Our results show that CYLD knockout leads to a decrease in stroke size and results in an improvement in functional outcome. Our immunofluorescence stainings of the penumbra area suggest that a decrease in neuronal programmed cell death contributes to the decrease in stroke size. This is in accordance with already published data, which show that inhibition of necroptosis leads to smaller strokes, that CYLD is part of the necroptosis cascade, and that a CYLD knockout is protective in traumatic brain injury. In addition, the finding that a CYLD knockout prevents neuronal programmed cell death is consistent with our finding that CYLD is mostly localized in neurons. The significant decrease of CYLD in the penumbra may hint at a neuronal survival mechanism by downregulation of proteins relevant for programmed cell death. Based on our results, we think that it is unlikely that CYLD plays a major role in ferroptosis. However, given the limitations of our model, we cannot fully exclude its involvement in the ferroptotic pathway.

In conclusion, we think that CYLD is involved in programmed cell death within the ischemic penumbra, and that it may be a target molecule for future stroke therapy. However, further research will be necessary in order to determine its clinical relevance.

5.2 DEUTSCH

9% aller Menschen weltweit sterben an einem Schlaganfall; zudem sind Schlaganfälle die sechsthäufigste Ursache für den Verlust von Lebensjahren. Trotz seines bedeutsamen negativen Einflusses auf die öffentliche Gesundheit sind die derzeit verfügbaren Therapiemöglichkeiten beim Schlaganfall begrenzt.

Das Entwickeln neuer Therapieansätze setzt die Kenntnis der Pathophysiologie des Schlaganfalls voraus. Der ischämische Schlaganfall wird durch den Verschluss eines zerebralen Blutgefäßes verursacht. Beim ischämischen Schlaganfall können zwei Bereiche unterschieden werden: der ischämische Kern, in welchem die zerebrale Durchblutung so gering ist, dass dortige Zellen binnen Minuten durch Nekrose zugrunde gehen, und die Penumbra, ein Bereich mit reduzierter Perfusion, in welchem die Gewebefunktion beeinträchtigt, die Gewebestruktur jedoch noch intakt ist, und in dem Zellen binnen Stunden durch Nekrose und programmierte Zelltodformen wie Apoptose, Nekroptose oder Ferroptose sterben.

CYLD ist eine K63-Deubiquitinase, die in der Nekroptosekaskade eine Rolle spielt. CYLD wurde außerdem mit Lipidperoxidation in Verbindung gebracht, die Teil der GPX4-vermittelten Ferroptose ist.

Aufgrund dieser Erkenntnisse haben wir entschieden, die Rolle von CYLD bei ischämischem Schlaganfall zu erforschen, um zu ermitteln, ob es ein mögliches Ziel für zukünftige Schlaganfalltherapien darstellt.

In unseren Experimenten verwendeten wir CYLD-Knockout-Mäuse. Wir führten eine Okklusion der Arteria Cerebri Media mittels eines silikonbeschichteten Fadens durch, maßen das Infarktvolume und die neurologische Funktion und verglichen die Resultate mit Wildtyp-Wurfgeschwistern. Wir untersuchten ebenfalls mittels Western Blot die CYLD-Expression nach Schlaganfall in der Penumbraregion. Zusätzlich lokalisierten wir CYLD im Gehirn mittels Immunfluoreszenz. Schlussendlich untersuchten wir die Beziehung zwischen CYLD und Ferroptose mittels eines von uns gezüchteten Doppel-Knockout-Modells mit einem permanenten CYLD- und einem induzierbaren neuronalen GPX4-Knockout.

Unsere Untersuchungen zeigten, dass CYLD innerhalb des Gehirns vor allem in Neuronen lokalisiert ist. Es findet sich perinukleär innerhalb des Zellkörpers, aber auch in apikalen Dendriten und in geringerem Maße im Zellkern. Wir konnten zeigen, dass

CYLD ^{-/-}-Mäuse im MCAo-Modell kleinere Schlaganfälle entwickeln als WT-Geschwistertiere. Sie zeigen außerdem geringere neurologische Ausfälle 24 Stunden nach MCA-Okklusion. Wir konnten jedoch keinen Unterschied in der Ödembildung zwischen beiden Gruppen feststellen. Zudem scheint die CYLD-Expression innerhalb der ischämischen Penumbra signifikant abzunehmen. In unserem CYLD/GPX4 Doppel-Knockout-Modell konnten wir keinen Unterschied bei Überleben oder neurologischer Funktion zwischen CYLD ^{-/-} und WT Mäusen feststellen.

Unsere Resultate zeigen, dass ein CYLD-Knockout tatsächlich zu einer Abnahme der Schlaganfallgröße und einer Verbesserung des neurologischen Outcomes führt. Unsere Immunfluoreszenzuntersuchung der Penumbra deutet auf eine Verminderung des neuronalen programmierten Zelltodes hin. Dies deckt sich mit bereits publizierten Daten, die zeigen, dass die Inhibition der Nekroptose zu kleineren Schlaganfällen führt, dass CYLD Teil der Nekroptosekaskade ist, und dass ein CYLD-Knockout protektiv bei traumatischer Hirnschädigung wirkt. Zusätzlich passt unser Ergebnis, dass ein CYLD-Knockout den neuronalen programmierten Zelltod behindert, zu der von uns beschriebenen neuronalen Lokalisation. Die signifikante Abnahme von CYLD in der Penumbra könnte auf einen neuronalen Überlebensmechanismus durch das Herunterregulieren für programmierten Zelltod relevanter Proteine wie CYLD hinweisen. Aufgrund unserer Ergebnisse vermuten wir, dass CYLD keine wesentliche Rolle bei Ferroptose spielt. Allerdings können wir aufgrund der Beschränkungen des von uns verwendeten Modells eine Beteiligung CYLDs an der Ferroptosekaskade nicht vollständig ausschließen.

Schlussfolgernd möchten wir festhalten, dass CYLD mit hoher Wahrscheinlichkeit eine Rolle beim programmierten Zelltod innerhalb der Penumbra spielt, und dass es sich um ein potentiell Ziel für zukünftige Schlaganfalltherapie handeln könnte. Allerdings sind weitere Untersuchungen notwendig, um dessen klinischen Nutzen zu erörtern.

6 ABBREVIATIONS

ACA	anterior cerebral artery
AMPA receptor	α -amino-3-hydroxy-5-methyl-4-isoxazolepropionic acid receptor
ATG	adenine-thymine-guanine; a start codon
ATP	adenosine triphosphate
BA	basilar artery
BCA assay	bicinchoninic acid assay
bp	base pairs
BSA	bovine serum albumin
CamKII α	Ca ²⁺ /calmodulin-dependent protein kinase II α
CBF	cerebral blood flow
CCD camera	charge-coupled device camera
cIAP	cellular inhibitor of apoptosis
C57BL/6	C57 black 6; inbred strain of laboratory mouse
Cre	cyclization recombinase
CSF	cerebrospinal fluid
CYLD	Cylindromatosis
DNA	desoxyribonucleic acid
dUTP	desoxyuridine triphosphate
ECG	electrocardiogram
ECL	enhanced chemiluminescence
FADD	Fas-associated death domain
fMCAo	filament middle cerebral artery occlusion model
GAP-GLY	cytoskeletal-associated protein-glycine-rich domains
GPX4	glutathione peroxidase 4
ICA	internal carotid artery
IDO	indoleamine 2,3-dioxygenase
IV	intravenous
LacZ	gene for β -galactosidase
LoxP	locus of X-over P1

MCA	middle cerebral artery
MMF	midazolam, medetomidine and fentanyl
NeuN	neuronal nuclei; neuron-specific nuclear protein
NF- κ B	nuclear factor κ -light-chain-enhancer of activated B cells
NMDA receptor	N-methyl-D-aspartate receptor
PCOM/ PComA	posterior communicating artery
PCR	polymerase chain reaction
PFA	paraformaldehyde
PHPGPX	glutathione peroxidase 4
PVDF	polyvinylidene difluoride
RIP1	receptor-interacting protein 1
RIP3	receptor-interacting protein 3
RIPA	radioimmunoprecipitation assay
ROS	reactive oxygen species
rt-PA	recombinant tissue-type Plasminogen Activator
RT-PCR	reverse transcriptase-PCR
SAH	subarachnoid hemorrhage
SCA	superior cerebellar artery
SD	standard deviation
siRNA	small interfering ribonucleic acid
SSRI	selective serotonin reuptake inhibitor
STAIR	Stroke Treatment Academic Industry Roundtable
TAK1	transforming growth factor beta-activated kinase 1
TBM	TRAF2 binding motif
TBS	tris-buffered saline
TBS-T	tris-buffered saline with Tween20
TNF α	tumor necrosis factor α
TNFR1	tumor necrosis factor receptor type 1
TRADD	TNFR1-associated death domain
TRAF2/TRAF5	TNFR-associated factor 2/5
tuj1	neuron-specific Class III β -tubulin

TUNEL	terminal deoxynucleotidyl transferase dUTP nick end labeling
UCH	ubiquitin carboxy-terminal hydrolases
WT	wild type
Xc ⁻	cystine/glutamate antiporter

7 ACKNOWLEDGEMENTS

First, I would like to thank my family and all of my friends, especially Katharina Knoll, for supporting me during my research.

I would also like to thank Prof. Dr. Nikolaus Plesnila, who helped me take my first steps into the world of science, and who aided me with the coordination and structure of my research project.

Special thanks also go to Dr. Farida Hellal, who supported me during most of my research, was always friendly and helpful, and taught me a lot about science in general. Moreover, I would like to thank Lilja Meißner, who helped me during the early phase of my research.

I would also like to thank the rest of our research team for their help and the great atmosphere in our laboratory, especially Uta Mamrak, Mitrajit Ghosh, Athanasios Loubopoulos, Kathrin Schüller, Sepiede Azghandi, Dominik Bühler, Iga Rynarzewska and Steffen Tiedt.

In addition, I would like to thank Carsten Culmsee and Reinhard Fässler for providing the knockout mouse models we have used in our experiments, and Prof. Dr. Martin Dichgans, the director of the Institute for Stroke and Dementia research.

Finally, I would like to thank Prof. Dr. Dr. Jürgen Heesemann, the former coordinator of the Ludwig-Maximilian-University's "Förderprogramm für Forschung und Lehre", which introduced me to Professor Plesnila's research group and provided financial support.

8 CURRICULUM VITAE

Personal Details

Name	Pierre Scheffler
Date of Birth	September 28, 1991
Place of Birth	Luxembourg
Nationality	German/Luxembourgish

Education

November 2016	Third part of the medical examination (Grade: “good”)
October 2015	Second part of the medical examination (Grade: “very good”)
2013 – 2022	Thesis at the Institute for Experimental Stroke Research as part of the FöFoLe-Programme (Förderprogramm für Forschung und Lehre)
August 2012	First part of the medical examination (Grade: 1.0)
2010-2017	Medical degree at Ludwig-Maximilians-Universität München
August 2010	Diplôme de fin d’études secondaires (Subject area: Latin – Natural sciences – Mathematics; Grade: “excellent”)
2003 – 2010	Secondary school: Athénée de Luxembourg

Work experience

Since July 2020	Residency in neurosurgery at University Hospital Freiburg
July 2017 – June 2020	Residency in neurosurgery at University Hospital Zurich
January – June 2017	Residency in neurology at the LMU Munich's University Hospital
June – October 2016	Medical elective in general surgery at the LMU Munich's University Hospital
May – June 2016	Medical elective in nephrology and infectious diseases at the University of North Carolina Hospitals, Chapel Hill
March – April 2016	Medical elective in cardiology at King's College London
November 2015 – March 2016	Medical elective in neurosurgery at University Hospital Zurich
February 2015	Medical elective in gastroenterology at the LMU Munich's University Hospital
September 2014	Medical elective in neurosurgery at the National Neuroscience Institute, Singapore
August 2013	Medical elective in the emergency department at University Hospital Zurich
February – March 2013	Medical elective in vascular surgery at Hôpital Kirchberg in Luxembourg

Scholarships

2014 – 2017	Scholarship by the German National Academic Foundation (Studienstiftung des deutschen Volkes)
2013 – 2014	Deutschlandstipendium

9 PRESENTATIONS AND PUBLICATIONS

Presentations

The role of CYLD in stroke

Retreat of the Institute for Stroke and Dementia Research, 2014

The role of CYLD in stroke

Colloquium of the program “Förderprogramm für Forschung und Lehre“, LMU Munich, Herrsching, May 9 2014

Posters

P. Scheffler, C. Schwicht, L. Meissner, F. Hellal, N. Plesnila

Contribution of the K63-deubiquitinase Cyldromatosis (CYLD) to neuronal cell death after focal cerebral ischemia

Brain 2015: XXVIIth international Symposium on Cerebral Blood Flow, Metabolism and Function; Vancouver, Canada, June 27-30, 2015

10 CITATIONS

- 1 Feigin, V. L. *et al.* Global and regional burden of stroke during 1990-2010: findings from the Global Burden of Disease Study 2010. *Lancet* **383**, 245-254 (2014).
- 2 Murakami, K., Kondo, T., Kawase, M. & Chan, P. H. The development of a new mouse model of global ischemia: focus on the relationships between ischemia duration, anesthesia, cerebral vasculature, and neuronal injury following global ischemia in mice. *Brain research* **780**, 304-310, doi:10.1016/s0006-8993(97)01217-1 (1998).
- 3 Sacco, R. L. *et al.* An updated definition of stroke for the 21st century: a statement for healthcare professionals from the American Heart Association/American Stroke Association. *Stroke* **44**, 2064-2089, doi:10.1161/STR.0b013e318296aeca (2013).
- 4 Auer, R. N. & Sutherland, G. R. Primary intracerebral hemorrhage: pathophysiology. *The Canadian journal of neurological sciences. Le journal canadien des sciences neurologiques* **32 Suppl 2**, S3-12 (2005).
- 5 Long, B., Koyfman, A. & Runyon, M. S. Subarachnoid Hemorrhage: Updates in Diagnosis and Management. *Emergency medicine clinics of North America* **35**, 803-824, doi:10.1016/j.emc.2017.07.001 (2017).
- 6 Donnan, G. A., Fisher, M., Macleod, M. & Davis, S. M. Stroke. *Lancet (London, England)* **371**, 1612-1623, doi:10.1016/s0140-6736(08)60694-7 (2008).
- 7 Thrift, A. G., Dewey, H. M., Macdonell, R. A., McNeil, J. J. & Donnan, G. A. Incidence of the major stroke subtypes: initial findings from the North East Melbourne stroke incidence study (NEMESIS). *Stroke* **32**, 1732-1738 (2001).
- 8 Murray, C. J. & Lopez, A. D. Mortality by cause for eight regions of the world: Global Burden of Disease Study. *Lancet* **349**, 1269-1276, doi:10.1016/S0140-6736(96)07493-4 (1997).
- 9 Luengo-Fernandez, R., Violato, M., Candio, P. & Leal, J. Economic burden of stroke across Europe: A population-based cost analysis. *European stroke journal* **5**, 17-25, doi:10.1177/2396987319883160 (2020).
- 10 Furie, K. L. & Jayaraman, M. V. 2018 Guidelines for the Early Management of Patients With Acute Ischemic Stroke. *Stroke* **49**, 509-510, doi:10.1161/STROKEAHA.118.020176 (2018).
- 11 Emberson, J. *et al.* Effect of treatment delay, age, and stroke severity on the effects of intravenous thrombolysis with alteplase for acute ischaemic stroke: a meta-analysis of individual patient data from randomised trials. *Lancet (London, England)* **384**, 1929-1935, doi:10.1016/S0140-6736(14)60584-5 (2014).
- 12 Demaerschalk, B. M. *et al.* Scientific Rationale for the Inclusion and Exclusion Criteria for Intravenous Alteplase in Acute Ischemic Stroke: A Statement for Healthcare Professionals From the American Heart Association/American Stroke Association. *Stroke* **47**, 581-641, doi:10.1161/str.0000000000000086 (2016).

- 13 de Los Rios la Rosa, F. *et al.* Eligibility for Intravenous Recombinant Tissue-Type Plasminogen Activator Within a Population: The Effect of the European Cooperative Acute Stroke Study (ECASS) III Trial. *Stroke* **43**, 1591-1595, doi:10.1161/strokeaha.111.645986 (2012).
- 14 Kleindorfer, D. *et al.* Eligibility for recombinant tissue plasminogen activator in acute ischemic stroke: a population-based study. *Stroke* **35**, e27-29, doi:10.1161/01.str.0000109767.11426.17 (2004).
- 15 Berkhemer, O. A. *et al.* A randomized trial of intraarterial treatment for acute ischemic stroke. *N Engl J Med* **372**, 11-20, doi:10.1056/NEJMoa1411587 (2015).
- 16 Jovin, T. G. *et al.* Thrombectomy within 8 hours after symptom onset in ischemic stroke. *N Engl J Med* **372**, 2296-2306, doi:10.1056/NEJMoa1503780 (2015).
- 17 Saver, J. L. *et al.* Stent-retriever thrombectomy after intravenous t-PA vs. t-PA alone in stroke. *N Engl J Med* **372**, 2285-2295, doi:10.1056/NEJMoa1415061 (2015).
- 18 Goyal, M. *et al.* Randomized assessment of rapid endovascular treatment of ischemic stroke. *N Engl J Med* **372**, 1019-1030, doi:10.1056/NEJMoa1414905 (2015).
- 19 Campbell, B. C. *et al.* Endovascular therapy for ischemic stroke with perfusion-imaging selection. *N Engl J Med* **372**, 1009-1018, doi:10.1056/NEJMoa1414792 (2015).
- 20 Bracard, S. *et al.* Mechanical thrombectomy after intravenous alteplase versus alteplase alone after stroke (THRACE): a randomised controlled trial. *Lancet Neurol* **15**, 1138-1147, doi:10.1016/S1474-4422(16)30177-6 (2016).
- 21 Langhorne, P., Williams, B. O., Gilchrist, W. & Howie, K. Do stroke units save lives? *Lancet (London, England)* **342**, 395-398 (1993).
- 22 Indredavik, B. *et al.* Benefit of a stroke unit: a randomized controlled trial. *Stroke* **22**, 1026-1031 (1991).
- 23 Vahedi, K. *et al.* Early decompressive surgery in malignant infarction of the middle cerebral artery: a pooled analysis of three randomised controlled trials. *Lancet Neurol* **6**, 215-222, doi:10.1016/s1474-4422(07)70036-4 (2007).
- 24 Raco, A., Caroli, E., Isidori, A. & Salvati, M. Management of acute cerebellar infarction: one institution's experience. *Neurosurgery* **53**, 1061-1065; discussion 1065-1066 (2003).
- 25 The International Stroke Trial (IST): a randomised trial of aspirin, subcutaneous heparin, both, or neither among 19435 patients with acute ischaemic stroke. International Stroke Trial Collaborative Group. *Lancet (London, England)* **349**, 1569-1581 (1997).
- 26 CAST: randomised placebo-controlled trial of early aspirin use in 20,000 patients with acute ischaemic stroke. CAST (Chinese Acute Stroke Trial) Collaborative Group. *Lancet (London, England)* **349**, 1641-1649 (1997).
- 27 Amarenco, P. *et al.* High-dose atorvastatin after stroke or transient ischemic attack. *N Engl J Med* **355**, 549-559, doi:10.1056/NEJMoa061894 (2006).

- 28 Siepmann, T. *et al.* Selective serotonin reuptake inhibitors to improve outcome in acute ischemic stroke: possible mechanisms and clinical evidence. *Brain and behavior* **5**, e00373, doi:10.1002/brb3.373 (2015).
- 29 Chollet, F. *et al.* Fluoxetine for motor recovery after acute ischaemic stroke (FLAME): a randomised placebo-controlled trial. *Lancet Neurol* **10**, 123-130, doi:10.1016/s1474-4422(10)70314-8 (2011).
- 30 Schmidt, H. D. & Duman, R. S. The role of neurotrophic factors in adult hippocampal neurogenesis, antidepressant treatments and animal models of depressive-like behavior. *Behavioural pharmacology* **18**, 391-418, doi:10.1097/FBP.0b013e3282ee2aa8 (2007).
- 31 Lim, C. M. *et al.* Fluoxetine affords robust neuroprotection in the postischemic brain via its anti-inflammatory effect. *Journal of neuroscience research* **87**, 1037-1045, doi:10.1002/jnr.21899 (2009).
- 32 Shin, T. K. *et al.* Fluoxetine and sertraline attenuate postischemic brain injury in mice. *The Korean journal of physiology & pharmacology : official journal of the Korean Physiological Society and the Korean Society of Pharmacology* **13**, 257-263, doi:10.4196/kjpp.2009.13.3.257 (2009).
- 33 Palvimaki, E. P., Laakso, A., Kuoppamaki, M., Syvalahti, E. & Hietala, J. Up-regulation of beta 1-adrenergic receptors in rat brain after chronic citalopram and fluoxetine treatments. *Psychopharmacology* **115**, 543-546 (1994).
- 34 Raichle, M. E. & Gusnard, D. A. Appraising the brain's energy budget. *Proc Natl Acad Sci U S A* **99**, 10237-10239, doi:10.1073/pnas.172399499 (2002).
- 35 Martin, R. L., Lloyd, H. G. & Cowan, A. I. The early events of oxygen and glucose deprivation: setting the scene for neuronal death? *Trends in neurosciences* **17**, 251-257 (1994).
- 36 Dirnagl, U., Iadecola, C. & Moskowitz, M. A. Pathobiology of ischaemic stroke: an integrated view. *Trends in neurosciences* **22**, 391-397 (1999).
- 37 Siesjo, B. K., Katsura, K. & Kristian, T. The biochemical basis of cerebral ischemic damage. *Journal of neurosurgical anesthesiology* **7**, 47-52 (1995).
- 38 Hossmann, K. A. Viability thresholds and the penumbra of focal ischemia. *Ann Neurol* **36**, 557-565, doi:10.1002/ana.410360404 (1994).
- 39 Obrenovitch, T. P. The ischaemic penumbra: twenty years on. *Cerebrovasc Brain Metab Rev* **7**, 297-323 (1995).
- 40 Nedergaard, M. & Astrup, J. Infarct rim: effect of hyperglycemia on direct current potential and [14C]2-deoxyglucose phosphorylation. *Journal of cerebral blood flow and metabolism : official journal of the International Society of Cerebral Blood Flow and Metabolism* **6**, 607-615, doi:10.1038/jcbfm.1986.108 (1986).
- 41 Kocher, M. Metabolic and hemodynamic activation of postischemic rat brain by cortical spreading depression. *Journal of cerebral blood flow and metabolism : official journal of the International Society of Cerebral Blood Flow and Metabolism* **10**, 564-571, doi:10.1038/jcbfm.1990.99 (1990).
- 42 Feuerstein, G., Wang, X. & Barone, F. C. Cytokines in brain ischemia--the role of TNF alpha. *Cellular and molecular neurobiology* **18**, 695-701 (1998).

- 43 L, L., X, W. & Z, Y. Ischemia-reperfusion Injury in the Brain: Mechanisms and Potential Therapeutic Strategies. *Biochemistry & pharmacology : open access* **5**, doi:10.4172/2167-0501.1000213 (2016).
- 44 Sanderson, T. H., Reynolds, C. A., Kumar, R., Przyklenk, K. & Huttemann, M. Molecular mechanisms of ischemia-reperfusion injury in brain: pivotal role of the mitochondrial membrane potential in reactive oxygen species generation. *Molecular neurobiology* **47**, 9-23, doi:10.1007/s12035-012-8344-z (2013).
- 45 Lambeth, J. D. NOX enzymes and the biology of reactive oxygen. *Nature reviews. Immunology* **4**, 181-189, doi:10.1038/nri1312 (2004).
- 46 Zhang, R.-L., Chopp, M., Chen, H. & Garcia, J. H. Temporal profile of ischemic tissue damage, neutrophil response, and vascular plugging following permanent and transient (2H) middle cerebral artery occlusion in the rat. *Journal of the Neurological Sciences* **125**, 3-10, doi:https://doi.org/10.1016/0022-510X(94)90234-8 (1994).
- 47 Khatri, R., McKinney, A. M., Swenson, B. & Janardhan, V. Blood-brain barrier, reperfusion injury, and hemorrhagic transformation in acute ischemic stroke. *Neurology* **79**, S52-57, doi:10.1212/WNL.0b013e3182697e70 (2012).
- 48 Broughton, B. R., Reutens, D. C. & Sobey, C. G. Apoptotic mechanisms after cerebral ischemia. *Stroke* **40**, e331-339, doi:10.1161/strokeaha.108.531632 (2009).
- 49 Zille, M. *et al.* Visualizing cell death in experimental focal cerebral ischemia: promises, problems, and perspectives. *Journal of cerebral blood flow and metabolism : official journal of the International Society of Cerebral Blood Flow and Metabolism* **32**, 213-231, doi:10.1038/jcbfm.2011.150 (2012).
- 50 Martin, L. J. *et al.* Neurodegeneration in excitotoxicity, global cerebral ischemia, and target deprivation: A perspective on the contributions of apoptosis and necrosis. *Brain research bulletin* **46**, 281-309, doi:10.1016/s0361-9230(98)00024-0 (1998).
- 51 Portera-Cailliau, C., Price, D. L. & Martin, L. J. Excitotoxic neuronal death in the immature brain is an apoptosis-necrosis morphological continuum. *The Journal of comparative neurology* **378**, 70-87 (1997).
- 52 Niizuma, K. *et al.* Mitochondrial and apoptotic neuronal death signaling pathways in cerebral ischemia. *Biochimica et biophysica acta* **1802**, 92-99, doi:10.1016/j.bbadis.2009.09.002 (2010).
- 53 Biggs, P. J. *et al.* Familial cylindromatosis (turban tumour syndrome) gene localised to chromosome 16q12-q13: evidence for its role as a tumour suppressor gene. *Nature genetics* **11**, 441-443, doi:10.1038/ng1295-441 (1995).
- 54 Young, A. L. *et al.* CYLD mutations underlie Brooke-Spiegler, familial cylindromatosis, and multiple familial trichoepithelioma syndromes. *Clinical genetics* **70**, 246-249, doi:10.1111/j.1399-0004.2006.00667.x (2006).
- 55 Bignell, G. R. *et al.* Identification of the familial cylindromatosis tumour-suppressor gene. *Nature genetics* **25**, 160-165, doi:10.1038/76006 (2000).

- 56 Glittenberg, M. & Ligoxygakis, P. CYLD: a multifunctional deubiquitinase. *Fly* **1**, 330-332 (2007).
- 57 Harhaj, E. W. & Dixit, V. M. Deubiquitinases in the regulation of NF- κ B signaling. *Cell research* **21**, 22-39, doi:10.1038/cr.2010.166 (2011).
- 58 Goldstein, G. *et al.* Isolation of a polypeptide that has lymphocyte-differentiating properties and is probably represented universally in living cells. *Proc Natl Acad Sci U S A* **72**, 11-15 (1975).
- 59 Kerscher, O., Felberbaum, R. & Hochstrasser, M. Modification of proteins by ubiquitin and ubiquitin-like proteins. *Annu Rev Cell Dev Biol* **22**, 159-180, doi:10.1146/annurev.cellbio.22.010605.093503 (2006).
- 60 Komander, D. The emerging complexity of protein ubiquitination. *Biochemical Society transactions* **37**, 937-953, doi:10.1042/bst0370937 (2009).
- 61 Komander, D. & Rape, M. The ubiquitin code. *Annual review of biochemistry* **81**, 203-229, doi:10.1146/annurev-biochem-060310-170328 (2012).
- 62 Ikeda, F. & Dikic, I. Atypical ubiquitin chains: new molecular signals. 'Protein Modifications: Beyond the Usual Suspects' review series. *EMBO Rep* **9**, 536-542, doi:10.1038/embo.2008.93 (2008).
- 63 Miranda, M. & Sorkin, A. Regulation of receptors and transporters by ubiquitination: new insights into surprisingly similar mechanisms. *Mol Interv* **7**, 157-167, doi:10.1124/mi.7.3.7 (2007).
- 64 Glickman, M. H. & Ciechanover, A. The ubiquitin-proteasome proteolytic pathway: destruction for the sake of construction. *Physiol Rev* **82**, 373-428, doi:10.1152/physrev.00027.2001 (2002).
- 65 Degterev, A. *et al.* Chemical inhibitor of nonapoptotic cell death with therapeutic potential for ischemic brain injury. *Nature chemical biology* **1**, 112-119, doi:10.1038/nchembio711 (2005).
- 66 Vandenabeele, P., Galluzzi, L., Vanden Berghe, T. & Kroemer, G. Molecular mechanisms of necroptosis: an ordered cellular explosion. *Nature reviews. Molecular cell biology* **11**, 700-714, doi:10.1038/nrm2970 (2010).
- 67 Hitomi, J. *et al.* Identification of a molecular signaling network that regulates a cellular necrotic cell death pathway. *Cell* **135**, 1311-1323, doi:10.1016/j.cell.2008.10.044 (2008).
- 68 Bertrand, M. J. *et al.* cIAP1 and cIAP2 facilitate cancer cell survival by functioning as E3 ligases that promote RIP1 ubiquitination. *Molecular cell* **30**, 689-700, doi:10.1016/j.molcel.2008.05.014 (2008).
- 69 Hacker, H. & Karin, M. Regulation and function of IKK and IKK-related kinases. *Science's STKE : signal transduction knowledge environment* **2006**, re13, doi:10.1126/stke.3572006re13 (2006).
- 70 Wooten, M. W. Function for NF- κ B in neuronal survival: regulation by atypical protein kinase C. *Journal of neuroscience research* **58**, 607-611 (1999).
- 71 Wang, L., Du, F. & Wang, X. TNF- α induces two distinct caspase-8 activation pathways. *Cell* **133**, 693-703, doi:10.1016/j.cell.2008.03.036 (2008).

- 72 Holler, N. *et al.* Fas triggers an alternative, caspase-8-independent cell death pathway using the kinase RIP as effector molecule. *Nature immunology* **1**, 489-495, doi:10.1038/82732 (2000).
- 73 Dixon, S. J. *et al.* Ferroptosis: an iron-dependent form of nonapoptotic cell death. *Cell* **149**, 1060-1072, doi:10.1016/j.cell.2012.03.042 (2012).
- 74 Imai, H. & Nakagawa, Y. Biological significance of phospholipid hydroperoxide glutathione peroxidase (PHGPx, GPx4) in mammalian cells. *Free Radic Biol Med* **34**, 145-169 (2003).
- 75 Sattler, W., Maiorino, M. & Stocker, R. Reduction of HDL- and LDL-associated cholesterylester and phospholipid hydroperoxides by phospholipid hydroperoxide glutathione peroxidase and Ebselen (PZ 51). *Arch Biochem Biophys* **309**, 214-221, doi:10.1006/abbi.1994.1105 (1994).
- 76 Yang, W. S. *et al.* Regulation of ferroptotic cancer cell death by GPX4. *Cell* **156**, 317-331, doi:10.1016/j.cell.2013.12.010 (2014).
- 77 Roveri, A., Maiorino, M. & Ursini, F. Enzymatic and immunological measurements of soluble and membrane-bound phospholipid-hydroperoxide glutathione peroxidase. *Methods Enzymol* **233**, 202-212 (1994).
- 78 Yoo, S. E. *et al.* Gpx4 ablation in adult mice results in a lethal phenotype accompanied by neuronal loss in brain. *Free Radic Biol Med* **52**, 1820-1827, doi:10.1016/j.freeradbiomed.2012.02.043 (2012).
- 79 Conrad, M. *et al.* 12/15-lipoxygenase-derived lipid peroxides control receptor tyrosine kinase signaling through oxidation of protein tyrosine phosphatases. *Proceedings of the National Academy of Sciences of the United States of America* **107**, 15774-15779, doi:10.1073/pnas.1007909107 (2010).
- 80 Diemert, S. *The role of p53 and CYLD in mitochondrial death pathways and mechanisms of neuronal necroptosis* Dr. rer. nat. thesis, Philipps-Universität Marburg, (2012).
- 81 Massoumi, R., Chmielarska, K., Hennecke, K., Pfeifer, A. & Fassler, R. Cyld inhibits tumor cell proliferation by blocking Bcl-3-dependent NF-kappaB signaling. *Cell* **125**, 665-677, doi:10.1016/j.cell.2006.03.041 (2006).
- 82 Sauer, B. Functional expression of the cre-lox site-specific recombination system in the yeast *Saccharomyces cerevisiae*. *Molecular and cellular biology* **7**, 2087-2096 (1987).
- 83 Feil, S., Valtcheva, N. & Feil, R. Inducible Cre mice. *Methods in molecular biology (Clifton, N.J.)* **530**, 343-363, doi:10.1007/978-1-59745-471-1_18 (2009).
- 84 Liu, X. B. & Murray, K. D. Neuronal excitability and calcium/calmodulin-dependent protein kinase type II: location, location, location. *Epilepsia* **53 Suppl 1**, 45-52, doi:10.1111/j.1528-1167.2012.03474.x (2012).
- 85 Liu, X. B. & Jones, E. G. Localization of alpha type II calcium calmodulin-dependent protein kinase at glutamatergic but not gamma-aminobutyric acid (GABAergic) synapses in thalamus and cerebral cortex. *Proc Natl Acad Sci U S A* **93**, 7332-7336 (1996).

- 86 Liu, X. & Jones, E. G. Alpha isoform of calcium-calmodulin dependent protein kinase II (CAM II kinase-alpha) restricted to excitatory synapses in the CA1 region of rat hippocampus. *Neuroreport* **8**, 1475-1479 (1997).
- 87 Seiler, A. *et al.* Glutathione peroxidase 4 senses and translates oxidative stress into 12/15-lipoxygenase dependent- and AIF-mediated cell death. *Cell Metab* **8**, 237-248, doi:10.1016/j.cmet.2008.07.005 (2008).
- 88 Vakili, A., Kataoka, H. & Plesnila, N. Role of arginine vasopressin V1 and V2 receptors for brain damage after transient focal cerebral ischemia. *J Cereb Blood Flow Metab* **25**, 1012-1019, doi:10.1038/sj.jcbfm.9600097 (2005).
- 89 Culmsee, C. *et al.* Apoptosis-inducing factor triggered by poly(ADP-ribose) polymerase and Bid mediates neuronal cell death after oxygen-glucose deprivation and focal cerebral ischemia. *J Neurosci* **25**, 10262-10272, doi:10.1523/JNEUROSCI.2818-05.2005 (2005).
- 90 Bederson, J. B. *et al.* Rat middle cerebral artery occlusion: evaluation of the model and development of a neurologic examination. *Stroke* **17**, 472-476 (1986).
- 91 Shapira, Y. *et al.* Experimental closed head injury in rats: mechanical, pathophysiologic, and neurologic properties. *Critical care medicine* **16**, 258-265 (1988).
- 92 Schulz, J. *et al.* LF16-0687 a novel non-peptide bradykinin B2 receptor antagonist reduces vasogenic brain edema from a focal lesion in rats. *Acta Neurochir Suppl* **76**, 137-139 (2000).
- 93 Schindelin, J. *et al.* Fiji: an open-source platform for biological-image analysis. *Nature Methods* **9**, 676-682, doi:10.1038/nmeth.2019 (2012).
- 94 Terpolilli, N. A. *et al.* Nitric oxide inhalation reduces brain damage, prevents mortality, and improves neurological outcome after subarachnoid hemorrhage by resolving early pial microvasospasms. *Journal of cerebral blood flow and metabolism : official journal of the International Society of Cerebral Blood Flow and Metabolism* **36**, 2096-2107, doi:10.1177/0271678X15605848 (2016).
- 95 Terpolilli, N. A., Kim, S.-W., Thal, S. C., Kuebler, W. M. & Plesnila, N. Inhaled nitric oxide reduces secondary brain damage after traumatic brain injury in mice. *Journal of cerebral blood flow and metabolism : official journal of the International Society of Cerebral Blood Flow and Metabolism* **33**, 311-318, doi:10.1038/jcbfm.2012.176 (2013).
- 96 Balbi, M., Koide, M., Wellman, G. C. & Plesnila, N. Inversion of neurovascular coupling after subarachnoid hemorrhage in vivo. *Journal of cerebral blood flow and metabolism : official journal of the International Society of Cerebral Blood Flow and Metabolism* **37**, 3625-3634, doi:10.1177/0271678X16686595 (2017).
- 97 Zan, Y. *et al.* Production of knockout rats using ENU mutagenesis and a yeast-based screening assay. *Nature biotechnology* **21**, 645-651, doi:10.1038/nbt830 (2003).
- 98 Sarsani, V. K. *et al.* The Genome of C57BL/6J "Eve", the Mother of the Laboratory Mouse Genome Reference Strain. *G3 (Bethesda, Md.)* **9**, 1795-1805, doi:10.1534/g3.119.400071 (2019).

- 99 Thal, S. C. & Plesnila, N. Non-invasive intraoperative monitoring of blood pressure and arterial pCO₂ during surgical anesthesia in mice. *J Neurosci Methods* **159**, 261-267, doi:10.1016/j.jneumeth.2006.07.016 (2007).
- 100 Davalos, A. *et al.* Citicoline in the treatment of acute ischaemic stroke: an international, randomised, multicentre, placebo-controlled study (ICTUS trial). *Lancet (London, England)* **380**, 349-357, doi:10.1016/s0140-6736(12)60813-7 (2012).
- 101 Ginsberg, M. D. *et al.* High-dose albumin treatment for acute ischaemic stroke (ALIAS) Part 2: a randomised, double-blind, phase 3, placebo-controlled trial. *Lancet Neurol* **12**, 1049-1058, doi:10.1016/s1474-4422(13)70223-0 (2013).
- 102 Mak, I. W., Evaniew, N. & Ghert, M. Lost in translation: animal models and clinical trials in cancer treatment. *American journal of translational research* **6**, 114-118 (2014).
- 103 Orset, C. *et al.* Efficacy of Alteplase in a Mouse Model of Acute Ischemic Stroke: A Retrospective Pooled Analysis. *Stroke* **47**, 1312-1318, doi:10.1161/strokeaha.116.012238 (2016).
- 104 Philip, M., Benatar, M., Fisher, M. & Savitz, S. I. Methodological quality of animal studies of neuroprotective agents currently in phase II/III acute ischemic stroke trials. *Stroke* **40**, 577-581, doi:10.1161/strokeaha.108.524330 (2009).
- 105 Recommendations for standards regarding preclinical neuroprotective and restorative drug development. *Stroke* **30**, 2752-2758 (1999).
- 106 Woodruff, T. M. *et al.* Pathophysiology, treatment, and animal and cellular models of human ischemic stroke. *Mol. Neurodegener.* **6**, 19, doi:10.1186/1750-1326-6-11 (2011).
- 107 Kirino, T. Delayed neuronal death in the gerbil hippocampus following ischemia. *Brain research* **239**, 57-69 (1982).
- 108 Yonekura, I., Kawahara, N., Nakatomi, H., Furuya, K. & Kirino, T. A model of global cerebral ischemia in C57 BL/6 mice. *Journal of cerebral blood flow and metabolism : official journal of the International Society of Cerebral Blood Flow and Metabolism* **24**, 151-158, doi:10.1097/01.Wcb.0000096063.84070.C1 (2004).
- 109 Pulsinelli, W. A. & Buchan, A. M. The four-vessel occlusion rat model: method for complete occlusion of vertebral arteries and control of collateral circulation. *Stroke* **19**, 913-914 (1988).
- 110 Brott, T. *et al.* Measurements of acute cerebral infarction: lesion size by computed tomography. *Stroke* **20**, 871-875 (1989).
- 111 Karpiak, S. E., Tagliavia, A. & Wakade, C. G. Animal models for the study of drugs in ischemic stroke. *Annual review of pharmacology and toxicology* **29**, 403-414, doi:10.1146/annurev.pa.29.040189.002155 (1989).
- 112 Mhairi Macrae, I. New models of focal cerebral ischaemia. *British journal of clinical pharmacology* **34**, 302-308 (1992).
- 113 Tamura, A., Graham, D. I., McCulloch, J. & Teasdale, G. M. Focal cerebral ischaemia in the rat: 1. Description of technique and early neuropathological

- consequences following middle cerebral artery occlusion. *Journal of cerebral blood flow and metabolism : official journal of the International Society of Cerebral Blood Flow and Metabolism* **1**, 53-60, doi:10.1038/jcbfm.1981.6 (1981).
- 114 Fluri, F., Schuhmann, M. K. & Kleinschnitz, C. Animal models of ischemic stroke and their application in clinical research. *Drug Des. Dev. Ther.* **9**, 3445-3454, doi:10.2147/dddt.S56071 (2015).
- 115 Markgraf, C. G. *et al.* Comparative histopathologic consequences of photothrombotic occlusion of the distal middle cerebral artery in Sprague-Dawley and Wistar rats. *Stroke* **24**, 286-292; discussion 292-283 (1993).
- 116 Watson, B. D., Dietrich, W. D., Busto, R., Wachtel, M. S. & Ginsberg, M. D. Induction of reproducible brain infarction by photochemically initiated thrombosis. *Ann Neurol* **17**, 497-504, doi:10.1002/ana.410170513 (1985).
- 117 Macrae, A. D. & Bloom, S. R. Endothelin an endocrine role. *Trends in endocrinology and metabolism: TEM* **3**, 153-157 (1992).
- 118 Gerriets, T. *et al.* The macrosphere model: evaluation of a new stroke model for permanent middle cerebral artery occlusion in rats. *Journal of neuroscience methods* **122**, 201-211 (2003).
- 119 Zhang, Z. *et al.* A new rat model of thrombotic focal cerebral ischemia. *Journal of cerebral blood flow and metabolism : official journal of the International Society of Cerebral Blood Flow and Metabolism* **17**, 123-135, doi:10.1097/00004647-199702000-00001 (1997).
- 120 Beech, J. S. *et al.* Further characterisation of a thromboembolic model of stroke in the rat. *Brain research* **895**, 18-24 (2001).
- 121 Carmichael, S. T. Rodent models of focal stroke: size, mechanism, and purpose. *NeuroRx : the journal of the American Society for Experimental NeuroTherapeutics* **2**, 396-409, doi:10.1602/neurorx.2.3.396 (2005).
- 122 Longa, E. Z., Weinstein, P. R., Carlson, S. & Cummins, R. Reversible middle cerebral artery occlusion without craniectomy in rats. *Stroke* **20**, 84-91 (1989).
- 123 Nagasawa, H. & Kogure, K. Correlation between cerebral blood flow and histologic changes in a new rat model of middle cerebral artery occlusion. *Stroke* **20**, 1037-1043 (1989).
- 124 Molina, C. A. *et al.* Timing of spontaneous recanalization and risk of hemorrhagic transformation in acute cardioembolic stroke. *Stroke* **32**, 1079-1084 (2001).
- 125 Garcia, J. H., Wagner, S., Liu, K. F. & Hu, X. J. Neurological deficit and extent of neuronal necrosis attributable to middle cerebral artery occlusion in rats. Statistical validation. *Stroke* **26**, 627-634; discussion 635, doi:10.1161/01.str.26.4.627 (1995).
- 126 Memezawa, H., Smith, M. L. & Siesjo, B. K. Penumbra tissues salvaged by reperfusion following middle cerebral artery occlusion in rats. *Stroke* **23**, 552-559 (1992).

- 127 Sakurada, O. *et al.* Measurement of local cerebral blood flow with iodo [14C] antipyrine. *The American journal of physiology* **234**, H59-66, doi:10.1152/ajpheart.1978.234.1.H59 (1978).
- 128 Tamura, A., Graham, D. I., McCulloch, J. & Teasdale, G. M. Focal cerebral ischaemia in the rat: 2. Regional cerebral blood flow determined by [14C]iodoantipyrine autoradiography following middle cerebral artery occlusion. *Journal of cerebral blood flow and metabolism : official journal of the International Society of Cerebral Blood Flow and Metabolism* **1**, 61-69, doi:10.1038/jcbfm.1981.7 (1981).
- 129 De Visscher, G., Haseldonckx, M. & Flameng, W. Fluorescent microsphere technique to measure cerebral blood flow in the rat. *Nature protocols* **1**, 2162-2170, doi:10.1038/nprot.2006.332 (2006).
- 130 Beckmann, N., Stirnimann, R. & Bochen, D. High-resolution magnetic resonance angiography of the mouse brain: application to murine focal cerebral ischemia models. *Journal of magnetic resonance (San Diego, Calif. : 1997)* **140**, 442-450, doi:10.1006/jmre.1999.1864 (1999).
- 131 Meng, W. *et al.* Effects of tissue type plasminogen activator in embolic versus mechanical models of focal cerebral ischemia in rats. *Journal of cerebral blood flow and metabolism : official journal of the International Society of Cerebral Blood Flow and Metabolism* **19**, 1316-1321, doi:10.1097/00004647-199912000-00004 (1999).
- 132 Ginsberg, M. D. *et al.* 11C-Iodoantipyrine for the measurement of regional cerebral blood flow by positron emission tomography. Validation studies. *Stroke* **12**, 745-750 (1981).
- 133 Rajan, V., Varghese, B., van Leeuwen, T. G. & Steenbergen, W. Review of methodological developments in laser Doppler flowmetry. *Lasers in medical science* **24**, 269-283, doi:10.1007/s10103-007-0524-0 (2009).
- 134 Dirnagl, U., Kaplan, B., Jacewicz, M. & Pulsinelli, W. Continuous measurement of cerebral cortical blood flow by laser-Doppler flowmetry in a rat stroke model. *Journal of cerebral blood flow and metabolism : official journal of the International Society of Cerebral Blood Flow and Metabolism* **9**, 589-596, doi:10.1038/jcbfm.1989.84 (1989).
- 135 Eyre, J. A., Essex, T. J., Flecknell, P. A., Bartholomew, P. H. & Sinclair, J. I. A comparison of measurements of cerebral blood flow in the rabbit using laser Doppler spectroscopy and radionuclide labelled microspheres. *Clinical physics and physiological measurement : an official journal of the Hospital Physicists' Association, Deutsche Gesellschaft fur Medizinische Physik and the European Federation of Organisations for Medical Physics* **9**, 65-74 (1988).
- 136 Fukuda, O., Endo, S., Kuwayama, N., Harada, J. & Takaku, A. The characteristics of laser-Doppler flowmetry for the measurement of regional cerebral blood flow. *Neurosurgery* **36**, 358-364, doi:10.1227/00006123-199502000-00016 (1995).
- 137 Katz, L., Ebmeyer, U., Safar, P., Radovsky, A. & Neumar, R. Outcome model of asphyxial cardiac arrest in rats. *Journal of cerebral blood flow and metabolism*

- : official journal of the International Society of Cerebral Blood Flow and Metabolism **15**, 1032-1039, doi:10.1038/jcbfm.1995.129 (1995).
- 138 Miyagi, Y., Carpenter, R. C., Meguro, T., Parent, A. D. & Zhang, J. H. Upregulation of rho A and rho kinase messenger RNAs in the basilar artery of a rat model of subarachnoid hemorrhage. *Journal of neurosurgery* **93**, 471-476, doi:10.3171/jns.2000.93.3.0471 (2000).
- 139 Scholler, K., Feiler, S., Anetsberger, S., Kim, S. W. & Plesnila, N. Contribution of bradykinin receptors to the development of secondary brain damage after experimental subarachnoid hemorrhage. *Neurosurgery* **68**, 1118-1123, doi:10.1227/NEU.0b013e31820a0024 (2011).
- 140 Hoffman, W. E., Thomas, C. & Albrecht, R. F. The effect of halothane and isoflurane on neurologic outcome following incomplete cerebral ischemia in the rat. *Anesthesia and analgesia* **76**, 279-283 (1993).
- 141 Zheng, S. & Zuo, Z. Isoflurane preconditioning induces neuroprotection against ischemia via activation of P38 mitogen-activated protein kinases. *Mol Pharmacol* **65**, 1172-1180, doi:10.1124/mol.65.5.1172 (2004).
- 142 Zhao, P. *et al.* Isoflurane postconditioning improved long-term neurological outcome possibly via inhibiting the mitochondrial permeability transition pore in neonatal rats after brain hypoxia-ischemia. *Neuroscience* **280**, 193-203, doi:10.1016/j.neuroscience.2014.09.006 (2014).
- 143 Zhang, H. P. *et al.* Isoflurane preconditioning induces neuroprotection by attenuating ubiquitin-conjugated protein aggregation in a mouse model of transient global cerebral ischemia. *Anesthesia and analgesia* **111**, 506-514, doi:10.1213/ANE.0b013e3181e45519 (2010).
- 144 Gray, J. J., Bickler, P. E., Fahlman, C. S., Zhan, X. & Schuyler, J. A. Isoflurane neuroprotection in hypoxic hippocampal slice cultures involves increases in intracellular Ca²⁺ and mitogen-activated protein kinases. *Anesthesiology* **102**, 606-615 (2005).
- 145 Khatibi, N. H. *et al.* Isoflurane posttreatment reduces brain injury after an intracerebral hemorrhagic stroke in mice. *Anesthesia and analgesia* **113**, 343-348, doi:10.1213/ANE.0b013e31821f9524 (2011).
- 146 Altay, O. *et al.* Isoflurane attenuates blood-brain barrier disruption in ipsilateral hemisphere after subarachnoid hemorrhage in mice. *Stroke* **43**, 2513-2516, doi:10.1161/strokeaha.112.661728 (2012).
- 147 Matchett, G. A., Allard, M. W., Martin, R. D. & Zhang, J. H. Neuroprotective effect of volatile anesthetic agents: molecular mechanisms. *Neurological research* **31**, 128-134, doi:10.1179/174313209x393546 (2009).
- 148 Karibe, H., Zarow, G. J., Graham, S. H. & Weinstein, P. R. Mild intransischemic hypothermia reduces postischemic hyperperfusion, delayed postischemic hypoperfusion, blood-brain barrier disruption, brain edema, and neuronal damage volume after temporary focal cerebral ischemia in rats. *Journal of cerebral blood flow and metabolism : official journal of the International Society of Cerebral Blood Flow and Metabolism* **14**, 620-627, doi:10.1038/jcbfm.1994.77 (1994).

- 149 Karibe, H., Chen, J., Zarow, G. J., Graham, S. H. & Weinstein, P. R. Delayed induction of mild hypothermia to reduce infarct volume after temporary middle cerebral artery occlusion in rats. *Journal of neurosurgery* **80**, 112-119, doi:10.3171/jns.1994.80.1.0112 (1994).
- 150 Minamisawa, H., Nordstrom, C. H., Smith, M. L. & Siesjo, B. K. The influence of mild body and brain hypothermia on ischemic brain damage. *Journal of cerebral blood flow and metabolism : official journal of the International Society of Cerebral Blood Flow and Metabolism* **10**, 365-374, doi:10.1038/jcbfm.1990.66 (1990).
- 151 Busto, R., Dietrich, W. D., Globus, M. Y. & Ginsberg, M. D. Postischemic moderate hypothermia inhibits CA1 hippocampal ischemic neuronal injury. *Neuroscience letters* **101**, 299-304 (1989).
- 152 Morikawa, E. *et al.* The significance of brain temperature in focal cerebral ischemia: histopathological consequences of middle cerebral artery occlusion in the rat. *Journal of cerebral blood flow and metabolism : official journal of the International Society of Cerebral Blood Flow and Metabolism* **12**, 380-389, doi:10.1038/jcbfm.1992.55 (1992).
- 153 Barber, P. A., Hoyte, L., Colbourne, F. & Buchan, A. M. Temperature-regulated model of focal ischemia in the mouse: a study with histopathological and behavioral outcomes. *Stroke* **35**, 1720-1725, doi:10.1161/01.STR.0000129653.22241.d7 (2004).
- 154 Wu, L. *et al.* Keep warm and get success: the role of postischemic temperature in the mouse middle cerebral artery occlusion model. *Brain research bulletin* **101**, 12-17, doi:10.1016/j.brainresbull.2013.12.003 (2014).
- 155 Gröger, M. *Rolle der Kinin Rezeptoren beim sekundären Hirnschaden nach transienter fokaler zerebraler Ischämie der Maus*, (2007).
- 156 Spector, R. G. Water content of the brain in anoxic-ischaemic encephalopathy in adult rats. *British journal of experimental pathology* **42**, 623-630 (1961).
- 157 Mayer, S. A. & Pulsinelli, W. A. Failure of GM1 ganglioside to influence outcome in experimental focal ischemia. *Stroke* **23**, 242-246, doi:10.1161/01.str.23.2.242 (1992).
- 158 Slivka, A., Murphy, E. & Horrocks, L. Cerebral edema after temporary and permanent middle cerebral artery occlusion in the rat. *Stroke* **26**, 1061-1065; discussion 1065-1066, doi:10.1161/01.str.26.6.1061 (1995).
- 159 Plesnila, N. *et al.* Role of bradykinin B2 receptors in the formation of vasogenic brain edema in rats. *J Neurotrauma* **18**, 1049-1058, doi:10.1089/08977150152693746 (2001).
- 160 Barone, F. C., Knudsen, D. J., Nelson, A. H., Feuerstein, G. Z. & Willette, R. N. Mouse strain differences in susceptibility to cerebral ischemia are related to cerebral vascular anatomy. *Journal of cerebral blood flow and metabolism : official journal of the International Society of Cerebral Blood Flow and Metabolism* **13**, 683-692, doi:10.1038/jcbfm.1993.87 (1993).

- 161 Gavrieli, Y., Sherman, Y. & Ben-Sasson, S. A. Identification of programmed cell death in situ via specific labeling of nuclear DNA fragmentation. *J Cell Biol* **119**, 493-501 (1992).
- 162 Grasl-Kraupp, B. *et al.* In situ detection of fragmented DNA (TUNEL assay) fails to discriminate among apoptosis, necrosis, and autolytic cell death: a cautionary note. *Hepatology* **21**, 1465-1468 (1995).
- 163 Negoescu, A. *et al.* In situ apoptotic cell labeling by the TUNEL method: improvement and evaluation on cell preparations. *J Histochem Cytochem* **44**, 959-968 (1996).
- 164 Negoescu, A., Guillermet, C., Lorimier, P., Brambilla, E. & Labat-Moleur, F. Importance of DNA fragmentation in apoptosis with regard to TUNEL specificity. *Biomed Pharmacother* **52**, 252-258, doi:10.1016/S0753-3322(98)80010-3 (1998).
- 165 Zhang, T. *et al.* CaMKII is a RIP3 substrate mediating ischemia- and oxidative stress-induced myocardial necroptosis. *Nature medicine* **22**, 175-182, doi:10.1038/nm.4017 (2016).
- 166 Zhu, Y., Cui, H., Xia, Y. & Gan, H. RIPK3-Mediated Necroptosis and Apoptosis Contributes to Renal Tubular Cell Progressive Loss and Chronic Kidney Disease Progression in Rats. *PloS one* **11**, e0156729, doi:10.1371/journal.pone.0156729 (2016).
- 167 Uhlén, M. *et al.* Proteomics. Tissue-based map of the human proteome. *Science (New York, N. Y.)* **347**, 1260419, doi:10.1126/science.1260419 (2015).
- 168 Wooten, M. W. *et al.* Essential role of sequestosome 1/p62 in regulating accumulation of Lys63-ubiquitinated proteins. *The Journal of biological chemistry* **283**, 6783-6789, doi:10.1074/jbc.M709496200 (2008).
- 169 Feng, T. *et al.* The p38/CYLD Pathway is Involved in Necroptosis Induced by Oxygen-glucose Deprivation Combined with ZVAD in Primary Cortical Neurons. *Neurochemical research* **42**, 2294-2304, doi:10.1007/s11064-017-2244-6 (2017).
- 170 Dosemeci, A., Thein, S., Yang, Y., Reese, T. S. & Tao-Cheng, J. H. CYLD, a deubiquitinase specific for lysine63-linked polyubiquitins, accumulates at the postsynaptic density in an activity-dependent manner. *Biochemical and biophysical research communications* **430**, 245-249, doi:10.1016/j.bbrc.2012.10.131 (2013).
- 171 Liu, S. *et al.* Necroptosis mediates TNF-induced toxicity of hippocampal neurons. *Biomed Res Int* **2014**, 290182, doi:10.1155/2014/290182 (2014).
- 172 Thein, S. *et al.* CaMKII mediates recruitment and activation of the deubiquitinase CYLD at the postsynaptic density. *PLoS One* **9**, e91312, doi:10.1371/journal.pone.0091312 (2014).
- 173 Ma, Q. *et al.* Proteasome-independent polyubiquitin linkage regulates synapse scaffolding, efficacy, and plasticity. *Proceedings of the National Academy of Sciences of the United States of America* **114**, E8760-e8769, doi:10.1073/pnas.1620153114 (2017).

- 174 Massoumi, R. *et al.* Down-regulation of CYLD expression by Snail promotes tumor progression in malignant melanoma. *The Journal of experimental medicine* **206**, 221-232, doi:10.1084/jem.20082044 (2009).
- 175 Espinosa, L. *et al.* The Notch/Hes1 pathway sustains NF-kappaB activation through CYLD repression in T cell leukemia. *Cancer cell* **18**, 268-281, doi:10.1016/j.ccr.2010.08.006 (2010).
- 176 Sahlgren, C., Gustafsson, M. V., Jin, S., Poellinger, L. & Lendahl, U. Notch signaling mediates hypoxia-induced tumor cell migration and invasion. *Proceedings of the National Academy of Sciences of the United States of America* **105**, 6392-6397, doi:10.1073/pnas.0802047105 (2008).
- 177 Liu, S., Kumar, S. M., Martin, J. S., Yang, R. & Xu, X. Snail1 mediates hypoxia-induced melanoma progression. *The American journal of pathology* **179**, 3020-3031, doi:10.1016/j.ajpath.2011.08.038 (2011).
- 178 Guo, J. *et al.* Hypoxia suppresses cylindromatosis (CYLD) expression to promote inflammation in glioblastoma: possible link to acquired resistance to anti-VEGF therapy. *Oncotarget* **5**, 6353-6364, doi:10.18632/oncotarget.2216 (2014).
- 179 Ganjam, G. K. *et al.* Cylindromatosis mediates neuronal cell death in vitro and in vivo. *Cell death and differentiation* **25**, 1394-1407, doi:10.1038/s41418-017-0046-7 (2018).
- 180 Lewen, A. *et al.* Oxidative stress-dependent release of mitochondrial cytochrome c after traumatic brain injury. *Journal of cerebral blood flow and metabolism : official journal of the International Society of Cerebral Blood Flow and Metabolism* **21**, 914-920, doi:10.1097/00004647-200108000-00003 (2001).
- 181 Robertson, C. L. Mitochondrial dysfunction contributes to cell death following traumatic brain injury in adult and immature animals. *Journal of bioenergetics and biomembranes* **36**, 363-368, doi:10.1023/B:JOB.0000041769.06954.e4 (2004).
- 182 Xing, C., Arai, K., Lo, E. H. & Hommel, M. Pathophysiologic cascades in ischemic stroke. *International journal of stroke : official journal of the International Stroke Society* **7**, 378-385, doi:10.1111/j.1747-4949.2012.00839.x (2012).
- 183 Prins, M., Greco, T., Alexander, D. & Giza, C. C. The pathophysiology of traumatic brain injury at a glance. *Disease models & mechanisms* **6**, 1307-1315, doi:10.1242/dmm.011585 (2013).
- 184 You, Z. *et al.* Necrostatin-1 reduces histopathology and improves functional outcome after controlled cortical impact in mice. *Journal of cerebral blood flow and metabolism : official journal of the International Society of Cerebral Blood Flow and Metabolism* **28**, 1564-1573, doi:10.1038/jcbfm.2008.44 (2008).
- 185 Moquin, D. M., McQuade, T. & Chan, F. K. CYLD deubiquitinates RIP1 in the TNFalpha-induced necrosome to facilitate kinase activation and programmed necrosis. *PLoS One* **8**, e76841, doi:10.1371/journal.pone.0076841 (2013).

- 186 Prendergast, G. C., Metz, R. & Muller, A. J. Towards a genetic definition of cancer-associated inflammation: role of the IDO pathway. *The American journal of pathology* **176**, 2082-2087, doi:10.2353/ajpath.2010.091173 (2010).
- 187 Kong, X., Gong, S., Su, L., Li, C. & Kong, Y. Neuroprotective effects of allicin on ischemia-reperfusion brain injury. *Oncotarget* **8**, 104492-104507, doi:10.18632/oncotarget.22355 (2017).
- 188 Rosenberg, G. A. Ischemic brain edema. *Prog Cardiovasc Dis* **42**, 209-216 (1999).
- 189 Winkler, E. A., Minter, D., Yue, J. K. & Manley, G. T. Cerebral Edema in Traumatic Brain Injury: Pathophysiology and Prospective Therapeutic Targets. *Neurosurgery clinics of North America* **27**, 473-488, doi:10.1016/j.nec.2016.05.008 (2016).
- 190 Alameda, J. P. *et al.* Functional inactivation of CYLD promotes the metastatic potential of tumor epidermal cells. *J Invest Dermatol* **133**, 1870-1878, doi:10.1038/jid.2013.76 (2013).
- 191 Alameda, J. P. *et al.* An inactivating CYLD mutation promotes skin tumor progression by conferring enhanced proliferative, survival and angiogenic properties to epidermal cancer cells. *Oncogene* **29**, 6522-6532, doi:10.1038/onc.2010.378 (2010).
- 192 Gao, J. *et al.* CYLD regulates angiogenesis by mediating vascular endothelial cell migration. *Blood* **115**, 4130-4137, doi:10.1182/blood-2009-10-248526 (2010).
- 193 Altun, M. *et al.* Activity-based chemical proteomics accelerates inhibitor development for deubiquitylating enzymes. *Chemistry & biology* **18**, 1401-1412, doi:10.1016/j.chembiol.2011.08.018 (2011).
- 194 Mullally, J. E., Moos, P. J., Edes, K. & Fitzpatrick, F. A. Cyclopentenone prostaglandins of the J series inhibit the ubiquitin isopeptidase activity of the proteasome pathway. *The Journal of biological chemistry* **276**, 30366-30373, doi:10.1074/jbc.M102198200 (2001).
- 195 Aleo, E., Henderson, C. J., Fontanini, A., Solazzo, B. & Brancolini, C. Identification of new compounds that trigger apoptosome-independent caspase activation and apoptosis. *Cancer research* **66**, 9235-9244, doi:10.1158/0008-5472.can-06-0702 (2006).
- 196 D'Arcy, P., Wang, X. & Linder, S. Deubiquitinase inhibition as a cancer therapeutic strategy. *Pharmacology & therapeutics* **147**, 32-54, doi:10.1016/j.pharmthera.2014.11.002 (2015).

Eidesstattliche Versicherung

Ich erkläre hiermit an Eides statt,

dass ich die vorliegende Dissertation mit dem Titel

Contribution of the K63-deubiquitinase Cyldromatosis (CYLD) to neuronal cell death after focal cerebral ischemia

selbständig verfasst, mich außer der angegebenen keiner weiteren Hilfsmittel bedient und alle Erkenntnisse, die aus dem Schrifttum ganz oder annähernd übernommen sind, als solche kenntlich gemacht und nach ihrer Herkunft unter Bezeichnung der Fundstelle einzeln nachgewiesen habe.

Ich erkläre des Weiteren, dass die hier vorgelegte Dissertation nicht in gleicher oder in ähnlicher Form bei einer anderen Stelle zur Erlangung eines akademischen Grades eingereicht wurde.

Freiburg, 01.05.2023

Pierre Scheffler